Remediation of Weathered Light Nonaqueous Phase Liquids by Persulfate: *In-Situ* Performance Assessment and Numerical Modeling

by

Golnoush Bolourani

A thesis
presented to the University of Waterloo
in fulfillment of the
thesis requirement for the degree of
Doctor of Philosophy
in
Civil Engineering

Waterloo, Ontario, Canada, 2021

Examining Committee Membership

The following served on the Examining Committee for this thesis. The decision of the Examining Committee is by majority vote.

External Examiner	Sarah Dickson-Anderson Professor	McMaster University Dept. of Civil Engineering
Supervisor(s)	Marios Ioannidis Professor	University of Waterloo Dept. of Chemical Engineering
	James Craig Professor	University of Waterloo Dept. of Civil & Environmental Engineering
Internal Member	Monica Emelko Professor	University of Waterloo Dept. of Civil & Environmental Engineering
Internal Member	Bruce MacVicar Professor	University of Waterloo Dept. of Civil & Environmental Engineering
Internal-external Member	Micheal Stone Professor	University of Waterloo Dept. of Geography & Environmental Management

Author's Declaration

This thesis consists of material, all of which I authored or co-authored: see Statement of Contributions included in the thesis. This is a true copy of the thesis, including any required final revisions, as accepted by my examiners.

I understand that my thesis may be made electronically available to the public.

Statement of Contributions

I am the sole author for Chapter 1. Exceptions to sole authorship of the material presented in this thesis are described below.

Chapters 2 and 3 of this thesis are partially adapted from an article submitted for publication to the Journal of Hazardous Materials, which is co-authored by myself and my supervisors Professor Ioannidis (Chemical Engineering) and Professor James R. Craig (Civil & Environmental Engineering). It should be noted that I have done all the work associated with designing the study, undertaking laboratory work, conducting data analysis and interpretation, performing computer programming and simulation. I have done the majority of the manuscript writing, with editorial and intellectual contributions by Drs. Ioannidis and Craig.

Chapter 4 of this thesis is partially adopted from previously submitted technical reports that I have done the majority of the manuscript writing with editorial contributions by personnel from an external consulting firm that supported the field activities. I was the lead researcher responsible for designing the study, coordinating and executing field work, collecting field samples, performing data analysis and interpretation, and preparing the manuscripts.

Abstract

Light nonaqueous phase liquids (LNAPLs) petroleum hydrocarbons (PHCs) subsurface contamination is complex and poses considerable risks to human health and the environment. The PHC contaminated sites are often difficult to access and remediate due to subsequent changes in composition and distribution of bulk LNAPL mass following the release. The cleanup process becomes even more challenging as the released product ages and leaves behind several weathered residual LNAPL blobs and ganglia that are heterogeneously distributed in the soil pores within the smear zone. The selection of a suitable remedial program is based on bench-scale treatability studies, and the duration of the program relies heavily on time-consuming, labor-intensive, and, therefore, expensive monitoring activities. *In situ* chemical oxidation (ISCO) using persulfate has been increasingly recognized as one of the most feasible and reliable tools for remediation of PHC contaminated sites. Despite this recognition, there is no modeling approach available that can capture a persulfate ISCO remediation system behavior, evaluate its efficiency and effectiveness, and assist with design optimization. Existing models that can estimate the efficiency of an ISCO remediation are greatly dependent on the availability of LNAPL mass, composition, architecture, and interphase mass transfer rate data. In reality, however, it is difficult, if not impossible, to determine many of these parameters at a weathered PHC contaminated site. The focus of the research was on developing a combined bench-scale and numerical modeling framework to assist with describing and capturing the persulfate ISCO system during the remediation activities of heavily weathered LNAPL PHC contaminated sites.

A series of bench-scale experiments were designed and implemented to support the development of a numerical model. Aquifer material was collected from a heavily weathered diesel contaminated site (Site). Since a common feature of the gas chromatography analysis of a heavily weathered PHC is the presence of an unresolved complex mixture (UCM) of components, pseudocomponents F2 and F3, based on PHC fractions, were defined to estimate fundamental kinetic data. Aqueous phase treatability studies were performed using a series of well-mixed batch reactors to provide information on the ability of various persulfate systems (unactivated, citric acid chelated-ferrous activated, and alkaline activated persulfate) to degrade pseudocomponents F2 and F3 detected in the Site groundwater. Two concentrations of persulfate (40 and 80 $g.L^{-1}$) and two different persulfate activators (alkaline and citric acid chelated ferrous) at a persulfate concentration of 40 $g.L^{-1}$ were evaluated for the weathered diesel fuel contaminated groundwater. The pH of ~12 in alkaline activation of persulfate resulted in the highest reduction of ~99% LNAPL mass in groundwater. Chemical kinetic parameters of the aqueous treatment studies were estimated using a numerical

approach in the modeling of soil columns. The alkaline activated and unactivated persulfate systems at a persulfate concentration of 40 $g.L^{-1}$ were selected for remediation of the contaminated soil using the flow interruption column method with multiple persulfate injections. The LNAPL mass reduction of ~50% and 80% for unactivated and alkaline activated systems, respectively, were achieved. The observed data were used to develop an explanatory and practically useful model considering dissolution, advective–dispersive transport, and complex oxidation reactions occurring in porous media during ISCO remediation. The simulations showed that after two persulfate injections, the LNAPL mass reduction was limited by the dissolution process, and no further mass reduction occurred upon additional exposure to more persulfate.

A Site-specific action plan was developed to scale up the bench-scale research to a pilot-scale for a demonstration study, where research data and findings in the laboratory were tested and evaluated under field conditions. A pilot area was selected at a historical Site with a weathered diesel fuel contaminated aquifer manifested as residual sources in soil and dissolved phase in groundwater. A comprehensive monitoring infra-structure was installed. In this unique pilot-scale experiment, the selected area was divided into three zones of treatment (TTZ), control (CZ), and a buffer area in between the TTZ and CZ. Two injection episodes were conducted at the pilot area. The unactivated persulfate system (or municipal water at CZ) was introduced into the subsurface of the treatment zone at locations/depths of PHCs impacts identified with laser-induced fluorescence (LIF) equipped with an ultra-violet optical screening tool (UVOST™) to maximize the opportunity of persulfate to degrade the dissolved F2 and F3 pseudocomponents. No injection activity was conducted at the buffer zone. The dissolved PHCs mass flux was monitored downstream of the pilot area across a transverse fence-line at 60 multilevel sampling points pre- and post-injection episodes. In general, the pilot test data indicate that the aqueous mass of F2 and F3 decreased following each injection episode; however, both the TTZ and CZ showed a similar decrease. Considering the lack of persulfate presence during 3-week monitoring in the post-injection samples collected from the CZ, oxidation of F2 and F3 in the CZ area with persulfate seems unlikely. One potential explanation can be that the injection of water caused a displacement of the dissolved phase and perhaps any mobile nonaqueous phase liquid. Another likely reason is that by injecting uncontaminated water into this area, oxygen was also supplemented to the subsurface and encouraged microbial activities. Generally, it is believed that oxygen is present within the smear zone, and given the age of this contaminated Site (~70 years), it is expected that aerobic bioremediation had long reached its operational limits. However, the latter explanation is in agreement with the results of groundwater treatment tests in control batch reactors in the absence of persulfate. The soil samples were collected and analyzed pre-injection activities, and

after completion of the injection, Episode 2 corresponding to nearby LIF elevated response data. Since the places that persulfate can reach during injection are mainly unknown, the post-injection soil samples were collected from ~0.5 m above to ~0.5 m below the depths that pre-injection core samples were collected. The values in the post-injection column are the average of concentrations F2 and F3 in the soil samples that were collected within the intervals mentioned above. Overall, collected soil samples within the TTZ showed a decrease of ~50% in F2 and F3. Samples collected from CZ showed higher concentrations of F2 and F3 compared to pre-injection samples. This observation is not uncommon in the field because of the heterogeneity in contaminant distributions. However, since the overall 50% decrease in contaminant in soil was observed in TTZ, it can be concluded that the two injection episodes at the pilot-scale area were successful and generally in agreement with model simulation results.

Acknowledgments

I would like to express my heartfelt gratitude and sincere appreciation to my supervisors Prof. Marios Ioannidis and Prof. James Craig. Their deep technical insight, extensive knowledge, expert advice, and incredible guidance have been invaluable and have made this Ph.D. research possible. I am forever grateful for their unparalleled support, phenomenal encouragements, and never-ending faith in me.

I would like to extend many thanks to the rest of my thesis committee, Prof. Monica Emelko, Prof. Bruce MacVicar, Prof. Sarah Dickson, and Prof. Mike Stone for their commitment in time, valuable comments, and participation in my defence.

To Mr. Wayne Noble, whose assistance and technical support during lab experiments made all the difference, thank you for making things actually work.

A big thank you to Mr. Bob Ingleton and Mr. Paul Johnson for their help and guidance with the field work throughout the year, especially on hot summer days and in Canadian winters.

Thank you, Ms. Shirley Chatten, for assisting with the analysis of countless soil and groundwater samples.

I am deeply indebted for the immense unconditional love and tremendous support of my wonderful family, both here on earth and on the other side, who have stood by me and cheered for me through all the ups and downs of this experience.

Dedication

To my parents, Parvin and Reza

Table of Contents

List of Figures

List of Tables

Chapter 1:
Introduction

1.1 Background

Petroleum hydrocarbon fuels (PHCs) have become an integral part of our daily lives. While they have significant contributions to our modern lifestyle over the past century, PHCs have been identified as a significant source of soil and groundwater contaminations. Because of fragmented information and ambiguous terminology of contaminations across the agencies, it is difficult to accurately obtain the number of PHC contaminated sites or the severity of the contamination. However, ~ 225,000 and ~19,000 petroleum impacted lands and properties have been recorded in the United States and Canada, respectively (FSCI, 2019; USEPA, 2021). It should be noted that the above records do not include the sites that fall under other federal, state, or provincial (Canada) agencies such as the Department of Defense (DoD) and Department of Energy (DoE). Given the prevalence of petroleum hydrocarbon-based fuel applications at these facilities, these numbers might be underestimated. More importantly, these numbers are expected to rise with ongoing accidental spills, inappropriate discharges, and the impact of climate change (e.g., hurricanes), etc. Despite industries' best efforts to comply with spill prevention regulations, as of September 2020, over 559,000 releases from federally regulated leaking underground storage tanks (LUSTs) have been reported in the United States (USEPA, 2020). Even with stricter environmental regulations and closer government oversight, Canada is not in a much better situation. For example, the Canada Energy Regulator has recorded an average of ~170,000 liters of oil spilled per year (between 2011 and 2014) over 73,000 kilometers of pipelines that it regulates (NRCAN, 2020). Even with the substantial amount of effort in recent years, a 2004 estimate from the USEPA (2004) projected that, by 2033, over $200 billion (USD) (not adjusted for inflation) would be required for cleanup of the contaminated sites. According to the Canadian Council of Ministers of the Environment (CCME) projections, under current policies, such spending can be as high as $40 billion (CAD) for Canadian sites (CCME, 2019). It should be noted that, in most cases, these estimates do not include the long-term operational and maintenance expenditure at sites that do not reach regulatory cleanup goals when remediation is no longer viable. The most challenging sites are those with persistent and residual contamination (i.e., weathered PHCs) recalcitrant to biodegradation and conventional treatment technologies. In most cases, these sites are the product of historical industrial operations related to storing, handling, and inappropriate disposal of petroleum fuels.

Light nonaqueous phase liquid (LNAPL) fuels, such as diesel fuel, are among the most frequent contaminations in the subsurface across North America (CL:AIRE, 2014). LNAPLs are a mixture of hundreds to thousands of organic compounds (i.e., alkanes, alkenes, and aromatics) in varying proportions (Potter & Simmons, 1998). The density of LNAPL is lower than water, such that upon reaching the water table, it spreads laterally across the water table. Seasonal fluctuations of water-table cause vertical distribution and, in some cases, entrapment of portion of LNAPL mass in the soil pores (Figure 1-1**)** (Reddi et al., 1998; Wiedemeier et al., 1999). Over time the entrapped (residual) LNAPL body undergoes weathering processes, including physical, chemical, and biodegradation transformations based on climate and *in situ* conditions. The weathering process results in significant compositional changes of LNAPL mass toward more recalcitrant, heavier molecular weight compounds. This weathered residual LNAPL can create an *in situ* reservoir in the form of entrapped blob or ganglia in pore space. This reservoir can act as a continuous and long-term source of PHC contaminations to groundwater through dissolution. Therefore, the environmental and human health risks of LNAPL may remain as long as residual LNAPL persist in the subsurface. Moreover, the residual LNAPL is less prone to further weathering and less likely to remediate even when using the most aggressive existing remedial technologies (Fingas, 2017; Johnston, 2010).

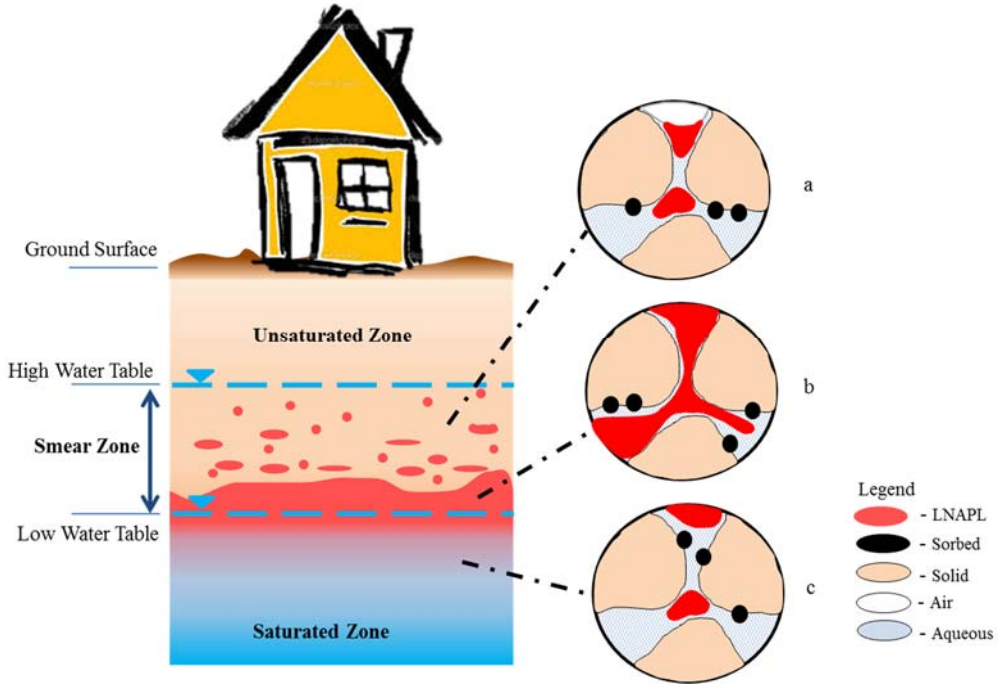

Figure 1-1: Simplified Conceptual Model of Smear Zone. In unsaturated zone (a) residual LNAPL in an unsaturated zone, (b) free moving LNAPL, and (c) residual LNAPL in a saturated zone

Since the danger of PHCs to human health and the environment has been increasingly recognized, remediation efforts to mitigate any potential or actual risk are currently at the forefront of environmental issues. Regulatory bodies and agencies have established guidelines and enforceable standards on maximum PHC concentration measurements in soil and groundwater for the protection of human and ecological health. Although considerable advances in remediation technologies have been made, existing technologies are unable to remove/destroy the weathered residual PHC mass sufficiently to reduce its dissolution into groundwater and thereby meet regulatory requirements. As such, many of these contaminated lands/properties remain unutilized and require prolonged and expensive remediation and ongoing monitoring activities (NRC, 2013). Identifying responsible party or parties to be held liable for remediation expenses are impractical in most cases, and taxpayers are left to deal with the cleanup bill.

One well-established technology for remediation of contaminated subsurface is *in situ* chemical oxidations (ISCO). ISCO requires the delivery of a chemical oxidant into the subsurface to react with hazardous contaminants in soil and groundwater and to alter them into less harmful chemical species. Persulfate has emerged as a strong and promising oxidant for ISCO applications, specifically for remediation of PHCs (Chen et al., 2016; Yang et al., 2019). Persulfate is capable of chemically oxidizing a wide range of PHCs both directly and through the generation of radical species (Liang et al., 2007). It can persist in the presence of aquifer material for weeks (Sra, K. S. et al., 2010). Considerable attention has been directed at this oxidant both in research and industry. Its use in ISCO has rapidly increased, as well as the crucial need for approaches and modeling tools that can provide insights into persulfate based ISCO (P-ISCO) system behavior, estimate performance expectations, and support remedial decision making (Lee et al., 2020; Siegrist et al., 2011; Yang et al., 2019). The literature on the oxidation of organics by persulfate is expanding; however, there are several research gaps to be explored with respect to its complex and real-world applications. The scope of P-ISCO studies with respect to the number and age of contaminants tends to be narrow and does not adequately cover the recalcitrant ones such as weathered residual sources. Addressing these problems demands improving existing and developing new remedial strategies. This highlights the need for further academic research in this area.

In this research, the effectiveness of various persulfate treatment strategies and the resultant mass removal/destruction behaviors in both groundwater and soil from a historical site impacted by weathered diesel fuel were investigated. Considering that the NAPL composition is often practically resolved only in terms of PHC fractions F1 to F4 (CCME, 2008), a phenomenological description was adopted for the oxidation by persulfate of PHC fractions treated as pseudocomponents and validated

this approach using experimental data for persulfate treatment of impacted groundwater in stirred batch reactors. Without further adjustment, the integration of persulfate oxidation kinetics within a one-dimensional model of dissolution, advection, and dispersion in porous media was implemented. The ability of this model to describe NAPL mass removal from soil columns during persulfate treatment – without and with activation by sodium hydroxide– was examined. Conclusions are drawn about the potential of this approach to estimate the extent of NAPL depletion during P-ISCO remediation that can inform remedial design in a field setting.

1.2 Research Objectives

The overall goals of this work are to provide a better understanding of persulfate ISCO for weathered LNAPL sites and improve upon remediation design and implementation. The research objectives mainly focus on the evaluation of the oxidation behavior of persulfate for decreasing LNAPL mass and mass flux from residual sources and the development of a model to guide future practice. As a result, the following objectives are set forth:

1. To investigate various persulfate treatment systems on mass destruction of dissolved multicomponent LNAPL in groundwater obtained from a historical site (Site), and estimate the nonlinear kinetic parameters for the chemical reactions;
2. To evaluate oxidation and the resultant mass removal/destruction behaviors of residual multicomponent LNAPL in impacted soil obtained from the Site under conditions more closely resembling the *in situ* conditions; and
3. To develop a numerical model for simulating multicomponent residual LNAPL dissolution and reactive transport that include complex oxidation reactions. The numerical approach can estimate the extent of residual LNAPL depletion in the soil through chemical oxidation, and the model can serve as an assessment tool to optimize remedial design and application at the field scale.

These objectives were addressed by investigating and evaluating the use of persulfate systems for the oxidation of weathered diesel impacted groundwater and soil through a detailed set of bench-scale studies that includes a series of batch and column tests to evaluate the effectiveness and efficiency of the persulfate systems in destroying weathered LNAPL mass. The results of these bench-scale studies were used to established persulfate based-ISCO end-points under ideal (i.e., laboratory) conditions. A numerical model was developed to simulate dissolution, advection, diffusion, and oxidation of residual LNAPL in soil. The results from these bench-scale experiments serve as a guide for pilot-scale investigations.

1.3 Thesis Outline

This thesis is comprised of four chapters; a general thesis introduction (Chapter 1), a review of the literature (Chapter 2), a bench-scale research approach (Chapter 3), and a pilot-scale study (Chapter 4). This chapter describes the research problem and lays out the objectives and what will be achieved by this study.

Chapter 2 reviews the existing literature on weathered petroleum light nonaqueous phase liquid contamination in soil and groundwater and their remediation using persulfate. A brief description of *in situ* chemical oxidation technology and the associated processes governing groundwater flow, interphase mass transfer, and contaminant's reactive transport provide the theoretical framework that guides this study.

Chapter 3 is the research-based experimental section investigating the feasibility and effectiveness of various persulfate-based systems for oxidation of weathered petroleum light nonaqueous phase liquid contamination in soil and groundwater. The experimental setup and methodology are described, and results are presented and discussed. This chapter also describes the development of a numerical model that facilitates the investigation of persulfate-based *in situ* chemical oxidation remediations. The model simultaneously solves the coupled mass-conservation governing equations of groundwater flow, complex chemical reactions, contaminants dissolutions, and advective-dispersive transport.

Chapter 4 is the research-based pilot-scale section investigating the feasibility of the persulfate system for remediation of a highly weathered LNAPL impacted subsurface in a "real-world" situation and to compare post-remediation results with the experimental data and numerical simulations in Chapter 3.

Chapter 5 is the final chapter of this thesis and summarizes the findings and contributions of the previous chapters. In addition, it provides recommendations for future work based on the limitations of the current study.

Chapter 2[1]:
Literature Review

This chapter presents a summary of the literature of prior research pertaining to *in situ* chemical oxidation (ISCO) treatment for remediation of weathered light nonaqueous phase liquid (LNAPL) contamination in soil and groundwater. A strong emphasis is placed on diesel range organic compounds and the use of persulfate as an oxidant for ISCO (P-ISCO).

2.1 Light Nonaqueous Phase Liquid Fuel Hydrocarbons

Petroleum hydrocarbon fuels, such as diesel fuel, are LNAPLs that are mixtures of aliphatic (saturated) and/or aromatic (unsaturated) organic compounds depending on the hydrocarbon source. When released into the environment, LNAPLs can infiltrate through the unsaturated zone and accumulate over the water table. The seasonal fluctuations of the water table cause a lateral spread of the LNAPL across the zone of oscillation (Steffy et al., 1995) and result in the trapping of a portion of the LNAPL's mass in the soil pores within the vicinity of the water table. Over time, the weathering processes change entrapped LNAPL's compositions, leaving behind the heavier and less volatile organic compounds that have low aqueous solubility (Drake et al., 2013; Powers et al., 1994). This residual entrapped LNAPL mass within the subsurface becomes progressively less susceptible to natural attenuation and conventional remedial technologies and may act as a lingering source of groundwater contaminations for centuries. Most current LNAPL-impacted sites are the result of past practices and unregulated activities whose human health and environmental consequences were not identified and fully understood at the time (Story & Yalkin, 2014).

Analysis of weathered petroleum hydrocarbon compounds (PHCs) by gas chromatography typically yields a substantial unresolved or unidentified portion that appears as a hump (Figure 2-1). This portion is referred to as an unresolved complex mixture (UCM) of hydrocarbons. The UCMs represent mixtures of hundreds or thousands of individual chemicals and have been adopted extensively as a quantitative descriptor of fuel hydrocarbons in environment studies (Thomas et al., 1995). However, since UCMs are not unique compounds, the mixture's physical and chemical properties such as density, viscosity, solubility, and LNAPL-water interfacial tension that govern their subsurface behavior remain largely unknown. There is a large of body P-ISCO literature describing PHCs' reactions and remediation based on quantifying individual compounds and/or total petroleum hydrocarbon (TPH) (Lemaire et al., 2011; Lominchar et al., 2018; Romero et al., 2009; Shafieiyoun & Thomson, 2019; Sra, K. S., Thomson, & Barker, 2013b).

[1] Some content from this chapter is also within a submitted article co-authored by myself and my supervisors Professor Ioannidis and Professor James R. Craig.

Meanwhile, there is a paucity of information on weathered PHCs despite the fact that many contaminated sites that are posing potential risks to human health harbour them (Brassington et al., 2007). Currently, policymakers and industry frequently use the results of existing single-species P-ISCO studies in establishing target cleanup criteria and remedial design for weathered PHC impacted sites. This is a challenging exercise and leads to an overestimation of the P-ISCO remedial benefits. First, because weathered PHC contaminations are complex mixtures. There is no single "best" compound or mixture of compounds that can adequately describe a weathered mixture's associated environmental risks, interaction with persulfate, intra-NAPL diffusion, and/or complex equilibrium partitioning in the subsurface over time. Second, TPH concentration measurements alone are insufficient for estimating critical transport parameters or potential risks to human health. Identical TPH concentration values may be comprised of very different constituents and consequently pose very different risks to human health and the environment (Weisman, 1998). One solution to these problems is the use of newer fraction-based analytical measures that have been adopted by many regulatory agencies for risk and toxicity assessment purposes. In this method, the broad spectrum of PHCs is fractionated into sub-fractions based on carbon chain length (CCME, 2008; Weisman, 1998). Fraction 1 (F1) or volatile PHCs represent C6 -C10, F2 or light extractable PHCs contains C10-C16, F3 or heavy extractable PHCs includes C16-C34, and F4 or extremely heavy extractable PHCs represent C34-C50 (CCME, 2008). Most compounds in a fraction share similar toxicity characteristics, environmental behavior, and transport properties. Therefore, once fractions are identified, fraction-specific parameters of relevant physical and chemical properties such as diffusion and reaction rate coefficients can be estimated (Edwards et al., 1997). In this research, the CCME (2008) classification approach was employed, and each PHC fraction was treated as a pseudocomponent.

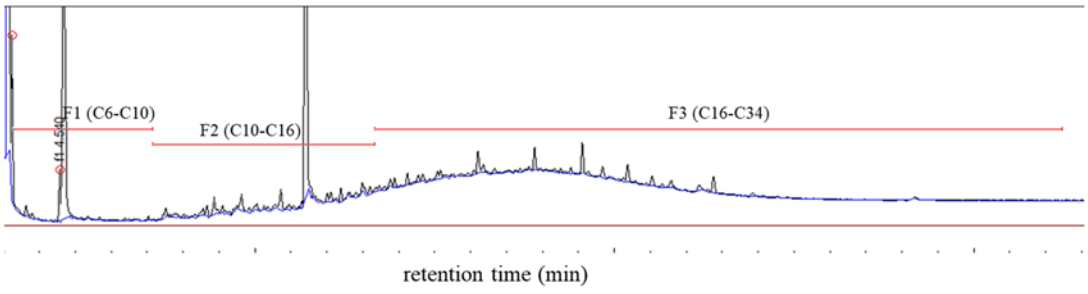

Figure 2-1: Example chromatogram profile of standard compounds (black) versus weathered diesel fuel (blue) from analysis of the groundwater collected at Site

2.2 *In Situ* Chemical Oxidation

In situ chemical oxidation is primarily considered a source zone treatment technology (Krembs et al., 2010) for organic contaminants. ISCO is conducted by delivery of a chemical oxidant into the contaminated subsurface with the goal of contaminant's mass destruction, transforming them into innocuous chemical species (Siegrist et al., 2011). The putative ISCO reagents include hydrogen peroxide, sodium persulfate, potassium permanganate, and ozone. Apart from ozone, which is in a gas form, other oxidants are commonly dissolved in water and made into a solution for ISCO purposes. ISCO may involve multiple iterations of oxidant delivery events and performance monitoring due to spatial variability in contaminant distribution, heterogeneity of aquifer, and limitation in mass transfer and transport mechanisms (Huling & Pivetz, 2006). The oxidant can be introduced into the subsurface employing varied delivery methods at different concentrations and mass loading rates (Siegrist et al., 2011). A summary of commonly used oxidant delivery methods is provided in Table 2-1.

Table 2-1: Conventional Oxidant Delivery Methods into Subsurface

Delivery Method	***Required Infrastructure***	***Applicable Depth (m)***	***Advantage***	***Disadvantage***
Direct push	Temporary boreholes advanced by the direct push technologies	30	Flexibility both in the location and vertical interval; small lateral displacement of contaminants	Equipment limitations, advancements of new boreholes for subsequent injections; small ROI due to the low injection pressure; not applicable in rocks/cobbles/boulders subsurface
Horizontal wells	Installation of temporary or permanent wells	30	Delivery of oxidant under infrastructure where vertical well installation or DPT is not feasible	Subsequent injections are restricted to the same location/depth
Fracturing (hydraulically or pneumatically)	Installation of injection wells slurry or air injections for hydraulic or pneumatic fracturing, respectively	Unlimited	Enhance ROI in low permeable zones	Lack of control over fracture pattern or radius of fracturing
Infiltration	Installation of trenches and galleries, dry wells, infiltration shaft, and pits within the vadose zone	Depth of vadose zone	Low maintenance cost; the constant presence of oxidant to address subsequent dissolution of contaminants	Limited zone of influence; depend upon vadose zone geology for vertical migration of oxidant solution
Injection wells	Installation of temporary or permanent wells	Unlimited	Installed wells can be used for subsequent injections; high injection pressures are possible	Subsequent injections are restricted to the same location/depth
Mechanical mixing	None	18	High contact time between oxidant and contaminants	Limited to the vertical operation of the mixing equipment
Sparge technologies (applicable only to ozone)	Installation of a network of injection sparging wells in the saturated zone	Unlimited	Installed wells can be used for subsequent injections; high injection pressures are possible	High vulnerability to nonideal transport mechanisms/preferential pathways; permeability reduction in the aquifer due to entrapped air; equipment limitations to provide the required pressure
Recirculation (injection-recovery-re-injection)	Installation of injection wells combined with extraction wells	Unlimited	Enhance ROI	Production of excess wastewater; high cost of operation and maintenance

2.2.1 Persulfate

Over the last few decades, the performance of hydrogen peroxide and permanganate for ISCO applications has been extensively explored (Petri et al., 2010). Although peroxide exhibits a widespread reactivity with PHCs, its low stability and generation of potential fugitive gases (e.g., oxygen) make it a weak candidate for the treatment of PHCs (Bogan & Trbovic, 2003; Schmidt et al., 2011; Yin & Allen, 1999). Permanganate is a more stable oxidant than hydrogen peroxide but is a selective one, and it produces manganese-oxide precipitations that might adversely affect the permeability of the subsurface (Huling & Pivetz, 2006). Use of persulfate ($S_2O_8^{2-}$) as an alternative oxidant for ISCO was promoted around 2000 because of its more comprehensive range of reactivity towards PHCs than peroxide and permanganate. Persulfate is a salt of peroxodisulphuric acid with strong oxidizing properties in the aqueous phase. Sodium persulfate ($Na_2S_2O_8$) (Figure 2-2) is commonly used for ISCO due to its low cost, high solubility, and stability (Petri et al., 2010). It can persist in the subsurface for several weeks (Sra et al., 2010).

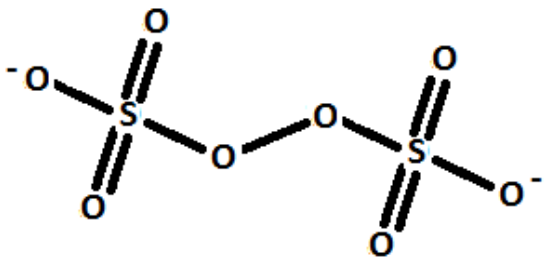

Figure 2-2: Persulfate Molecular Structure

2.2.2 Persulfate Activation Methods

Direct (or unactivated) persulfate reactions refer to the oxidization of PHCs without the initial presence of the free radicals. Persulfate can be activated through different methods and form potent sulfate ($SO_4^{-\bullet}$) and hydroxyl ($OH^{\bullet}$) radicals, and potentially several other radical-based oxygen species. These radical species possess higher oxidation potentials compared to the persulfate anion (House, 1962; Kolthoff & Miller, 1951) and are less selective in oxidizing a greater variety of PHCs (Block et al., 2004). Despite these advantages, activation of persulfate can decrease its persistency in the subsurface. Therefore, decisions on whether to activate persulfate or which activation method to use essentially rely on the rate and timescale at which the contaminant of concerns oxidize (Block et al., 2004; Crimi & Taylor, 2007). Different choices of activation methods for persulfate in ISCO include the use of heat, chelated iron, or alkaline activation.

Thermal activation of persulfate is generally achieved at ~60°C and produces sulfate radicals. This method of activation is less prevalent in the vicinity of flammable organic compounds such as PHCs.

Certain transition metal ions, such as ferrous iron (Fe(II)), can promote the generation of free radicals when combined with persulfate (Anipsitakis & Dionysiou, 2004). Typically, a chelating reagent such as citric acid (CA) is added to the mix to increase the solubility of iron at neutral pH (Liang et al., 2004a; Liang et al., 2004b). The molar ratio of CA to Fe(II) is one of the determining factors in the activation process, and a CA: Fe molar ratio of 0.2 to 2 is recommended for persulfate activation (Sra et al., 2010). In most existing studies, the citrate chelated ferrous iron activation method is used for PHCs of gasoline in the range that includes F1 and F2 PHCs. Both Killian et al. (2007) and Sra (2010) utilized this activation method for remediation of benzene, toluene, ethylbenzene, and xylenes (collectively called BTEX) and achieved near destruction of all compounds. The former authors observed that benzene and toluene, which have a lower molecular weight in a BTEX mixture, were oxidized to a greater extent (~99%) than the higher molecular weight BTEX compounds (ethylbenzene and xylenes), whose concentration were reduced by ~85%. Given that this method is one of the most popular persulfate activation methods (Tsitonaki, Aikaterini et al., 2010), additional investigations are required to evaluate the applicability and efficiency of this method for the treatment of weathered PHCs.

At high alkaline conditions (pH≥10), persulfate decomposes and generates sulfate and hydroxyl radicals (Furman et al., 2010). Strong bases such as sodium hydroxide (NaOH) are often used for alkaline activation of persulfate at pH ranges of 11 and 13 (Block et al., 2004; Siegal et al., 2009). Studies conducted to date to establish the performance efficiency of the alkaline activation method for the degradation of PHCs have been narrow and contradictory. In several studies, when alkaline activation of persulfate was employed, complete or near-complete PHC mass reduction was reported, while in some others, under comparable conditions, persulfate could not effectively destroy the PHCs (Liang et al., 2008; Sra et al., 2013). In a study by Zhao et al. (2013), unactivated, alkaline, and chelated iron activated persulfate were compared based upon mass destruction of 16 aromatic hydrocarbons that are commonly found in gasoline and diesel fuel. The oxidative treatment removal of these compounds was lowest in alkaline-activated persulfate among the systems evaluated. Meanwhile, Block et al. (2004) recommended that alkaline activation was best applied for mass destruction of recalcitrant contaminants, particularly in situations in which faster remediation is desired. Most published studies that focus on PHCs either conducted on dissolved PHCs in the aqueous phase (Crimi & Taylor, 2007; Sra et al., 2013a), slurry tests for contaminated solids (Chen et al., 2016; Lominchar et al., 2018), or use fresh PHC materials in spiked soil. Lack of information on the

performance of alkaline-activated persulfate for mass reduction of aged residuals presents additional difficulty in interpreting results for a P-ISCO field application. This ambiguity demands further research to evaluate alkaline-activated persulfate effectiveness for PHCs impacted subsurface at historical sites. A summary of available literature on LNAPL PHC oxidation with persulfate is provided in Table 2-2.

Table 2-2 : Summary of Literature on Persulfate Chemical oxidation of LNAPL PHCs

Study	Study Type	System type	Source	Target Compounds	Activator System	Persulfate Concentration (as $Na_2S_2O_8$)	Temperature of study (ºC)	Test duration	Major Findings
Neta et al. (1977)	Aqueous	Batch	Spiked	Benzenes	Unactivated	0.2 to 1.2%	Ambient	as the reactors were completed	1) Reaction rates of SO4* with contaminates are reported 2) The primary oxidation mechanism was identified as electron transfer
Cuypers et al. (2000)	Soil	Batch	Field Sample	PAHs	Thermal	~3.6 wt%	70	3 hrs	1) Less condensed natural organic matter was oxidized initially, and the sorbed PAHs were oxidized afterward
Cuypers et al. (2002)	Soil	Batch	Field Sample	PAHs	Thermal	~3.6 wt%	70	3 hrs	1) O-alkyl and carboxyl are more susceptible to persulfate oxidation 2) Aromatic or aliphatic are less susceptible to persulfate oxidation
Block et al. (2004)	Soil	Batch	Spiked	28 VOCs (of which only BTEX and styrene are LNAPL among reported contaminants)	Fe(II) Fe(III) Fe(III)-EDTA (Fe: 550 mg/L and pH 2-3, 7-8) Hydrogen Peroxide (0.9-5%) Alkaline (pH 11+)	0.02 to 10 wt%	Ambient	8 to 21 days	1) Mild oxidation (unactivated persulfate) for destruction of BTEX 2) Strong oxidation (Fe-EDTA activated persulfate) for the destruction of chlorinated ethenes or chloro-benzenes 3) Aggressive oxidation (alkaline-persulfate, combined peroxide and persulfate, or heated persulfate) for the destruction of chlorinated ethanes or methanes
Huang et al. (2005)	Aqueous	Batch	Spiked	BTEX, styrene, naphthalene, acetone, trimethylbenzene, propylbenzene, butylbenzene	Thermal	0.01 to 0.05 wt%	20, 30, 40	72 hrs	1) At 20 ºC, ~34 to 66% destruction of contaminant were observed 2) At 30 ºC, ~80 to 98% destruction of contaminant were observed 3) At 40 ºC, ~94 to 100% to 66% destruction of contaminant were observed 4) It is noted that acetone had a negative degradation rate at all the temperature
Nadim et al (2005)	Soil	Batch	Spiked	16 PAHs	Fe(II):EDTA (3.33:1) [(250 mg/L-, 375 mg/L- and 500 mg/L-Fe(II)]	~0.5 wt%	20 to 25	24 hrs	Fe II-EDTA degraded PAHs by 75-100%
	Aqueous				Thermal		20, 30, 40		Results were not available to laboratory errors
Crimi & Taylor (2007)	Soil	Batch	Spike	BTEX naphthalene	CA:Fe (2:10, 2:1) CA-Fe:OX (1:2, 1:10) Alkaline (pH11) Hydrogen Peroxide:persulfate (0.0035 to 10:1)	~0.16 to 17 wt%	20	21 days	1) CA-Fe persulfate solution had better performance than alkaline or hydrogen systems for both BTEX destruction (~55 to 100%) and oxidant persistence 2) No difference in the effectiveness of oxidant solutions was observed in spike versus field soils systems 3) Contaminant extent and rate of degradation are contaminants- and porous media type-dependent
Killian et al. (2007)	Soil	Batch	Field Sample	BTEX PAHs	Fe (0.45 wt%) CA:Fe (5:1, 50:2)	2 wt% and 31.5 wt%	Ambient	7-19 days	1) Chelated iron (95% and 85% removal efficiency of BTEX and PAHs, respectively) is a superior activator than sequential addition of iron (86% and 56% removal efficiency of BTEX and PAHs, respectively) 2) Sequential (double dose) of chelated iron activated persulfate reduced BTEX and PAHs by 99% and 92%. 3) Light weight molecular weight compounds were oxidized faster than heavier ones
Liang et al. (2008)	Aqueous	Batch	Spiked	BTEX	Fe(II) and Fe(II)-HPCD (500-4000 mg/L as Fe 25.4 g/L HBCD or 17.5 mM)	Persulfate:BTEX molar ratios of 20:1 and 100:1	20	30 days	1) the degradation half-lives of aqueous phase BTEX ranged from 3.0 to 23.1 days and 1.5 to 20.3 days in aqueous and soil slurry systems, respectively 2) HPCD and EDTA may be less susceptible to chelated Fe2+ while CA was found a more suitable chelating agent in the iron activated persulfate system
	Soil				Unactivated	Unactivated (0.5 to 2.5 wt%)	20	30 days	

Table 2-2 (CONT.) : Summary of Literature on Persulfate Chemical oxidation of LNAPL PHCs

Study	Study Type	System type	Source	Target Compounds	Activator System	Persulfate Concentration (as $Na_2S_2O_8$)	Temperature of study (ºC)	Test duration	Major Findings
Do et al. (2009)	Soil	Batch	Spiked	Fresh diesel fuel	Fe(II) ($FeCl_2$, $FeSO_4$) (0.2 - 4 mM) Co(II) ($CoCl_2$, $CoSO_4$) (0.2 - 4 mM) pH (3, 6, and 9)	Peroxymonosulfate PMS:M^+(200:3, 2:10-100, 200, 400, 500]	Ambient	7 hrs	1) CoCl2 and PMS solution provided the best removal efficiency 2) A minimum of 2 mM of Co(II) was required to achieve ~30% destruction of diesel 3) Increase in PMS: Co(II) led to higher removal of diesel 3) Single and sequential (5 to 10 times) solution injection led to 47% and 88% removal of diesel4) Diesel degradations were 20%, 17%, and 13%, at pH values of 3, 6, and 9, respectively
Do et al. (2010)	Soil	Batch	Spiked	Fresh diesel fuel	Fe(II) (0.5 to 10mM) (Fe:Persulfate 1:100, 200, 500, 1000), goethite, hematite, magnetite, and manganese oxide (1, 5, and 7%)	~ 0.1 to 2 wt%	25	12 hrs	1) The effectiveness of goethite, hematite, magnetite, and manganese oxide on the ability of persulfate (PS) with/without Fe(II) to remediate fresh diesel-contaminated soil was evaluated. 2) The optimum contaminant removal was observed at pH 3, and the molar ratio of PS:Fe(II) was 100:1. 3) All methods showed some removal of the contaminant ~20% to 40%. PS activated with manganese oxide worked best in removing the diesel in the presence of Fe(II). 4) Persulfate showed a strong dependency on concentrations of Fe(II), and higher concentrations of Fe(II) acted as a scavenger for persulfate.
Liang & Guo (2010)	Aqueous	Batch	Spiked	Naphthalene	zerovalent iron (ZVI) (1 g)	1 wt%	Ambient	120 min	1) Concentration gradient between the solid and aqueous phases of naphthalene particles caused naphthalene particles to dissolve and oxidize by $SO^{\bullet}_4$
Yen et al. (2011)	Soil	Batch	Spiked	Fresh diesel and fuel oil	Fe(II):Persulfate (10:1, 100:1) In situ Fe	10 and 20 wt%	25	150 days	1) The higher persulfate and ferrous ion concentrations (similar molar ratio systems), the higher diesel degradation rates 2) Treatment systems showed between 25 to 55% reductions of contaminants in spiked and weathered samples 3) Removal efficiencies of unactivated and activated treatment systems were comparable, indicating that in situ metal is effective in activating the persulfate 4) A two-stage diesel degradation was observed in the batch experiments: a rapid and slow stage 5) Fuel oil degradation efficiency was comparable to diesel fuel 6) Persistence of persulfate in the systems lasted more than five months
			Field sample	Weathered diesel	Fe(II):Persulfate (10:1) unactivated (in situ Fe)	20 wt%		60 days	
Liang & Guo (2012)	Soil	Batch	Spiked	Fresh diesel fuel	Alkaline (CaO and NaOH) (0.05-2 M) Hydrogen Peroxide (0.66 and 3.30 M) Hydrogen Peroxide/alkaline (pH 12) heat/alkaline (pH 12) heat	0.1-0.5 M	20 and 50	7-28 days	1) Highest diesel degradation rate of 56 % in 7 days was observed in a peroxide/persulfate system of 3.3:0.5 2) NaOH or CaO persulfate system showed a maximum of 30% diesel degradation 3) Results indicated that using increasing alkalinity of the oxidation solution increased decomposition of persulfate with no significant effect on diesel degradation
Kambhu et al. (2012)	Aqueous	Batch	Spiked	BTEX	Fe(II) candles ZVI candles Mixed persulfate + Fe(II) + citric acid candles	Various	Ambient	2 days	1) Oxidant candles were a mixture of $Na_2S_2O_8$:paraffin (2.25:1) in a circular shape candles of 2.38 cm long (diameters of 0.71 or 1.27 cm) 2) $FeSO_4$ or ZVI activator candles were used for activation purposes 3) Rapid transformation of BTEX was observed within 12 hrs
Usman et al. (2012b)	Soil	Batch	Spiked	weathered PAHs and fresh crude oil reported as TPH	Magnetite activated	2.3 wt%	Ambient	1 week	1) Weathered PAH mass removal efficiency was between 70 and 80% in the magnetite activated system 2) Crude oil mass removal efficiency was between 80 and 90% in the magnetite activated system

Table 2-2 (CONT.) : Summary of Literature on Persulfate Chemical oxidation of LNAPL PHCs

Study	Study Type	System type	Source	Target Compounds	Activator System	Persulfate Concentration (as $Na_2S_2O_8$)	Temperature of study (ºC)	Test duration	Major Findings
Usman et al. (2012a)	Soil	Batch	Spiked and Filed sample	Fluorenone and a mixtre of PAHs	Magnetite activated soluble Fe(II) [oxidant:Fe(II) (1:1)] and unactivated	2.3 wt%	Ambient	1 week	1) Magnetite activate persulfate showed 70-80% while soluble Fe(II) and unactivated showed 5-20% of reduction of PAHs in spiked sand 2) Oxidation of Fluorenone was MRS activated while less than 20% in other two oxidant system 2) No PAHs removal was observed from the field sample soil 3) PAH degradation efficiency is highly on the dependant PAH availability and soil matrix
Al-Shamsi & Thomson (2013)	Aqueous	Batch	Spiked	Naphthalene	nZVI Naphthalebe:persulfate:nZVI (1:20:20)	0.26 g/L	20.5	18 hrs	1) 99% and 10% naphthalene reductions in nZVI-activated persulfate and nZVI treatment systems, respectively, were observed 2) X-ray photoelectron spectroscopy analyses showed that nZVI particle surfaces were passivated 3) Passivated nZVI activated persulfate appeared to have a better degradation efficiency than Fe^{2+} and granular ZVI activated persulfate systems
Lemaire et al. (2013)	Soil	Column	Spiked and Field sample	16 PAHs	Hydrogen peroxide (H_2O_2: $Na_2S_2O_8$ =5:1)	90 g/L	Ambient	12 hrs	1) Maximum PAH removal of 30% and 55% were observed in field soils and spiked soils, respectively 2) High carbonate content was contributed to a drawback for radical reactions in field samples in addition to poor PAH availability in these samples
Sra et al. (2013)	Aqueous	Batch	Spiked	Fresh Gasoline Fuel	Unactivated CA:Fe(II) 1:1 (Fe(II) 150 and 300 mg/L) Hydrogen peroxide (0.1 and 1 M) Alkaline (pH 11and 13)	1 and 20 g/L	Ambient	28 days	1) 1 g/L unactivated persulfate systems did not show ability to remove PHC F1 significantly while PHC F2 decreased by 75% within 10 days 2) 20 g/L persulfate in both activated and unactivated systems removed PHC F1 by 50-97% significantly while PHC F2 decreased by 75% within 10 days 3) 40–60% reduction of PHC F2 was observed in natural activation treatment systems while 20-40% reduction of PHC F2 was observed in CA-Fe(II) and pH-13 treatment systems 4) PHC F2 was degraded by 50-70% in the peroxide controls
Sra et al. (2013)	Aqueous	Field Scale	Spiked	BTEX trimethylbenzene naphthalene	Unactivated (2000 L)	20 g/L	Ambient	10+ months	1) The decrease in the cumulative mass of contaminants was 60 to 80% due to persulfate oxidation. 2) A partial rebound of 40 to 80% of contaminant concentrations was observed up to Day 315
Usman et al. (2013)	Soil	Column	Spiked	a mixtre of weatherd PAHs	MRS oxidant:Fe(II)(1:1)	2.3 wt%	Ambient	4 days	1) Oxidant system showed 63-70% degradation of PAHs 2) No mobilization of dissolved organic compounds out of the system was observed 3) Oxidant system showed less reactivity towards high molecular weight PAHs.
Yan & Lo (2013)	Soil	Batch	Spiked	Naphthalene	Fe-EDTA (persulfate:FeEDTA:naphthalene 150:10:1, 225:10:1 and 300:10:1) Fe-EDDS (persulfate:FeEDDS:naphthalene 150:50:1, 150:75:1, 150:100:1, 225:10:1 and 300:10:1).	3 to 6 g/L	20	10 hrs	1) Naphthalene removals of 89% and 75% were observed in persulfate: Fe-EDTA:naphthalene (300:10:1) and persulfate:Fe-EDDS:naphthalene (150:75:1), respectively
	Aqueous							7 hrs	1) Naphthalene removal was highest at 60% in persulfate:FeEDDS:naphthalene (150:75:1) treatment systems 2) persulfate consumed more by EDDS than EDTA, so EDTA was found to be a more suitable iron chelating agent
Zhao et al. (2013)	Soil	Batch	Field samples	a mixtre of weatherd PAHs	Thermal (40, 50, 60) CA-Fe (ferrous iron: persulfate 1:10, 1:4, 1:2) alkaline (10, 11, 12) hydrogen peroxide (H_2O_2: $Na_2S_2O_8$ = 1:100, 1:10, 1:1)	60 g/L	Various	72 hrs	1) Maximum PAHs degradation of 99.1% and persulfate consumption of 0.45–1.38 g/kg soil were observed in thermal activated treatment systems 2) CA-Fe treatment systems showed persulfate consumption of 0.91–1.22 g/kg soil and PAHs removal of 73.3–82.9% 3) Oxidant consumptions and PAH removals were comparable in hydrogen peroxide activated, alkaline activated, and unactivated persulfate treatment systems
Liao et al. (2014)	Soil	Batch	Field samples	a mixtre of weatherd PAHs	Thermal activation and unactivated	238 g/L	50 for thermal activation Ambient for unactivated	4 and 24 hrs	1) Significant PAH compositional changes was observed in pre- and post- oxidation soil 2) overall, both unactivated and thermally activated persulfate oxidation of PAH-contaminated soil resulted in PAH mass removal compared to the control system, however, the oxidant efficiency was limited in a naturally contaminated soil representing aged conditions compared to the comparable studies

Table 2-2 (CONT.) : Summary of Literature on Persulfate Chemical oxidation of LNAPL PHCs

Study	Study Type	System type	Source	Target Compounds	Activator System	Persulfate Concentration (as $Na_2S_2O_8$)	Temperature of study (ºC)	Test duration	Major Findings
Wu et al. (2015)	Soil	Batch	Field samples	Wathered PHC reported as TPH	Unactivated, thermal activation, CA-Fe (1:1), and hydrogen peroxide (H2O2: Na2S2O8 = 100, 10, 1), alkaline activation (pH=9, 11, & 12)	238	40, 70, and 100 fi thermal activation, ambient for the rest	24 hrs	1) TPH removal efficiency was 3% in unactivated, ~40.1% in CA-Fe activated, ~32% in alkaline activated, 21% in hydrogen peroxide activated, ~16% in thermal activated persulfate systems. 2) the age of contamination resulted in decrease in remediation efficiency compared to the comparable studies
Chen et al. (2016)	Soil	Batch	Field samples	Wathered diesel reported as TPH	Unactivated	10, 30,50, and 100 g/L	Ambient	120 days	1) TPH degradation of increased by increasing persulfate concentrations and were 66, 72, 78, and 93% for 10, 30,50, and 100 g/L, respectively. 2) Persulfate persisted in all treatment reactors to various degrees until for duration of the experiment, except for reactors with 10 g/L concentration of persulfate that persulfate was not detected from day 80 onward.
Lominchar et al. (2018)	Soil	Batch	Field sample	Weathered diesel reported as TPH	Alkaline activation (pH>12) NaOH: persulfate =2 & 4	25, 50, and 100 g/L	Ambient	56 days	1) TPH removal efficiency was 100% NaOH:persulfate = 4 at persulfate concentration of 100 g/L while in other systems were between 60 and 77%.
Yang et al. (2020)	Soil	Column	Spiked	Benzene and toluene	100 mL ferrous iron (100 mg/L): 100 mL of persulfate solution	10 g/L	Ambient	enough time to inject ~18 PV of oxidant solution	1) The activated peruslfate system was compared to the hydrogen peroxide system, and it was concluded that hydrogen peroxide system was more effective in reducing the mass of the PHC. Both systems achived 100% removal but persulfate system reached that mass reduction with injection of ~13 PV while only injection 6 PV of the hydrogen peroxide solution was needed for same mass reduction.
	Aqueous	Batch				10, 50, and 100 g/L		5 hrs	

Notes:

BTEX- refers to the chemicals benzene, toluene, ethylbenzene and xylene
PAHs- polycyclic aromatic hydrocarbon group was included in the summary because they are the least desnse DNAPLs
EDTA- Ethylenediaminetetraacetic acid
HPCD- hydroxypropyl-I-cyclodextrin
EDDS- Ethylenediamine-N,N'-disuccinic acid

2.2.3 Persulfate Reaction Kinetics with LNAPL Hydrocarbons

Many of the persulfate reactions with fuel hydrocarbons are thermodynamically favorable. The mass balance law for the reaction between persulfate and an organic compound can be described written as (Tsitonaki, A. et al., 2008):

$$\frac{d[C_xH_y]}{dt} = -k[C_xH_y]^{n_{PHC}}[S_2O_8^{2-}]^{n_{ox}} \quad (2.1)$$

In the above equation, k is the reaction rate coefficient with respect to the organic compound, and n_{PHC} and n_{ox} are the reaction orders for PHC compound and persulfate, respectively. In the majority of studies to date, it is assumed that the oxidant concentration remains constant for the duration of the experiment, and n_{PHC} is assumed to be unity, modifying Equation (2.1) as:

$$\frac{d[C_xH_y]}{dt} = -k'[C_xH_y] \quad (2.2)$$

where k' is defined as pseudo-first-order reaction rate coefficient and is the product of k and initial persulfate concentration. In some studies, it was observed that degradation of organic compounds has a multiple-stage degradation process and is nonlinear, notably, at longer experimental times (>10 days) (Biswas, 2011; Lominchar et al., 2018; Yen et al., 2011). Tratnyek et al. (2009) noted this trend in their data; nevertheless, they decided only to fit the initial portion using the pseudo-first-order for practical purposes. Shafieiyoun et al. (2018) used soil columns to study the ability of persulfate in the oxidation of a multicomponent NAPL mixture. The soil used in the study was collected from a contaminated site; however, the study only focused on the detected NAPL components with known concentrations. Their attempt to estimate second-order reaction rate coefficients for any of the components was not successful even by adopting idealized conditions (per authors' admission), including the assumption of infinite dispersion. The exact persulfate reaction mechanism with a PHC mixture is unknown. Regardless of the initial unactivated or activated condition, persulfate can potentially react with daughter products and generate reactive radicals that complicate kinetics investigations (Tratnyek et al., 2009). In light of the above information, it is not desirable to overtly apply a pseudo-first-order model to persulfate oxidation reactions with weathered PHCs. An extensive literature review indicates that with the exception of one peer-reviewed publication (Mendes et al., 2020), only pseudo-first-order kinetics are reported. Mendes et al. ran a 4-hour batch experiment with naphthalene (NAP) spiked soil at a concentration of 80 mg NAP/kg soil. A 6.5 mL of persulfate solution (~18 $g.L^{-1}$) was activated by 1 mL of ferrous sulfate (~4 $g.L^{-1}$) and was

added to 3.75 g of spiked soil in a 20 mL vial. The experimental data were best fitted to pseudo-zero-order kinetics; however, the authors have reported both first- and second-order rate reactions. In this research, pseudocomponents (based on PHC fractions) are defined, and a numerical approach is developed to estimate fundamental kinetic data such as nonlinear reaction rate constants.

2.3 Interphase Mass Transfer and Reactive Mass Transport

A comprehensive, realistic ISCO modeling framework with the ability to conservatively access remediation effectiveness can be used to provide an understanding of the system behavior and greatly assist with remedial design and optimization. Most standard model tools approved by the USEPA are for groundwater flow and contaminant transport applications. As of now, models that can capture *in situ* persulfate oxidation, a weathered residual source, and the relevant complex processes are lacking. Several analytical and numerical solution approaches have been developed for remediation of residual NAPL source; however, they either address some of the processes (Frind et al., 1999; Molson et al., 2002) or are based on unrealistic and overly simplified physical models (Shafieiyoun & Thomson, 2019).

Several governing equations are considered for the simulation of a P-ISCO of a residual NAPL source in the subsurface, including groundwater flow, residual NAPL dissolution, advective-dispersive transport, and chemical reactions for oxidation of dissolved phase. The NAPL desorption was assumed negligible (Appendix C). By assuming that the linear driving force can represent LNAPL interphase mass transfer (as done by, e.g., Frind et al., 1999 or Powers et al., 1994), the following one-dimensional partial differential equation can capture spatial and temporal concentration changes for the *i*th component of an LNAPL mixture during ISCO processes:

$$\frac{\partial C_i}{\partial t} = -v\frac{\partial C_i}{\partial x} + \frac{\partial}{\partial x}\left(D_i\frac{\partial C_i}{\partial x}\right) + k_{diss}\alpha_i\left(C_{S_i} - C_i\right) - k_i {C_i}^{n_i} C_{ox}^{m_i} \qquad (2.3)$$

where v (cm.day^{-1}) is average linear groundwater velocity, D_i (cm^2.day^{-1}) are the hydrodynamic dispersion coefficients for persulfate and i^{th} component, respectively. C_{S_i} (g.L^{-1}) is the solubility limit, k_{diss} (cm.day^{-1}) mass transfer coefficient, and α_i (cm^{-1}) is the LNAPL- water specific (but unknown) interfacial tension. C_{ox} is the concentration of oxidant, n_i and m_i are the exponents in the reaction rate expressions.

Mass transfer coefficient is commonly determined based on Gilland-Sherwood number (Sh), an empirical nondimensional expression, that relates NAPL-water interphase mass transport resistance to the molecular mass transfer resistance in terms of fluid and porous medium properties:

$$Sh = \frac{k_{diss}\, l_p}{D_{m_i}} \tag{2.4}$$

In the above equation l_p (cm) is a characteristic length and can be defined in the range of pore scale (Zhao & Ioannidis, 2003) to laboratory scale (Powers et al., 1994), to field scale (Parker & Park, 2004). D_{m_i}(cm^2.day^{-1}) is the molecular diffusion coefficient of *i*th the component in a NAPL mixture. Most researchers avoid quantifying k_{diss} and instead, use lumped mass transfer rate coefficient, K_l (day^{-1}), which is the product of k_{diss} and α_i. Due to the heterogeneous nature of porous media structure, NAPL geometry, and NAPL wettability that makes the quantification of α_i difficult (Sahloul et al., 2002). Miller et al. (1990) provided a modified definition of Sherwood number, Sh', that has been defined as a function of NAPL-water total specific interfacial tension and median grain size (d_{50}):

$$Sh = \frac{K_l\, d_{50}^2}{D_{m_i}} \tag{2.5}$$

Most existing Sherwood number expressions are developed based on laboratory-scale experiments using simplified NAPL blob geometry of single NAPL sphere models or lumped domain models (by assuming uniformly distributed NAPL saturations) (e.g., Imhoff et al., 1994; Miller et al., 1990). In reality, however, a residual NAPL source zone is a collection of subzones of trapped blobs and ganglia of complex geometries within the soil pore network (Figure 2-3). The orientations of these NAPL subzones to preferential flow paths play an essential role in overall NAPL dissolution within the contaminated aquifer and NAPL availability for P-ISCO remediation. Different flow passing scenarios can be applied for the same interfacial area due to pore-scale structure and NAPL architecture (Agaoglu et al., 2016). Another issue with the formulation of many of the existing Sherwood formulations is the assumption that water is the wetting liquid. During the dissolution process, the composition of a NAPL mixture changes, which can result in an alternation of the degree of wettability or shift of the system to a NAPL-wet state (or vice versa) depending on the remaining components and compositions. Zhao and Ioannidis's (2003) research shows that in a NAPL-wetting system, the available interfacial area for mass transfer is larger than a water-wetting system at a comparable NAPL saturation and pore-scale structure and results in higher NAPL dissolution. In addition to the above issues, the solution to Equations 2.3 requires identification and knowledge of the composition of each component within a multicomponent NAPL mixture. However, weathered NAPLs at contaminated sites are comprised of hundreds of thousands of unknown components. The existing modeling studies have been based on (1) a single component selected from a NAPL mixture or, at best, (2) a mixture of known (and fresh) components. In a recent modeling effort to evaluate the intra-NAPL

diffusion and its effect on dissolution in the presence of persulfate oxidation, a flow-through chamber was used in a horizontal position (Shafieiyoun & Thomson, 2019). A rectangular cuboid NAPL body was placed at the bottom of the chamber, and the experiments were conducted in the absence of porous media. Only the top surface area (length x width) of the rectangular cuboid was exposed to the flowing persulfate solution. The isolated multicomponent NAPL mixture had a similar composition to the NAPL used in the Shafieiyoun et al. (2018) study. The authors claim that their reactive transport model generates "realistic parameters (i.e., mass transfer rate coefficients, equilibrium concentration of NAPL constituents, activity coefficients, and NAPL characteristics)." As described in earlier sections, the problematic multicomponent NAPL contaminations in the subsurface consist of several entrapped NAPL bodies. The above parameters cannot be determined realistically when NAPL source zone architecture[2] and preferential flow in porous media are entirely disregarded. Although their model is theoretically appealing, its practical utility has limited value for the assessment of NAPL dissolution and to assist with the design and optimization of a P-ISCO remedial program.

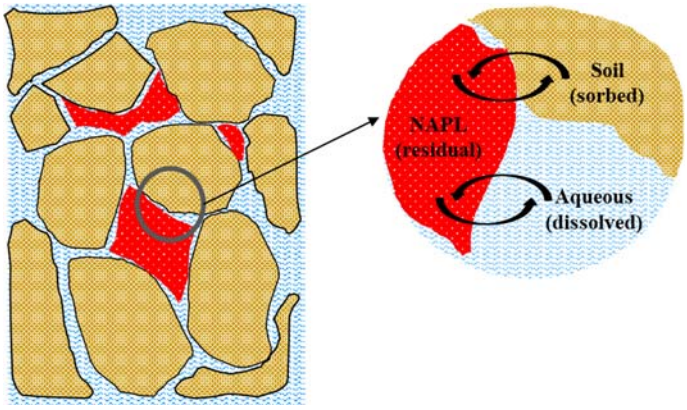

Figure 2-3: Conceptual model of NAPL, aqueous, and solid phase in the saturated zone

2.4 Summary

Over the past two decades, persulfate-based ISCO has gained increasing attention for remediation of petroleum NAPL contaminated subsurface. Its economic feasibility, ability to oxidize a wide range of recalcitrant organic contaminants, and persistency in the subsurface have made it an attractive oxidant for

[2] Source zone architecture is defined as number, geometry, special distribution, and collective saturation of NAPL subzones within the contaminated aquifer that composed the overall source zone (Sale & McWhorter, 2001)

field applications. The current upsurge in scientific publications on persulfate-based ISCO technology suggests confidence and optimism on the part of academic researchers and non-academic stakeholders about the future of the technology. However, the majority of petroleum NAPL focused remediation research with the technology has been done on a single compound or mixture of known compounds, primarily from fresh products and often in the absence of porous media. The literature available on persulfate-based ISCO treatment of weathered NAPL contaminated soil is scarce and very limited in scope. One of the missing and highly desired tools, aligned with data from realistic design and execution of laboratory trials that can provide a better reflection of the *in situ* system behavior, is developing modeling and simulation capabilities that provide researchers and practitioners acceptable explanatory powers to explore and access various remediation scenarios, offer reliable support for decision-making, and enable remedial design optimization.

Chapter 3[3]:
Persulfate oxidation to remediate soil contaminated by weathered multicomponent nonaqueous phase liquid: Column experiments and modeling

3.1 Overview

In this chapter, a mathematical model is formulated to help explain and access both activated and unactivated persulfate efficiency for mass destruction of weathered residual multicomponent light nonaqueous phase liquid (LNAPL). The model can simulate coupled processes of residual LNAPL dissolution, advective-dispersive transport, and complex oxidation of dissolved phase reactions. As part of this study, detailed aqueous batch and flow interruption (Brusseau et al., 1989) soil column experiments were designed and implemented for the purpose of model parameterization. Efforts were made to capture physical and chemical processes at a level that is applicable to complex in situ conditions. This research is unique in several aspects. To the author's knowledge, this is the first time an investigation has defined an LNAPL pseudocomponent based contaminants' toxicity and successfully estimated their complex nonlinear kinetic characteristics in persulfate oxidations reactions. This is the most comprehensive study presenting a physical model for persulfate-based *in situ* chemical oxidation (P-ISCO) under laboratory conditions that closely resemble *in situ* environments with respect to the heterogeneous distribution of residual NAPL mass oxidant to solids mass ratio and multiple oxidant delivery iterations. This is the first reasonably realistic numerical approach for simulating P-ISCO degradation of weathered residual sources in a transport model that can serve as a guidance tool for performance assessment in field-scale applications.

3.2 Introduction

Petroleum hydrocarbon (PHC) mixtures such as diesel fuel are light nonaqueous phase liquid (LNAPL) contaminants frequently encountered at sites across North America (CL: AIRE, 2014; Tomlinson et al., 2017). LNAPLs have a lower density than water and, upon release to the environment, migrate downward in the vadose zone and tend to accumulate in the vicinity of the water table. Movement of the water table results in spreading, disconnection trapping of LNAPL in the form of ganglia (blobs) within soil pores, and the establishment of an immobile residual LNAPL saturation in a so-called smear zone. Weathering of

[3] Most content from this chapter is also within a submitted article co-authored by myself and my supervisors Professor Ioannidis and Professor James R. Craig.

LNAPL causes significant compositional, physical, and chemical changes in the PHC mixture, resulting in more viscous and less soluble compounds than the original mixture (Fingas, 2017). This residual weathered LNAPL acts as a long-term, continuous source of groundwater contamination through dissolution, which persists until it is naturally attenuated or actively remediated (Powers et al., 1996).

The destruction and potentially complete mineralization of PHCs in contaminated soil and groundwater by *in situ* chemical oxidation using persulfate as the oxidant (P-ISCO) has received considerable attention (Huling & Pivetz, 2006; Lominchar et al., 2018; Siegrist et al., 2011). Persulfate has a broader range of reactivity towards PHCs than permanganate (Crimi & Taylor, 2007; Watts, Richard J. & Teel, 2006) and, unlike peroxide, can persist in the subsurface for several weeks (Matzek & Carter, 2016) without producing by-products that can alter the permeability of the subsurface (Conrad et al., 2002; Heiderscheidt et al., 2008; Watts & Teel, 2006). Persulfate can produce powerful free radicals (e.g., $SO_4^{-\bullet}$, $OH^{\bullet}$) upon activation to potentially enhance the oxidation rate of organic compounds. The understanding of persulfate activation has increased considerably in the past twenty years, and various activation methods have been proposed to increase the efficiency of the oxidation process for the destruction of PHCs (Matzek & Carter, 2016).

Many studies on P-ISCO for PHC remediation have been conducted in batch systems (Huang et al., 2005; Kambhu et al., 2012). Persulfate in a batch reactor has unlimited residence time and an unrealistic oxidant-to-solids mass ratio (Lominchar et al., 2018). Batch tests are therefore likely to overestimate the efficiency and effectiveness of the oxidation process in the field. Furthermore, the bulk of the literature on P-ISCO research has been focused mainly on a single representative compound selected from a PHC mixture (Liang et al., 2011 a,b; Yan & Lo, 2013), with limited effort to investigate the oxidation of weathered petroleum mixtures (Yang et al., 2019). Yet, a key characteristic of many LNAPLs at field sites is that these liquids are a complex mixture of hundreds of organic contaminants, which significantly complicates the remediation process and its mathematical description using models of reactive transport in porous media. At many, if not all, contaminated sites, remediation of PHCs is strongly limited by their multicomponent nature (Banerjee, 1984; Miller & Weber, 1984; Mukherji et al., 1997). Intra-NAPL diffusion and complex equilibrium partitioning at the NAPL-aqueous interface result in a decrease of the dissolution rate over time that is very difficult to predict (Brahma & Harmon, 2003). The LNAPL present at most contaminated sites is so heavily weathered that gas chromatography analysis only leads to a hump or unresolved complex mixture (UCM) in the chromatogram, meaning that the individual compounds cannot be identified or quantified. Therefore, although conceptually valuable, current findings regarding the fate of individual compounds cannot be extrapolated to design a P-ISCO system for contaminated sites impacted by highly

weathered recalcitrant PHC mixtures. The relevance of reaction rate kinetics discerned from batch tests with a single or few fresh PHCs to P-ISCO in the field is not clear. With few exceptions (Mendes et al., 2020), most studies of the persulfate oxidation rate have reported only pseudo-first-order kinetics (Huang et al., 2005; Sra et al., 2013; Tratnyek et al., 2009), limiting the applicability of the kinetic parameters estimated. For practical application of P-ISCO in a field setting, where reactant concentrations are certain to vary significantly in space, the reactivity of complex weathered LNAPLs with persulfate must be described with sufficient accuracy to access the outcome of P-ISCO remediation strategies. To the best of our knowledge, this objective has yet to be met.

Despite the increased interest in P-ISCO for research and commercial application, an experimentally validated model that could be used to examine different P-ISCO remediation scenarios is presently lacking. Predicting the outcome of P-ISCO in the subsurface is indeed a formidable task since it requires simulating the coupled processes of non-equilibrium dissolution of a weathered multicomponent NAPL of incompletely known composition advective–dispersive transport in a multicomponent aqueous phase in the presence of complex oxidation reactions with incompletely known kinetics. In the absence of a model with explanatory capacity, the design and implementation at the field scale have relied upon on-field experience, bench and pilot tests, and observational methods (Siegrist et al., 2011). In a significant recent work, Shafieiyoun and Thomson (2019) have attempted to account for some of the complexities of P-ISCO of multicomponent LNAPLs. Seeking to elucidate the effect of intra-NAPL diffusion on contaminant dissolution and subsequent oxidation by persulfate in a flowing aqueous phase, these authors formulated a model appropriate for a single isolated NAPL blob of known chemical composition and simple shape. Shafieiyoun & Thomson (2019) assumed second-order oxidation rate coefficients and sought to calibrate their model against experiments conducted in a microfluidic system of simple geometry. They found evidence for NAPL-persulfate interactions inhibiting interphase mass transfer, but the relevance of this finding for P-ISCO within porous media requires further investigation. While necessary for resolving intra-NAPL concentration gradients, the assumptions of known initial NAPL composition and simple geometry are at odds with reality in a field setting. Multiple NAPL bodies are heterogeneously distributed within porous media, their relative orientation to the flow path varies (Agaoglu et al., 2016), the NAPL-water interfacial area for mass transfer depends crucially on pore structure and wettability (Zhao & Ioannidis, 2003), and the time evolution of the chemical composition of each NAPL body is markedly different. These limitations provide strong motivation for investigating P-ISCO in one-dimensional soil columns.

In this thesis, the effectiveness of various persulfate treatment strategies and the resultant mass removal/destruction behaviors in both groundwater and soil from a historical site impacted by weathered diesel fuel w Considering that the NAPL composition is often practically resolved only in terms of PHC fractions F1 to F4 (CCME, 2008), we adopt a phenomenological description for the oxidation by persulfate of PHC fractions treated as pseudocomponents and validate this approach using experimental data for persulfate treatment of impacted groundwater in stirred batch reactors. Without further adjustment of the reaction kinetic parameters, we then consider the integration of persulfate oxidation kinetics within a one-dimensional model of dissolution, advection, and dispersion in porous media. The ability of this model to describe NAPL mass removal from soil columns during persulfate treatment – without and with activation by sodium hydroxide– is examined. Conclusions are drawn about the potential of this approach to estimate the extent of NAPL depletion during P-ISCO remediation that can inform remedial design in a field setting.

3.3 Experimental Design

3.3.1 Materials and Methods

3.3.1.1 Chemicals

Sodium persulfate ($Na_2S_2O_8$, reagent grade, ≥ 98%, Sigma-Aldrich Co., Milwaukee, WI), ferrous sulfate heptahydrate ($FeSO_4 \cdot 7H_2O$, J.T. Baker, Phillipsburg, NJ), citric acid anhydrous ($C_6H_8O_7$, Fisher, Fair Lawns, NJ), sodium hydroxide (NaOH, Sigma-Aldrich Co., St. Louis, MO), naphthalene ($C_{10}H_8$, GLC purity ≥ 99%, BDH Inc., Toronto, ON), and sodium azide (NaN_3, EMD Chemicals Inc., Gibbstown, NJ) were utilized without further purification. Chemicals for persulfate concentration analysis included ACS grade ferrous ammonium sulfate (FAS) ($Fe(NH_4)_2(SO_4)_2 \cdot 6H_2O$), EMD Chemicals Inc., Gibbstown, NJ), ammonium thiocyanate (NH_4SCN) (J.T. Baker, Phillipsburg, NJ) and sulfuric acid (H_2SO_4) (EMD chemicals Inc., Gibbstown, NJ). Dichloromethane (CH_2Cl_2, purity ≥ 99.8%, Sigma-Aldrich Co., St. Louis, MO) was used as a partitioning solvent for PHC analysis. Aqueous solutions of the chemicals were prepared, if required, using Milli-Q® water.

3.3.1.2 Contaminated subsurface Soil

Soil and groundwater were collected from a weather diesel fuel contaminated Site located in Ontario[4]. Chapter 4 provides detailed sample collection methodologies. Generally, an appropriate number of ~1.5 m

[4] Due to a confidentially agreement signed by the research team the location of the Site cannot be disclosed

long soil cores in dedicated clear acetate liners were collected (Figure 3-1 (a)) and subsampled in the laboratory for analysis of F2 and F3. Soil samples from the soil cores with elevated concentrations of the pseudocomponents were used for soil treatability studies. The contaminated soil used in this experiment was sourced from the smear zone at approximate depths of 6 to 9 m bgs and was characterized as medium to coarse textured native permeable sand with median grain size (d_{50}) of 0.071 cm and uniformity index ($U_i = d_{60}/d_{10}$) of 1.2. Groundwater samples were collected from 12 multilevel well transects containing 60 sampling points from 6 to 9 m bgs (Figure 3-1 (b)) utilizing a low flow (0.2 $L.min^{-1}$ or less) purge sampling technique via Masterflex L/S 12VDC peristaltic pump (Model 7533-40). Samples were collected in amber glass containers containing 10% sodium azide preservative. The groundwater samples were placed in coolers, maintained at ~4°C for transport to the laboratory for analysis to confirm the elevated level of PHC F2 and F3.

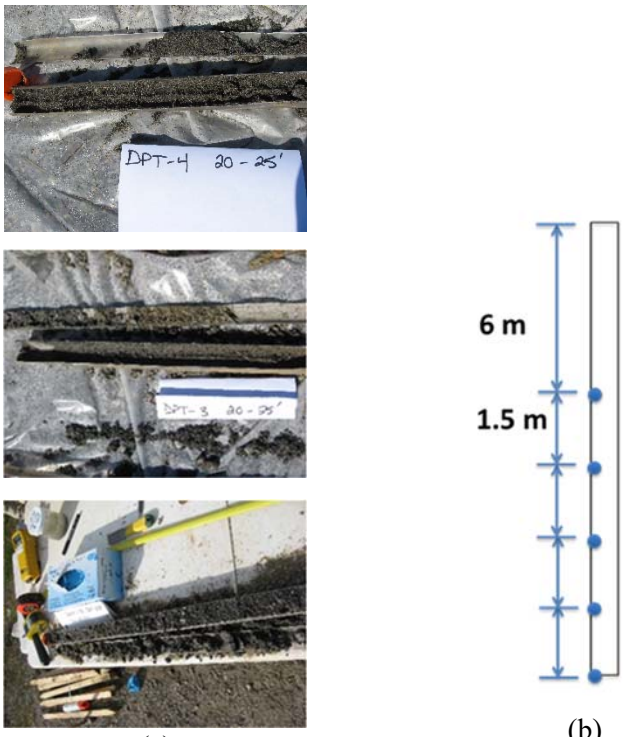

(a) (b)

Figure 3-1: a) Soil cores collected at the Site b) Schematic diagram of multilevel well used for groundwater sample collection

The concentration of F 2 and F3 in groundwater averaged 4626.7 and 4402.4 $\mu g.L^{-1}$, respectively. Due to circumstances beyond research team control, the alkaline activated and unactivated columns were packed with soil obtained from different cores. In 40-unactivated columns, the concentration of PHC F2 and F3 in

soil were averaged 538.6 and 1441.6 mg-NAPL per kg-soil, respectively. In alkaline columns, the concentration of PHC F2 and F3 in soil were averaged 1663.4 and 4675.6 mg-NAPL per kg-soil, respectively. Table 3-1 presents the physico-chemical properties of F2 and F3. The F2 and F3 data were determined by averaging the properties of the most common compounds found in diesel fuel range PHCs (Gustafson et al., 1997).

Table 3-1: Physico-Chemical Properties Organic Phases

Property	***Symbol***	***Units***	***F2***	***F3***
Density	ρ	$g.cm^{-3}$	0.88	0.98
Solubility	C_S	$g.L^{-1}$	8.70E-03[iii]	1.01E-02[iii]
Free liquid diffusivity	D_L	$cm^2.day^{-1}$	1.146E-02[iii]	2.840E-02[iii]

3.3.2 Analytical Methods

Pseudocomponent F2 and F3 analyses were performed following the applicable sections of the Canadian Council of Ministers of the Environment (CCME) method "Reference Method for the Canada-Wide Standard for Petroleum Hydrocarbons (CWS-PHC) in Soil – Tier 1 Method" (MOE Method DECPH-E3421/CCME). In general, the pseudocomponents were extracted from the aqueous and soil samples using solvent partition and analyzed by HP 5890 capillary gas chromatograph (GC) equipped with an HP7673A autosampler and a flame ionization detector. Dichloromethane (1 mL) was added to 5 mL of groundwater samples in glass vials and sealed with an aluminum crimp cap and Teflon septum. The vials were then shaken on their sides at 350 rpm on a platform shaker for 20 min. Upon completion of shaking, the vials were reverted for 30 min to allow the phases to separate. For soil samples, ~10 g of collected soil samples were placed in 20 mL glass vials containing ~15 mL of dichloromethane and shaken for 18 hours and then were allowed to settle. A gas-tight glass syringe was employed to transfer 1 mL of the solvent phase from the vials to Teflon-sealed auto-sampler vials into HP 5890 capillary GC equipped with a flame ionization detector. The bulk PHC fractions F2 (C10 to C16) included integration of all area counts on a PHC chromatogram beginning just after the decane (nC10) peak to the apex of the peak hexadecane (nC16) peak. The bulk PHC fractions F3 (C16 to C34) included integration of all area counts on a PHC chromatogram beginning just after the hexadecane (nC16) peak to the apex of the peak tetratriacontane (nC34) peak. The reader is referred to Appendix A for further details. Persulfate concentration analysis was

performed following Liang et al.'s (2008) method for unactivated and alkaline activated persulfate analysis. The Huang et al. (2002) method was performed to analyze the chelated ferrous activated persulfate to eliminate the interfering effect of ferric ions that are produced during the activation process. An Orion pH meter (model 290A) was used to measure pH. Oxidation-reduction potential (ORP) was measured by an Orion® ORP probe (Model A325). An Orion (5 Start portable multi-parameter meter) was used to measure electrical conductivity (EC).

3.3.3 Natural Oxidant Demand

One of the challenges in ISCO design is the oxidant loading rate to achieve the treatment objective. The non-target reactants reduced metals, and natural oxidant matters (NOM) can be major oxidant sink by increasing the persulfate consumption or decomposition rate, hence, impose a background oxidant demand. This natural oxidant demand (NOD) generally completes with target contaminants and reduces persulfate efficiency and performance. A series of well-mixed triplicate slurry batch tests were performed to determine the potential NOD values of unimpacted soil for unactivated persulfate systems. The unimpacted soil was collected from the same Site. The oxidant loading rates, mass oxidant per mass subsurface soil) varied from 5 to 50 $g_{persulfate}.kg^{-1}_{soil}$. The initial concentrations of 5, 20, 30, and 40 $g.L^{-1}$ were added to 50 g of soil in 125-mL clear glass vials with Teflon® screw-cap septum to achieve the oxidant loading rates of 5, 20, 30, and 40 $g_{persulfate}.kg^{-1}_{soil}$, respectively. In addition, two other experiments at the persulfate loading rates of 20 and 50 $g_{persulfate}.kg^{-1}_{soil}$ where the persulfate concentration of 30 $g.L^{-1}$ was added to 75 and 40 g of soil, respectively. A small aliquot (~2 mL) of the supernatant was withdrawn from each reactor after 8, 15, and 29 days. The reactors were manually shaken initially and after each sampling event and maintained at a temperature of ~20ºC in the dark for the duration of the experiment. The reader is referred to Appendix B for further details.

3.3.4 Groundwater Treatability Studies in Batch Reactors

A series of well-mixed batch experiments were conducted to evaluate the ability of non-activated and alkaline-activated persulfate systems to destroy dissolved phase F2 and F3 PHC. The trials for evaluation of the unactivated persulfate were conducted at two concentrations of 40 $g.L^{-1}$ (40-unactivated) and 80 $g.L^{-1}$ (80-unactivated). The data obtained from the 80-unactivated reactors were assessed the degree to which the rate of the PHC oxidation increased when the concentration of persulfate increases from 40 $g.L^{-1}$ to 80 $g.L^{-1}$. For activated systems, a concentration of 40 $g.L^{-1}$ of persulfate was used. The reported values of ORP at the research Site range from -400 to +6 millivolts (mV) and suggest a reducing condition (Golder, 2009).

Once groundwater is in contact with the atmosphere, the introduction of oxygen raises the ORP values, and aerobic bioactivity could resume (EPA, 2013). The PHC control reactors were prepared that contained only groundwater to account for the potential biodegradation of the F2 and F3 pseudocomponents. Biocide control reactors (BIO-CTRL) were designed to block the potential aerobic bioactivity by the addition of a sodium azide solution. The alkaline-activated treatment (ALK) reactors were to evaluate the performance of persulfate at high pH values (=~12) in activated persulfate systems. Since at higher pH values, some organic compounds may undergo hydrolysis reactions (Sra, 2010), pH Control reactors (pH-CTRL) were established to assess if hydrolysis alone can play a role in the F2 and F3 mass reduction. The dissolved PHCs in groundwater at the Site is a complex LNAPL mixture containing hundreds of thousands of components that cannot be identified individually. To verify the effectiveness of the persulfate system (e.g., 40-unactivated), a single PHC was selected and dissolved in Milli-Q® water for a proof-of-concept test. Naphthalene has been widely utilized for research on PHC oxidation (Liang and Guo, 2010) and was selected as a single component of PHC in this study. The data from these reactors were used for comparison of persulfate performance for multiple compounds versus single compound oxidation. Groundwater collected from the Site with elevated concentrations of the F2 and F3 was selected and mixed in a glass container. Aliquots of 450 mL of the mixed groundwater were dispensed to 1300 mL clear glass reactors and capped with the Mininert™ valves. Sodium persulfate was added to the groundwater in treatment reactors to attain the desired concentrations. In both elevated pH control and alkaline-activated treatment reactors, elevated pH was achieved by incrementally adding sodium hydroxide. Chelated-ferrous (CA-Fe) trials were performed at 300 $mg.L^{-1}$ Fe (II) concentration chelated with citric acid (CA) at a molar ratio of 1:1. Approximately 7 mL of sodium azide solution (10% w/v) was added to the groundwater in biocide control reactors. Single PHC treatment reactors (Naphthalene) were prepared using Milli-Q® water (instead of groundwater) that was spiked with naphthalene to achieve a concentration of ~5 $mg.L^{-1}$. Enough headspace was left in the reactors to avoid pressure buildup due to the generation of gases. All tests were implemented in triplicates. The reactors were placed on an orbital shaker (300 revolutions per minute) at a temperature of ~20°C in the dark. Temporal 20 mL samples from each reactor were collected until the concentrations of the F2 and F3 were either non-detectable or constant for three consecutive measurements. Based on the available studies of oxidation of the diesel range organics, a two-stage organic compound removal was expected: a fast reduction of the organic compounds (4 to 7 days) followed by a significant decrease in oxidation rate (Yen et al., 2011). As such, samples from each reactor were collected daily for the first week, every 3 days for the next 14 days, and every other week thereafter until concentrations of pseudocomponents were non-detect or plateaued. A total of 13 sampling events was conducted over 56

days.

3.3.5 Soil Treatability Studies in Flow-Through Columns

The objective of these tests was to evaluate the performance of two persulfate systems, unactivated and alkaline-activated, for F2 and F3 mass reduction/removal in the impacted soils. These two persulfate systems were selected based on their performance efficiency and practicality attributes during groundwater treatments studies. A series of soil column experiments were performed by employing a flow interruption method to mimic desirable *in situ* conditions with respect to oxidant-to-solid mass ratio and to provide sufficient reaction time. Two sets of control columns were run in parallel and operated similar to treatment columns, however, in the absence of persulfate solution. The PHC control columns (CTRL) were injected with Milli-Q® during each injection period. These control reactors were implemented to assess F2 and F3 losses without being subjected to oxidation reactions and to determine the contribution of potential aerobic bioactivity in contaminant mass reduction in the soil. As described in groundwater treatment studies, PHCs at elevated pH might undergo hydrolysis reactions; and so, pH control reactors (pH-CTRL) were operated at a pH of ~12 to investigate the effect of hydrolysis in the PHC mass reduction in soil. A 40 $g.L^{-1}$ persulfate concentration solution (yielding 5 $g_{oxidant}.kg^{-1}_{soil}$). The treatment plan included five injection episodes at an oxidant loading rate to determine the extent of NAPL mass removal. This treatment plan is considered a heavy application, as previous studies of ISCO at the field scale report only two persulfate injection episodes (Krembs, 2008). The rationale for selecting this concentration was that in literature, total oxidant loading (g-persulfate per kg bulk media) ranges between 0.3 to 34 $g_{oxidant}.kg^{-1}_{soil}$, with a median of ~5 $g_{oxidant}.kg^{-1}_{soil}$ (Krembs et al., 2010).

3.3.5.1 Soil Column Preparations

Impacted aquifer soil collected from the Site was homogenized and packed in polyvinyl chloride (PVC) columns (Figure 3-2). To avoid handling difficulties, only grain size <2 millimeters (mm) was used. The column length was 10 cm with an inside diameter (ID) of 3.8 cm. Each column was equipped with two filters consisting of glass beads (Potter Industries Ltd.) with a mean diameter of 0.7 mm, a thin layer of glass wool (Pyrex, VWR), and stainless-steel screens (#80 screen mesh) at each end to encourage uniform flow and to retain the soil. The weathered PHC impacted soil was added in ~ 0.5 cm lifts and packed. During packing, representative samples were collected at ~2 cm intervals to determine the initial concentration/mass of the F2 and F3 in soil. The packed columns were weighed and connected to a peristaltic pump (Model Masterflex L/S 12) to maintain a fixed flow rate and positioned to operate in an

up-flow mode to avoid channeling of the influent solution. Initially, all the packed columns were fed Milli-Q® water for water saturation at a flow rate of 0.02 mL.min^{-1} until ~40 mL of water was collected from the effluent. The saturated columns were weighed, and the pore volume (PV) of the columns was estimated. Then three pore volumes of Milli-Q® water were injected, and effluent samples were collected and analyzed for analysis F2 and F3 to establish baseline conditions.

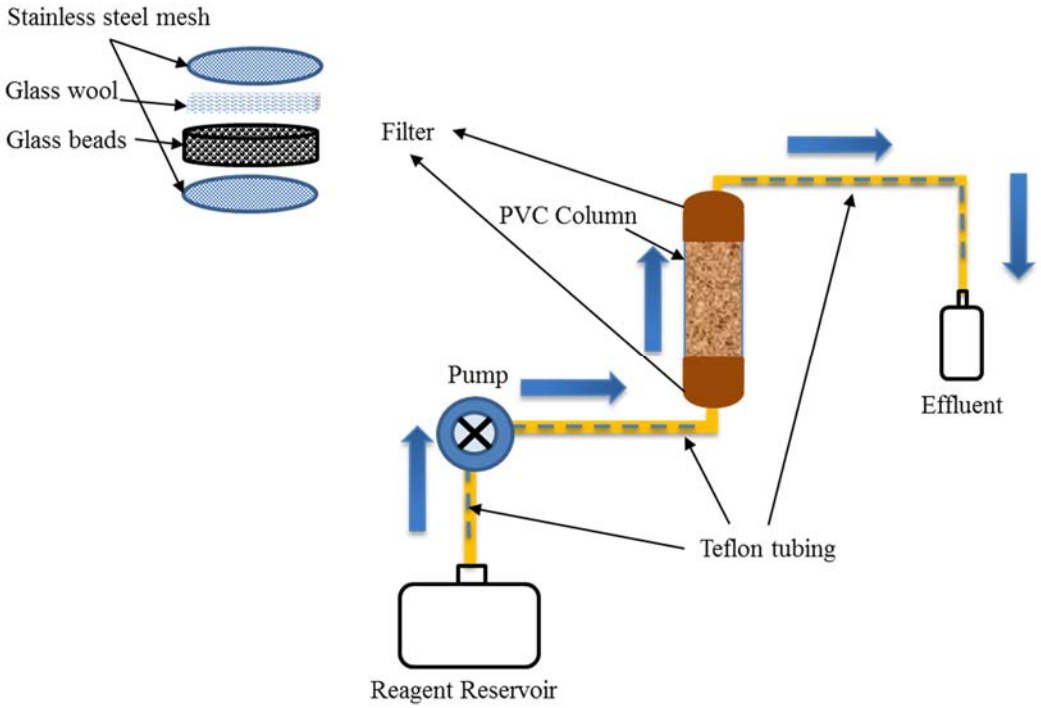

Figure 3-2: Schematic of Column Design

3.3.5.2 Injection Episodes and Samplings

The reagent solutions were prepared and stored in an injection reservoir prior to each injection episode. Each episode consisted of three periods. Period I was identified with the injection (at a constant flow rate of 0.2 mL.min^{-1}) of the reagent solution until consistent electric conductivity, confirming the breakthrough of the persulfate solution, was established downstream. The columns were then clamped at both sides for the reactions to occur. In Period II, which lasted for 5 days, the opportunity for prolonged residence time was provided with the objective of maximizing the mass reduction of LNAPL under no-flow conditions. In Period III, the columns were unclamped and flushed (at a constant flow rate of 0.05 mL.min^{-1}) with 4 PVs of Milli-Q® water in order to remove the residual persulfate and to establish a new baseline for the

subsequent treatment episode. Rebound conditions, if any, prior to each injection episode were established. Throughout the experiment, the flow rate was verified periodically by volume measurements of the column effluent. At the completion of the experiment, columns were disassembled, sliced in half through their length, and sectioned in 2 cm increments (~10 g subsamples), and collected for analysis of F2 and F3 pseudocomponents. All column tests were conducted in triplicate to capture variability.

3.4 Conceptual and Mathematical Models

Despite advances in ISCO technologies, the behavior of a complex system of advection-dispersion-dissolution-reaction during a P-ISCO of a multicomponent LNAPL phase in porous media is still associated with significant uncertainties that could significantly impact performance and effectiveness remedial plans and make modeling intractable unless simplifying assumptions are made. The approach taken here is to adopt a phenomenological description of LNAPL oxidation by persulfate. The LNAPL is not described in terms of the concentrations of individual chemical species in a mixture but in terms of PHC fractions F2 and F3. These pseudocomponents undergo dissolution into the aqueous phase, oxidation by persulfate, and are transported in soil by advection and dispersion. Our conceptual models rely on three key assumptions: (1) oxidation reactions lead to complete mineralization of F2 and F3 compounds to CO_2 and H_2O; (2) inorganic geochemical processes are not significant; (3) persulfate is completely soluble and does not precipitate under the test conditions. In this chapter, a comprehensive numerical model is developed to simulate the coupled processes of multicomponent NAPL dissolution, oxidation reactions, advective–dispersive transport within a saturated system.

3.4.1 Simulation of Batch Tests

The conceptual model includes a well-mixed aqueous phase (groundwater) containing dissolved LNAPL from residual weathered multicomponent sources (Figure 3-3). The aqueous phase also contains oxidant systems. It is assumed that oxidant, F2, and F3 are only available in the dissolved phase in the aqueous phase, and all reactions occur in the aqueous phase. The proposed model is isolated, meaning it assumes the domain is free of an LNAPL source and aquifer solid in order to reduce the complexity of reactions and parameters involved. In the development of the model, the interest was placed on estimating a reasonable set of kinetic parameters for oxidation of dissolved weathered diesel fuel compounds by fitting the model to experimental data.

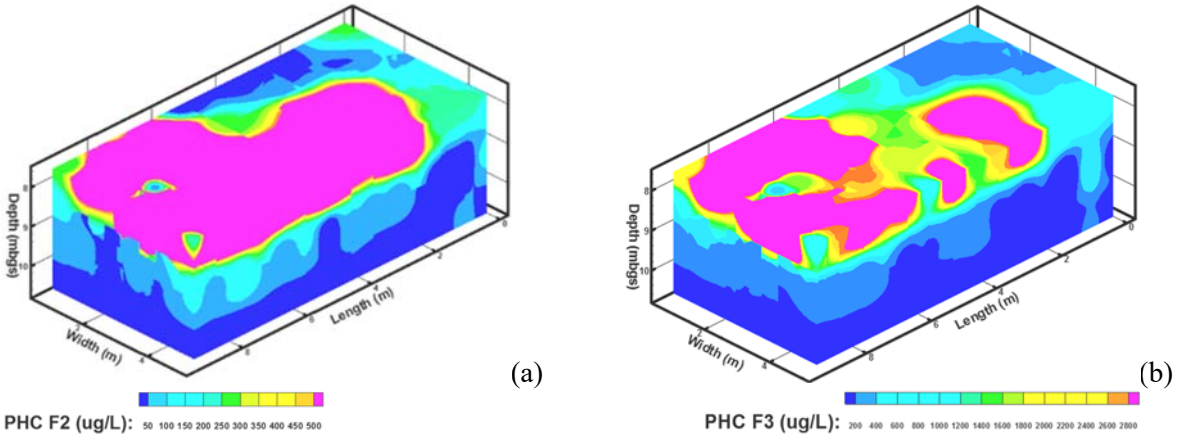

Figure 3-3: Dissolved LNAPL plume within the saturated zone at the Site (a) F2 and (b) F3

The following coupled differential equations were developed from the mass balance of persulfate and pseudocomponents during oxidation reactions:

$$\frac{dC_{ox}}{dt} = -\beta_{F2} k_{F2} C_{F2}^{n_{F2}} C_{0x}^{m_{F2}} - \beta_{F3} k_{F3} C_{F3}^{n_{F3}} C_{ox}^{m_{F3}} \tag{3.1}$$

$$\frac{dC_{F2}}{dt} = -k_{F2} C_{F2}^{n_{F2}} C_{0x}^{m_{F2}} \tag{3.2}$$

$$\frac{dC_{F3}}{dt} = -k_{F3} C_{F3}^{n_{F3}} C_{ox}^{m_{F3}} \tag{3.3}$$

In the above equations, $\beta_{F2}\ and\ \beta_{F3}$ are apparent stoichiometric coefficients for F2 and F3, respectively, whereas $C_{ox}, C_{F2}, and\ C_{F3}$ are the concentrations of persulfate, F2, and F3, respectively. The parameters $k_{F2}\ and\ k_{F3}$ are the reaction rate constants and the parameters $m_{F2},\ m_{F3}, n_{F2}, and\ n_{F3}$ are the exponents in the reaction rate expressions. These rate expressions are entirely empirical in nature and contain no information about the mechanisms of PHC oxidation by persulfate. Their value is limited to their potential to quantify the dependence of reaction rates upon the oxidant and LNAPL compound group concentrations in terms of a set of parameters ($\beta_{F2},\ \beta_{F3},\ k_{F2}, k_{F3}\ , m_{F2},\ m_{F3},\ n_{F2}, and\ n_{F3}$). In this work, the model Equations (3.1)-(3.3) were readily integrated in MATLAB using a low-order implicit method (ode23s). The eight parameters (concentration exponents, stoichiometric coefficients, and reaction rate constants) assumed to describe the oxidation kinetics of diesel fuel components in the aqueous phase were estimated by fitting the solutions to the experimental data obtained from treatability tests in batch reactors.

3.4.2 Simulation of Column Tests

The mathematical model described in this section is intended to represent a smear zone of uniformly distributed, highly-weathered residual multi-component LNAPL (diesel fuel) (Figure 3-4). The model is based on the following assumptions: (1) aqueous phase flow is one-dimensional, (2) LNAPL is immobile, (3) LNAPL dissolution into the aqueous phase and oxidation have a negligible effect on the hydraulic conductivity, (4) LNAPL is described as a mixture of two pseudocomponents, F2 and F3 PHC, (5) oxidation of F2 and F3 PHC follows the kinetics described by Equations (3.4)-(3.6) with the parameter values determined from batch treatability tests, (6) sorption of F2 and F3 PHC on the soil may be neglected (Appendix C).

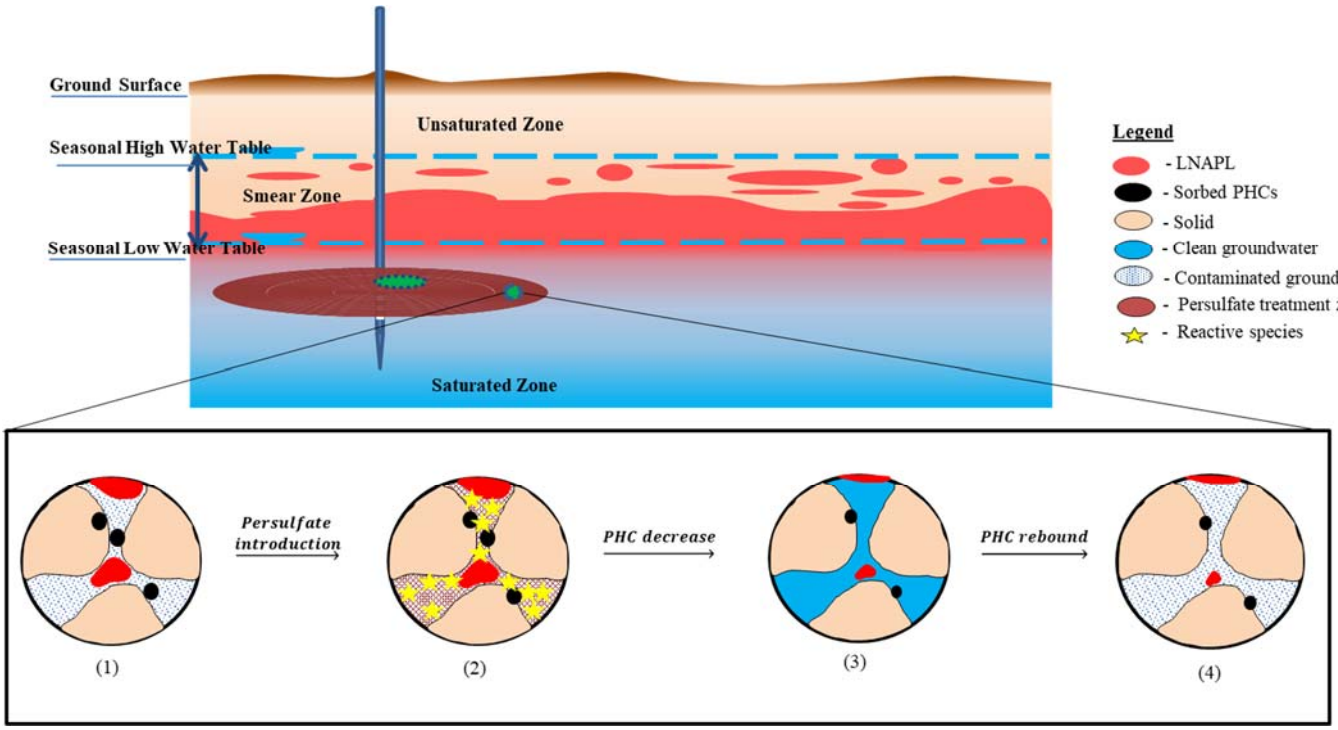

Figure 3-4: An idealized oxidant delivery model where the injected oxidant travels an even radius in all horizontal directions from the point of injection. Then it ideally oxidizes the dissolved PHCs and promotes further dissolution of PHCs from LNAPL.

Assuming a linear relationship between the dissolution rate of LNAPL and the difference between the effective solubility of F2 and F3 PHC pseudocomponents and their concentration in the flowing aqueous phase (e.g., Frind et al., 1999), the following statements of mass conservation may be written for persulfate, F2 PHC, and F3 PHC in the aqueous phase:

$$\frac{\partial C_{ox}}{\partial t} = -v\frac{\partial C_{ox}}{x} + \frac{\partial}{\partial x}\left(D_{ox}\frac{\partial C_{ox}}{\partial x}\right) - k_{NOM}\, C_{ox} - \beta_{F2}\, k_{F2} C_{F2}{}^{n_{F2}} C_{ox}^{m_{F2}} - \beta_{F3}\, k_{F3} C_{F3}{}^{n_{F3}} C_{ox}^{m_{F3}} \quad (3.4)$$

$$\frac{\partial C_{F2}}{\partial t} = -v\frac{\partial C_{F2}}{\partial x} + \frac{\partial}{\partial x}\left(D_{F2}\frac{\partial C_{F2}}{\partial x}\right) + K_L\alpha_{F2}\left(C_{S_{F_2}} - C_{F2}\right) - k_{F2} C_{F2}{}^{n_{F2}} C_{ox}^{m_{F2}} \quad (3.5)$$

$$\frac{\partial C_{F2}}{\partial \mathrm{t}} = -v\frac{\partial C_{F2}}{\partial \mathrm{x}} + \frac{\partial}{\partial \mathrm{x}}\left(\mathrm{D}_{F2}\frac{\partial C_{F2}}{\partial \mathrm{x}}\right) + K_L\alpha_{F3}\left(C_{S_{F_2}} - C_{F2}\right) - \mathrm{k}_{F2} C_{F2}{}^{\mathrm{n}_{F2}} C_{ox}^{m_{F2}} \quad (3.6)$$

where v (cm.day^{-1}) is average linear groundwater velocity, D_{ox}, D_{F2}, and D_{F3} (cm^2.day^{-1}) is the hydrodynamic dispersion coefficients for persulfate and F2 and F3 pseudocomponents, respectively. $C_{S_{F2}}$ and $C_{S_{F3}}$ (g.L^{-1}) are the solubility limit for F2 and F3, respectively. and $K_L\alpha_{F2}$and $K_L\alpha_{F3}$(day^{-1}) are the lumped mass transfer rate coefficients, and k_{NOM} is the rate coefficient describing the loss of persulfate via the first-order reaction with the soil's natural organic matter (Sra, 2010). The following initial and boundary conditions are consistent with the column tests (Table 3-2):

Table 3-2: Initial and Boundary Conditions

Periods	***Initial condition***	***Inlet Boundary condition***	***Outlet Boundary condition***
Injection (I)	$C_{ox}(x,0) = 0$ $C_{F_i}(x,0) = C_{S_{F_i}}$	$C_{ox}(0,t) = C_{ox_{inj}}$ $\frac{\partial C_{F_i}}{\partial x}(0,t) = 0$	$\frac{\partial C_{ox}}{\partial x}(L,t) = 0$ $\frac{\partial C_{F_i}}{\partial x}(L,t) = 0$
No Flow (II)	$C_{ox}(x,0) = C_{ox_{inj}}$ $C_{F_i}(x,0) = 0$	$C_{ox}(0,t) = 0$ $\frac{\partial C_{F_i}}{\partial x}(0,t) = 0$	
Flushing (III)	$C_{ox}(x,0) = 0$ $C_{F_i}(x,0) = 0$	$C_{ox}(0,t) = 0$ $\frac{\partial C_{F_i}}{\partial x}(0,t) = 0$	

The model defined by Equations (3.4)-(3.6) contains the following fixed parameters. Parameters describing the reaction kinetics (β_{F2}, β_{F3}, k_{F2}, k_{F3} , m_{F2}, m_{F3}, $n_{F2}, and\ n_{F3}$) were determined a priori from groundwater treatability tests – their values are listed in Table 3-3. The rate coefficient k_{NOM} was taken equal to 0.1 day^{-1} (Sra, 2010). The hydrodynamic dispersion coefficients of persulfate, F2, and F3 were estimated as follows:

$$D = \frac{\phi D_o}{\tau} + \alpha_L v \quad (3.7)$$

where ϕ = 0.32 is the column porosity, α_L = 0.22 cm is the column longitudinal dispersivity - both determined experimentally - and τ = 1.5 is an estimate of the tortuosity (Domenico & Schwartz, 1990; Perkins & Johnston, 1963) . The modified Sherwood number correlation developed by Powers et al. (1994) was used to determine the F2 and F3 lumped mass transfer rate coefficients during period III of Episode 1:

$$Sh' = 4.13 Re'^{0.06} * \left(\frac{d_{50}}{d_M}\right)^{0.67} * U_i^{0.37} * \left(\frac{\theta_n}{\theta_{n_o}}\right)^{\beta} \tag{3.8}$$

$$\beta = 0.518 + 0.114 * \left(\frac{d_{50}}{d_M}\right) + 0.10 * U_i \tag{3.9}$$

Here $Re'(= v\rho_w d_{50}/\mu_w)$ is defined in terms of interstitial velocity (v), d_M (= 0.05 cm) is representative of medium to coarse sand grain size (as defined by the United States Department of Agriculture), and θ_{n_o} is the initial volumetric fraction of NAPL retained by porous media. Note that knowledge of θ_{n_o} is not required for determining $K_L\alpha$ using Equation (3.8) during Episode 1, since $\theta_n = \theta_{n_o}$ in that case. Note also that the mathematical model does not include conservation statements for free-phase PHC and, for this reason, it does not predict the spatiotemporal evolution of θ_n. Thus, the values of $K_L\alpha$ for subsequent episodes cannot be predicted using Equation (3.8) and are treated as adjustable parameters. This is true also for $K_L\alpha$ during Period II (all Episodes) when $Re' = 0$, and Equation (3.8) does not apply. In this work, the model equations were solved numerically using the method of lines (Schiesser, 1991) in which the parabolic partial differential equations (PDEs) are discretized in space, but the time is left continuous. The numerical model was developed using a finite difference method. The resulting system is a coupled set of ODEs that were solved simultaneously in MATLAB using a low-order implicit method (ode23s). The lumped mass transfer rate coefficients were fitted to the experimental effluent concentration data using a trial-and-error approach.

3.5 Results and Discussion

Kinetic parameters for oxidation reactions of F2 and F3 pseudocomponent were estimated by numerically solving the coupled mass balance equations of groundwater treatment systems. These estimated parameters were then used to estimate the dissolution coefficient rates for Period II and III by numerically simulating the coupled PDE (Equations (3.4)-(3.6)) of the ADDR equations developed for the column tests.

3.5.1 Natural Oxidant Demand Studies

Triplicate data sets were averaged to identify changes in persulfate concentration in the presence of unimpacted aquifer soil. The results indicated that the loss of persulfate during 15 days of the experiment was between 8 to 32-percent. By day 30, the reactors at concentrations of 5 $g.L^{-1}$ lost over 70% of their persulfate to NOD. However, the loss was at 35% at a concentration of 40 $g.L^{-1}$ over the same time period. Persulfate loss at 40 $g.L^{-1}$ was 11% in the first 15 days. The reaction of persulfate with NOM is not negligible for this soil. A K_{NOM} of 0.1 day^{-1} was determined for this study.

3.5.2 Groundwater Treatment Studies

Figure 3-5 shows normalized F2 and F3 concentration, pH profile, and electrical conductivity over the course of the experiment. Each data point is an average of the three replicates. The bars at each data point represent the confidence limits computed at 0.95. A mixed-effects Analysis of Variance (ANOVA) model was used to compare the treatment systems. The two unactivated persulfate treatments did not differ significantly (P = 0.397 for F2 and P = 0.239 for F3) from each other. Analytical data from the CTRL showed a decrease in the concentration of F2 (~60%) and F3 (~50%) pseudocomponent. Since persulfate was not present in these reactors, the degradation of PHC contaminants in groundwater can be attributed to microbial activity. In 40-unactivated reactors, F2 and F3 were reduced by 80- and 67-percent at the end of the experiment. However, multiple comparisons of results of 40-unactivated and control reactors over time showed insignificant differences in reduction of F2 and F3 (P = 0.112 and 0.083, respectively) between these two reactors, confirming that aerobic biodegrading, if applicable, could potentially perform similar to 40-unactivated persulfate treatment. Moreover, the comparison of the results of F2 in pH control and the 40-unactivated system was also statistically insignificant (P = 0.090). This can potentially imply that alkaline hydrolysis of the F2 at high pH is comparable to the performance of persulfate at 40 $g.L^{-1}$ for degradation of F2 mass. However, this observation is in contraction with Sra's (2010) results that reported no evidence of hydrolysis of gasoline range organics (F1 and F2) at pH values of 11 and 13. The F3 analytical results of pH control showed significant fluctuations during the course of the experiment and did not allow to produce a meaningful interpretation of data. The comparisons also revealed that alkaline-activated reactors were superior in both rate and extent of F2 and F3 mass reduction among all reactors. In alkaline-activated reactors, the concentration of F2 and F3 had a drastic decrease (~99%) within the first 3 days. Although PHCs' mass reduction results in the chelated-ferrous activated reactors were comparable to the ones in the alkaline-activated reactors by the end of the experiment, it took 35 days to achieve

statistically insignificant differences in F2 (P = 0.105) and F3 (P = 0.092) concentrations, between these two reactors. With the exception of chelated-ferrous activated reactors, in general, groundwater test results showed a rapid reaction rate followed by a much slower (or plateau) reaction rate for all the treatment systems. In chelated-ferrous activated reactors, F2 and F3 concentrations were gradually declined for the first 35 days (>85%) and then almost plateaued for the subsequent 21 days. Persulfate reduction was the lowest in 80-unactivated among all treatment reactors at 13-percent, followed by 40-unactivated (22%), naphthalene (25%), alkaline-activated reactors (30%), and chelated-ferrous activated reactors (40%), indicating that enough persulfate was still available in all reactors to the end.

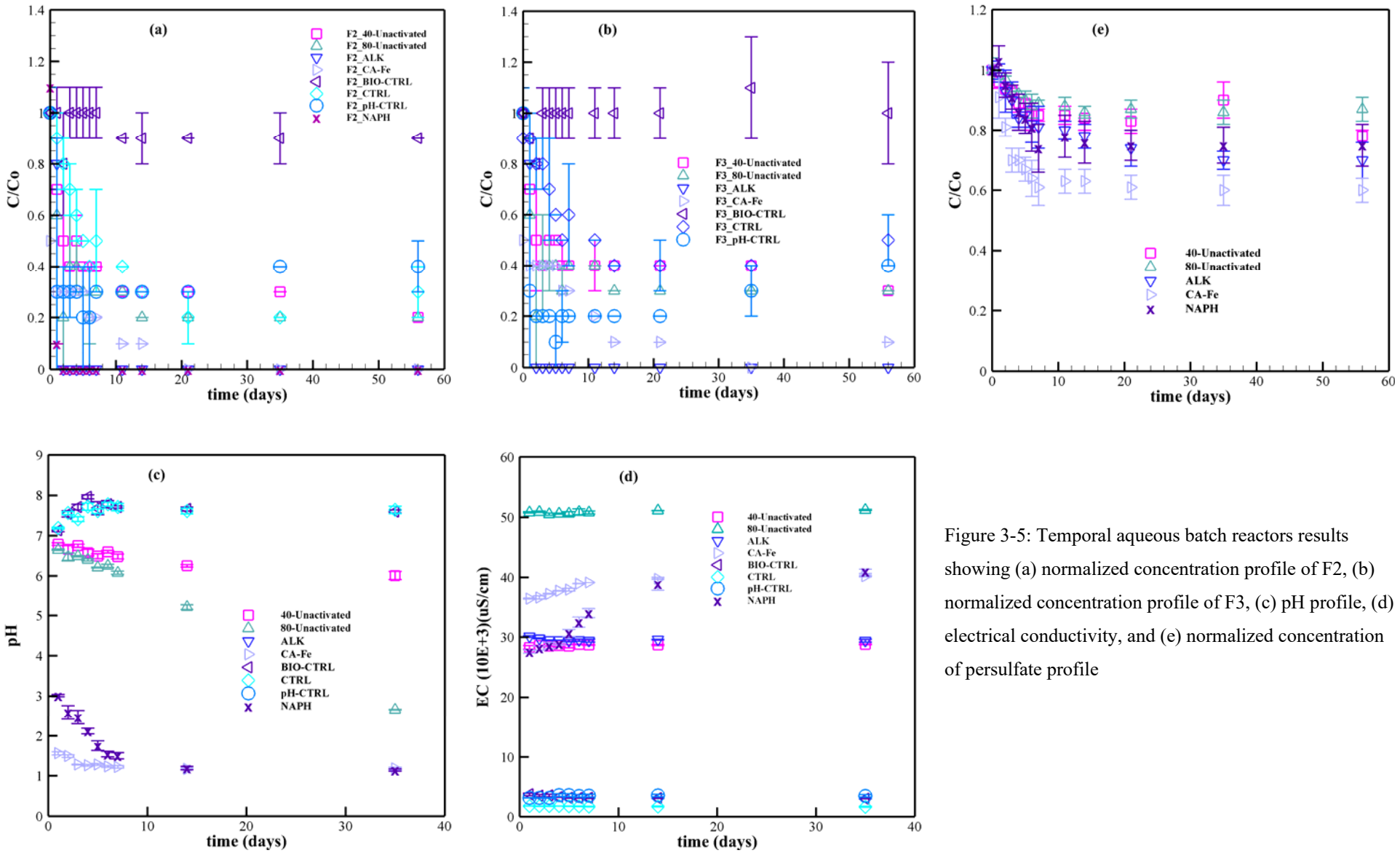

Figure 3-5: Temporal aqueous batch reactors results showing (a) normalized concentration profile of F2, (b) normalized concentration profile of F3, (c) pH profile, (d) electrical conductivity, and (e) normalized concentration of persulfate profile

Groundwater experimental data were numerically simulated to determine the best combination of kinetic parameters for oxidation of F2 and F3. The estimated parameters for treatment systems are presented in Table 3-3. The parameters' temporal changes were assumed negligible. Comparisons between observed data and model-simulated aqueous phase concentrations derived from simulating the numerical model are presented in Figure 3-6 a-d for each pseudocomponent and persulfate. These figures indicate minor differences, especially for the F2 and F3 in alkaline-activated and chelated-ferrous activated systems, between simulated and experimental values, that can be attributed to the complex kinetic pathways and multiple intermediate conformations during the oxidation process before reaching the final compounds.

Table 3-3: Estimated Oxidation Kinetic Parameters for F2 & F3

Fraction	Systems	β	k	n	m
F2	40-unactivated	780	12.5E-2 ($g^{-3.35}$ $L^{3.35}$ day^{-1})	2.3	2.05
	80-unactivated	780	12.5E-2 ($g^{-3.35}$ $L^{3.35}$ day^{-1})	2.3	2.05
	ALK	1200	0.21 ($g^{-2.36}$ $L^{2.36}$ day^{-1})	1.76	1.6
	CA-Fe	4990	4.5 ($g^{-3.29}$ $L^{3.29}$ day^{-1})	2.39	1.9
F3	40-unactivated	1530	9.5E-2 ($g^{-4.26}$ $L^{4.26}$ day^{-1})	2.66	2.6
	80-unactivated	1530	9.5E-2 ($g^{-4.26}$ $L^{4.26}$ day^{-1})	2.66	2.6
	ALK	1500	0.1 ($g^{-3.31}$ $L^{3.31}$ day^{-1})	2.01	2.3
	CA-Fe	5750	6.9 ($g^{-4.67}$ $L^{4.67}$ day^{-1})	2.97	2.7

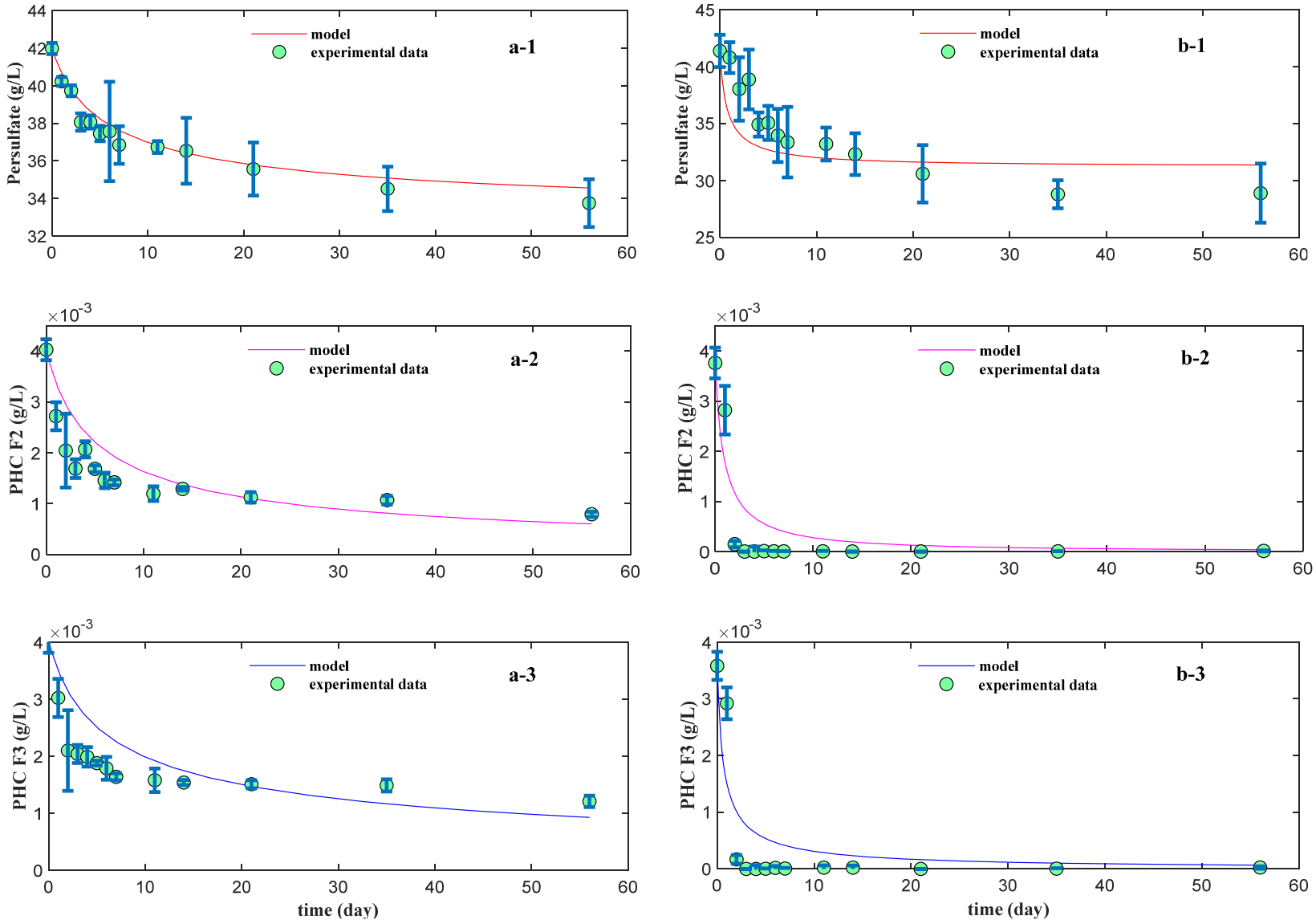

Figure 3-6: Comparison of observed and simulated aqueous phase concentrations of F2, F3, and persulfate of 40 $g.L^{-1}$ in groundwater for (a) unactivated and (b) alkaline-activated systems

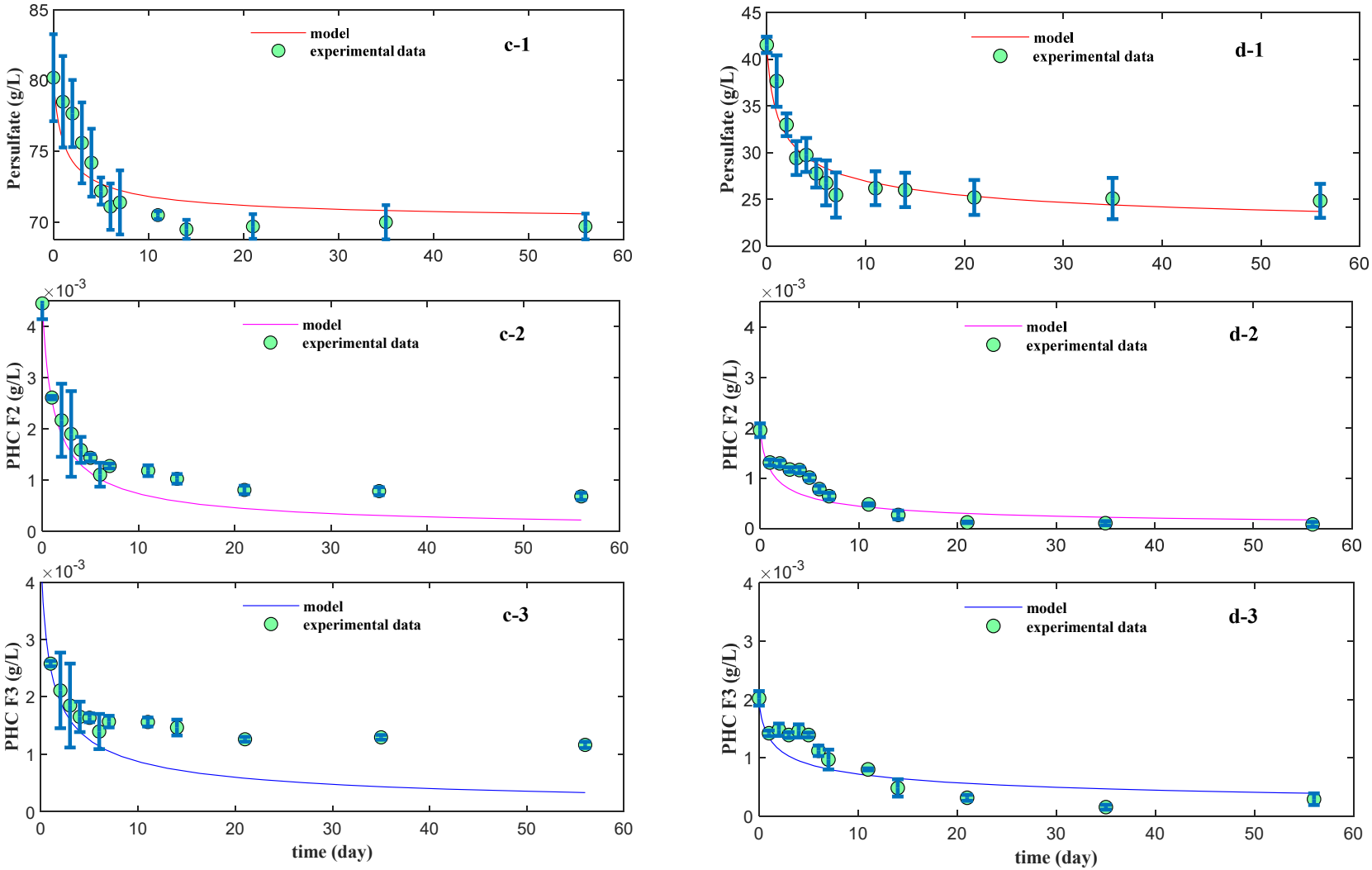

Figure 3-6 (Cont.): Comparison of observed and simulated aqueous phase concentrations of F2, F3, and persulfate in groundwater for (c) 80-unactivated (80 g.L^{-1}) and (d) CA-Fe systems

3.5.3 Soil Treatment Studies

Figure 3-7 a and b illustrate the normalized F2 and F3 effluent concentration data from the first collected pore volume after the reaction period for each column. In general, the concentrations of pseudocomponents in the effluent were significantly reduced compared to their initial values. Since this observation was made both in treatment and control columns, it can be concluded that the initial effluents' values (prior to commerce injections) contained LNAPL bodies (in addition to dissolved PHCs) that were not visible to the naked eyes.

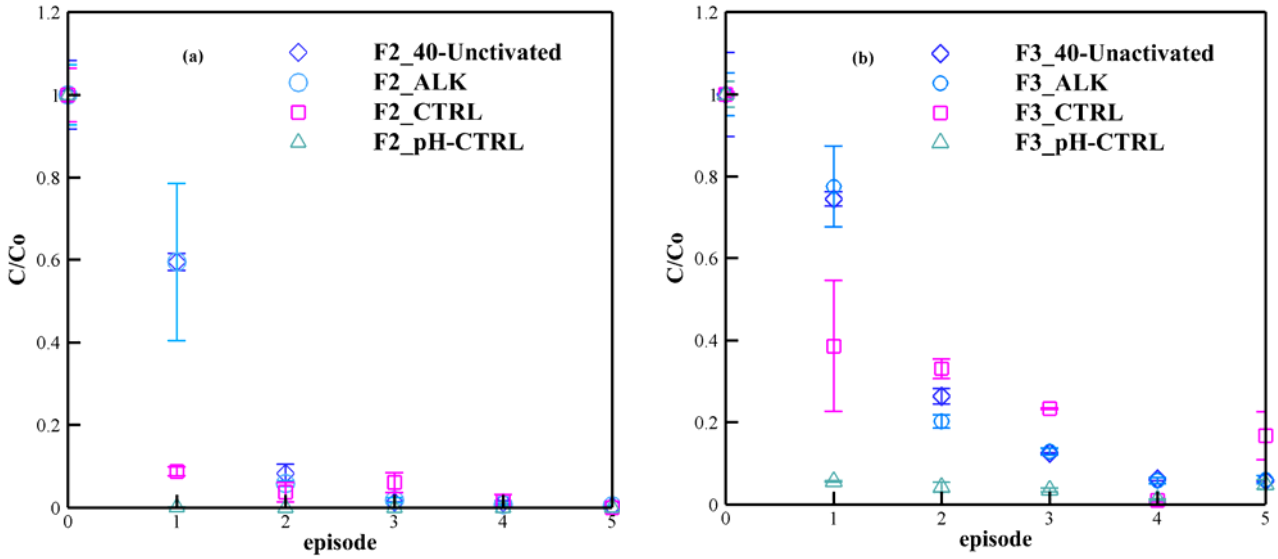

Figure 3-7: Normalized analytical results of the 1st pore volume of effluent during column tests for each injection episode (a) normalized concentration profile of F2, (b) normalized concentration profile of F3

Data from treatment column tests were presented as a plot of average aqueous effluent concentration (from triplicates tests) versus time in Figure 3-8 for column experiments 40-unactivated and alkaline-activated persulfate. The figure also shows the simulated results from simulated models with solid lines. With no exception, persulfate is depleted during Period II (no flow) in the columns as a result of reactions with NOM and PHC. The significant rebound of the PHC concentrations after Episode 1 is evident in the results from both unactivated and alkaline-activated persulfate systems, which is due to diffusion-driven dissolution of LNAPL in columns sealed in preparation for Episode 2. That this rebound is not observed after Episode 3, when a similar opportunity exists for PHC concentrations to build up in the columns, similarly suggests a significant reduction of the remaining LNAPL mass and a concomitant reduction in LNAPL dissolution rate (Miller et al., 1990; Powers et al., 1994). The mathematical model described by Equations (3.4)-(3.6) is seen to provide an adequate description of the effluent concentrations of F2, F3, and persulfate for both alkaline-activated and unactivated persulfate systems.

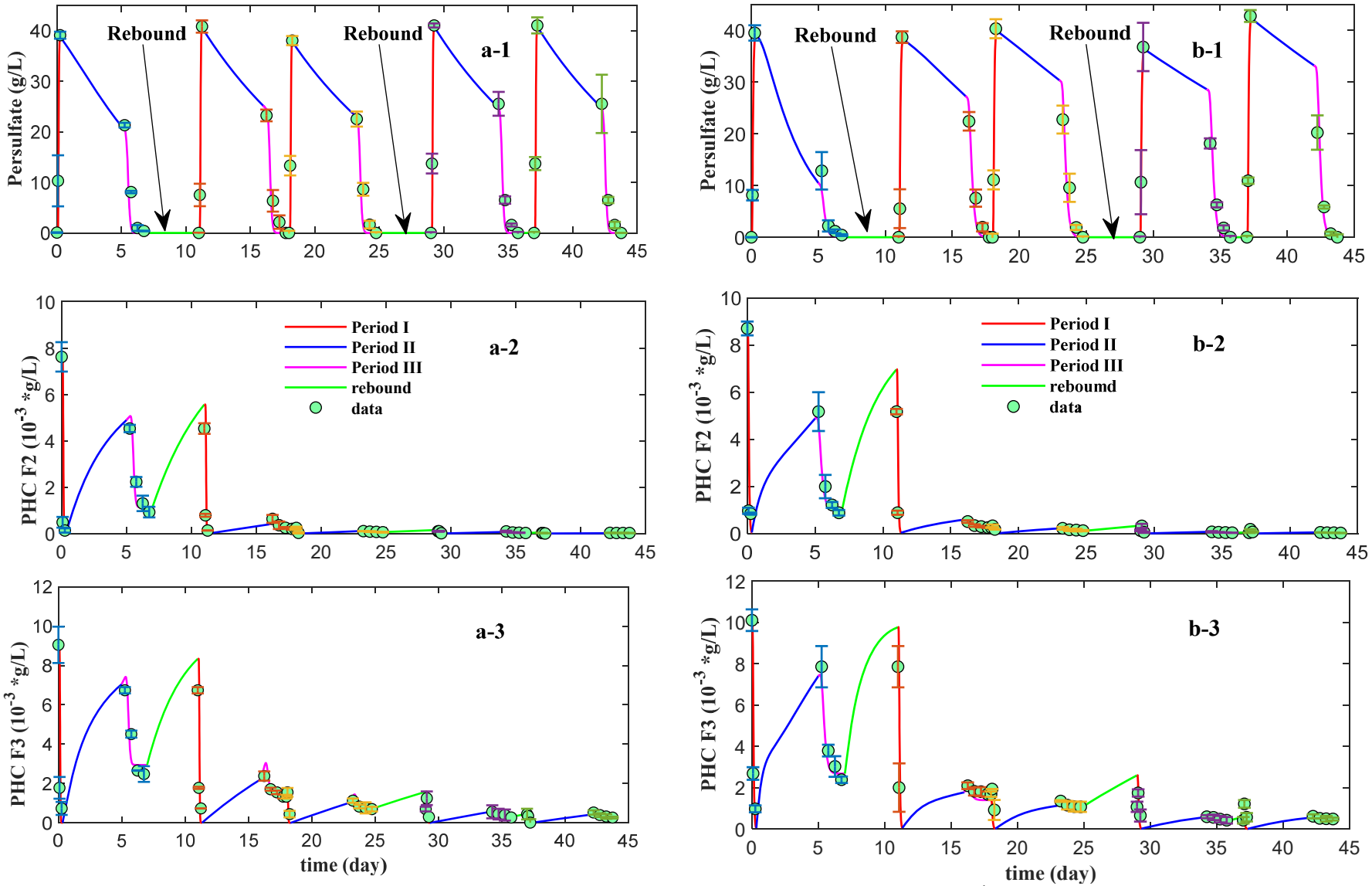

Figure 3-8: Comparison of observed and simulated effluent concentrations of F2, F3, and persulfate (40 $g.L^{-1}$) in groundwater for (a) unactivated and (b) alkaline-activated

An independent check on the consistency of the model is afforded by an overall mass balance on the mass of PHC fractions F2 and F3. The total mass of F2 and F3 removed by advection and oxidation after five Episodes can be predicted from the model by integration over time, and this mass can be compared to the difference between the initial and final mass of F2 and F3 determined experimentally. This comparison, shown in Figure 3-9, reveals substantial agreement between simulation and experiment, even though it was not used as a calibration target. Especially, 78% of F2 and 80% of F3 mass initially present was removed following treatment alkaline-activated persulfate (compared to simulated results of 78% of F2 and F3 mass removal). On the contrary, experimental results show that 52% of F2 and 48% of F3 mass removal with unactivated persulfate (simulation provided 44% of F2 and 32% of F3 mass removal). The model provides an excellent prediction of LNAPL mass removal in the alkaline-activated system, whereas LNAPL mass removal in the unactivated system is somewhat underestimated. Overall, the agreement between simulation and experiment is quite satisfactory, considering the simplicity of the model.

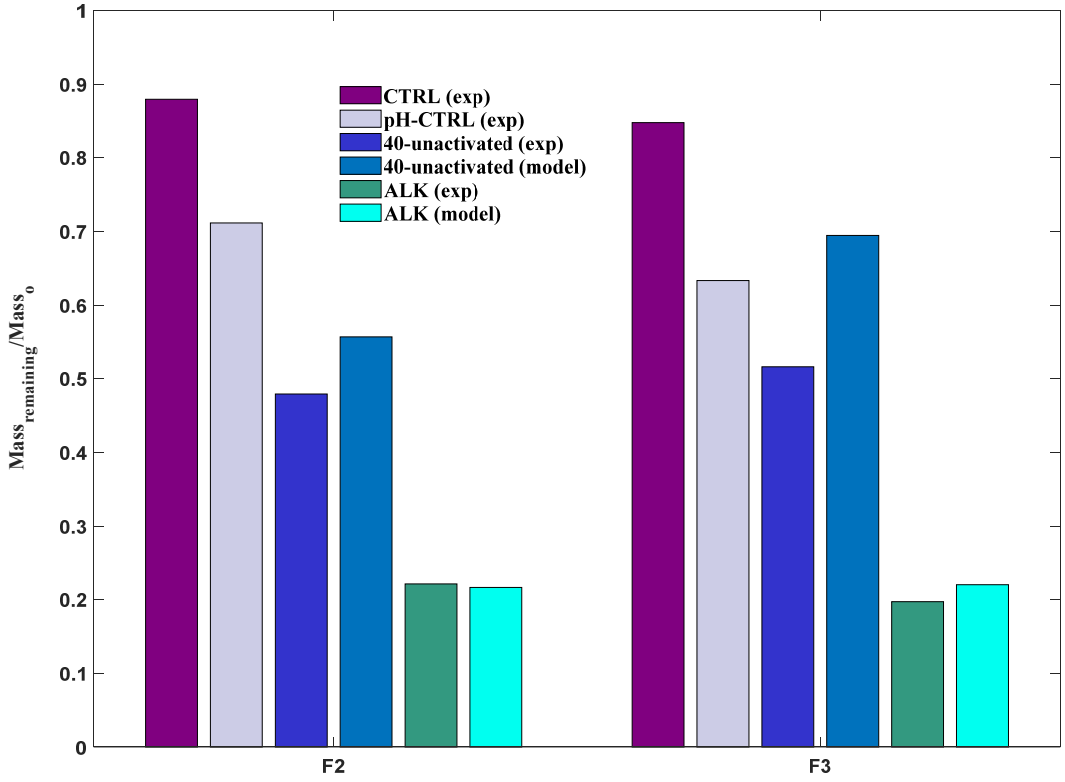

Figure 3-9: Normalized observed versus simulated PHC F2 and F3 mass remaining in soil columns

Analytical results of control columns show that 12% of F2 and 29% of F3 original mass was reduced from the soil, while in pH control columns, mass reduction of F2 and F3 was 15% and 37%, respectively. In both control and pH control columns, the LNAPL mass reduction occurs due to dissolution, advection, and potentially some other processes that have not been defined in Equations (3-4)-(3-6). The higher reduction in the pH control system compared to the control system can be the result of LNAPL

compounds hydrolysis reactions at the elevated pH (Sra, 2010). Attempts were made to fit both control and pH control systems' experimental data to the theoretical expressions; however, the results do not appear to fit the facts very satisfactorily. In the case of the control system, the simulation captured the effluent profile of both pseudocomponents well. However, the model grossly underestimated the LNAPL mass loss at the end of the experiment. Since these columns were injected with Milli-Q water, aerobic bioactivity may be the cause of the LNAPL mass reduction in control columns and observed differences between experimental and simulated data. This model was found to be unsuitable for fitting the pH control system's data due to the irregular fluctuation of effluent concentrations.

Further insight into LNAPL mass removal is provided in Figure 3-10, which shows that the amount of mass removed by oxidation was substantial during Episode 1 but negligible during subsequent episodes. PHC cannot be degraded by persulfate at a rate greater than the rate it becomes available in the aqueous phase by dissolution. In turn, the dissolution rates of PHC fractions F2 and F3 are determined by their effective solubility in the aqueous phase and the corresponding lumped mass transfer rate coefficient. Recall that the effective solubilities $C_{S_{F2}}$ and $C_{S_{F3}}$ are assumed constant (see Table 3-1) and that the mass transfer rate coefficients ($K_L\alpha$) are treated as adjustable parameters in the simulation, with the exception of $K_L\alpha$ during Period III of Episode 1. As shown in Figure 3-11, the $K_L\alpha$ values which suffice to describe the effluent concentrations (see Figure 3-8) and cumulative LNAPL mass removal (see Figure 3-10) decrease monotonically to very small values from Episode 1 to Episode 5. This trend is observed in both alkaline-activated and unactivated persulfate systems and is certainly consistent with a reduction of LNAPL saturation (see Equation (3.8)). Estimates of the LNAPL saturation (Brost & DeVaull, 2000) prior to persulfate injection, after Episode 1, and after all Episodes, summarized in Table 3-4, support this interpretation. Nevertheless, it must be noted that the $K_L\alpha$ values reported in Figure 3-11are estimated using a model that assumes $C_{S_{F2}}$ and $C_{S_{F3}}$ are constant over time. Changes in the composition of F2 and F3 over time may reasonably be expected to result in the reduction of the effective solubility of PHC fractions F2 and F3 over time, which would also be reflected in the model as lower $K_L\alpha$ values. As shown in Table 3-4, LNAPL saturations after Episode 1 and Episode 3 are not greatly different, but significant PHC rebound is observed only after Episode 1 (see Figure 3-8). This observation is consistent with the reduction of $C_{S_{F2}}$and $C_{S_{F3}}$ are constant over time. Figure 3-11 also shows that higher $K_L\alpha$ values are realized during treatment with alkaline-activated persulfate. A possible explanation for this observation is increased solubility of PHC resulting from the presence of surfactants. It is well known that organic acids (e.g., carboxylic acid) are potential intermediate products of the oxidation of diesel fuel (Langbehn & Steinhart, 1994; Lu, 1994). When exposed to aqueous solutions of high pH, organic acids can form

natural surfactants that improve the solubilization of F2 and F3 constituents (deZabala & Radke, 1986; Hauswirth et al., 2012).

Table 3-4: Residual LNAPL Saturation in the Soil Columns

LNAPL	***Initial (measured)***		***after Episode 1 (simulated)***		***Final (measured)***	
	Unactivated	*Alkaline activated*	*Unactivated*	*Alkaline activated*	*Unactivated*	*Alkaline activated*
F2	0.4%	1.1%	0.2%	0.3%	0.2%	0.3%
F3	0.9%	2.7%	0.6%	1.1%	0.4%	0.6%
Total	1.2%	3.9%	0.8%	1.4%	0.6%	0.8%

Generally, $K_L\alpha$ values are expected to increase with velocity. However, in alkaline-activated columns, for both F2 and F3, $K_L\alpha$ values in Period II (no flow/reaction period) of Episode 1 (Figure 3-11b) were greater than the $K_L\alpha$ values of Period III (flushing period) for the same episode. It is suggested that two mechanisms are contributing to this inconsistency. First, as mentioned above, when alkali contacts organic acids in the LNAPL, potentially water-soluble and surface-active products can be formed (deZabala & Radke, 1986), which would increase the LNAPL dissolution. Second, it has been observed that at lower LNAPL saturations (<4%), shorter column retention times outweighed increasing mass transfer rate as velocity increased (Miller et al., 1990).

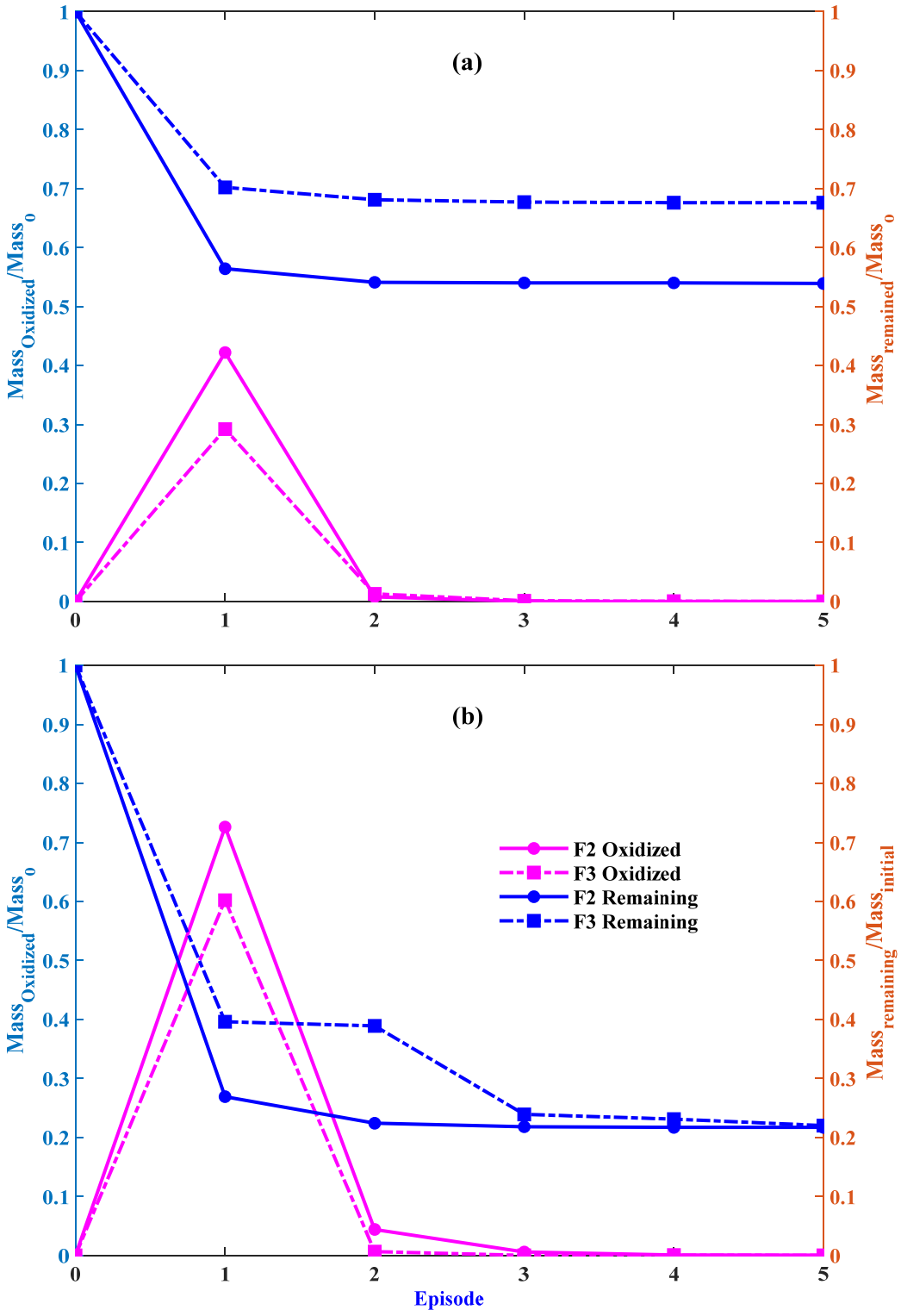

Figure 3-10: Simulated normalized LNAPL mass change in the soil during each episode of at persulfate concentration of 40 $g.L^{-1}$ (a) unactivated and (b) alkaline-activated

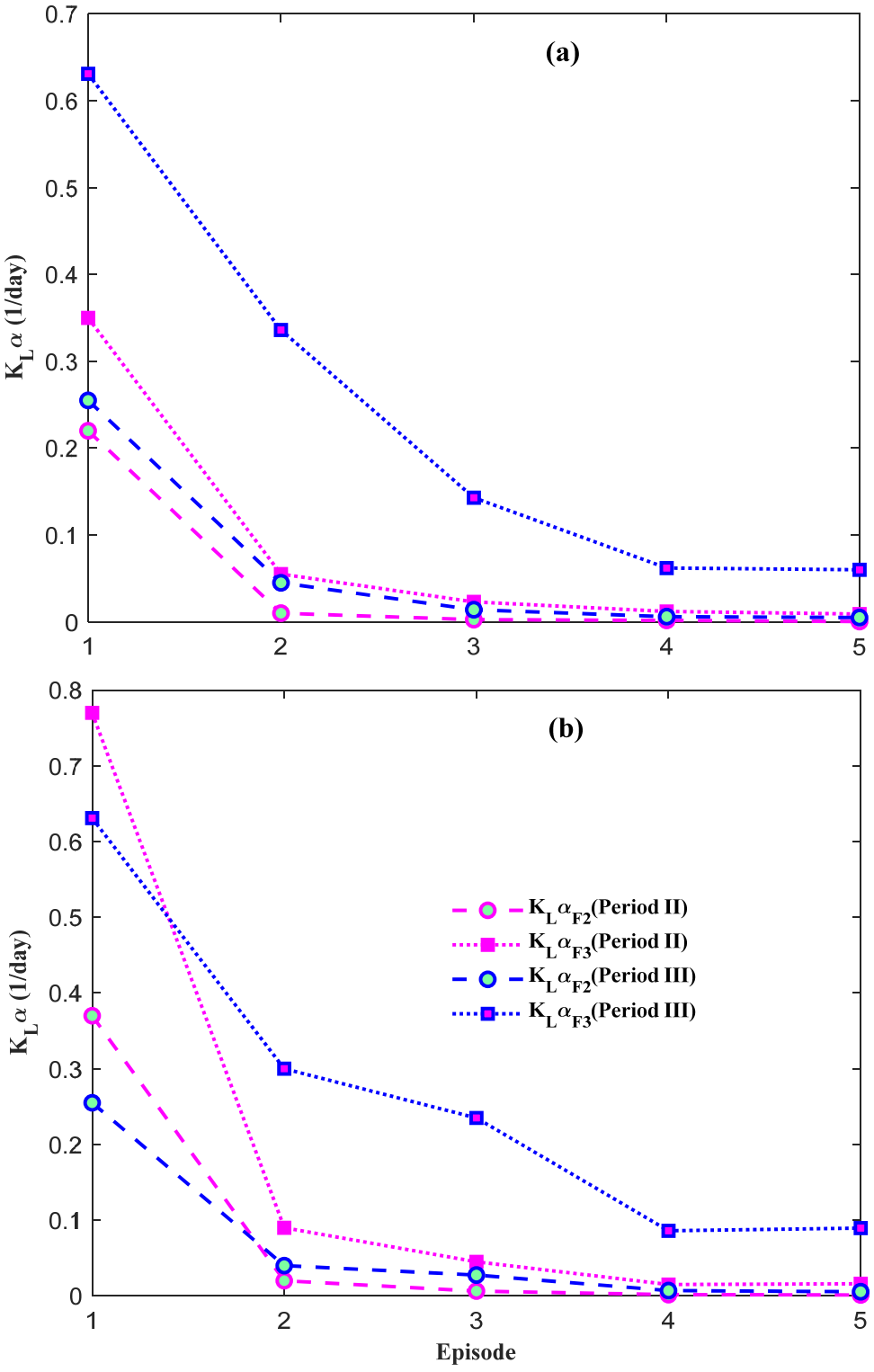

Figure 3-11: Simulated dissolution rate coefficient during Period II (no flow) and Period III (flushing) each episode of treatment with (a) unactivated and (b) alkaline-activated persulfate.

3.6 Conclusion

A simplified continuum model of *in situ* chemical oxidation (ISCO) of weathered PHC liquid contaminants by persulfate is developed and validated against experimental data from a real site contaminated by a heavily weathered diesel fuel. Treatment of impacted groundwater with alkaline-activated (pH ~ 12) and unactivated persulfate in batch reactors was used to calibrate a phenomenological model of the oxidation of main PHC fractions. Treatment of PHC-impacted soil was studied in soil columns using a flow interruption method and multiple injections of alkaline-activated and unactivated persulfate. An LNAPL mass reduction of ~50% and 80% was achieved in the unactivated and alkaline-activated systems, respectively. The continuum model, which accounts for non-equilibrium dissolution, advective–dispersive transport, and oxidation reactions of persulfate with main PHC fraction (treated as pseudo-components) and natural organic matter, adequately describes both LNAPL mass removal and effluent concentration data. Together, experiments and simulations show that LNAPL mass reduction is limited by dissolution and that repeated injection of persulfate becomes ineffective. The mathematical model integrates site-specific experimental data to link quantitative LNAPL mass removal to soil and contaminant properties, thereby enabling the rational design of oxidant injection strategies at field scales without having to represent the hundreds of individual PHC components of the contamination.

Chapter 4:
Pilot-Scale Remediation Design and Implementation

4.1 Overview

A site-specific action plan was developed to scale up the bench scale research to a pilot scale for a demonstration study, where research data and findings in the laboratory were tested and evaluated under field conditions. A pilot area was selected at a historical site (Site) with weathered diesel fuel contaminated aquifer with the presence of residual source in soil and dissolved phase in groundwater (Figure 4-1). A comprehensive monitoring infrastructure was installed. In this unique pilot-scale experiment, the selected area was divided into three zones of treatment, control, and a buffer area in between them. The unactivated persulfate system or municipal water was introduced into the subsurface of the treatment zone at locations/depths of high petroleum hydrocarbons (PHCs) impacts identified with laser-induced fluorescence (LIF) equipped with an ultra-violet optical screening tool (UVOST™) (Ling & Chen, 2014) to maximize the opportunity of persulfate to degrade the dissolved F2 and F3 pseudocomponents. No injection activity was conducted at the buffer zone. The dissolved PHCs mass flux was monitored downstream of the pilot area across a transverse fence-line at 60 multilevel sampling points pre-and post-injection episodes. The specific goals of this field effort were to (1) evaluate the efficiency of the persulfate system in decreasing or eliminating the LNAPL mass flux; (2) Compare contaminants' mass changes post – ISCO with numerical simulations in Chapter 3. The design and implementation of this field experiment are defined here with a partial discussion of the long-term monitoring results; incomplete access to long-term monitoring data has limited the depth of this investigation.

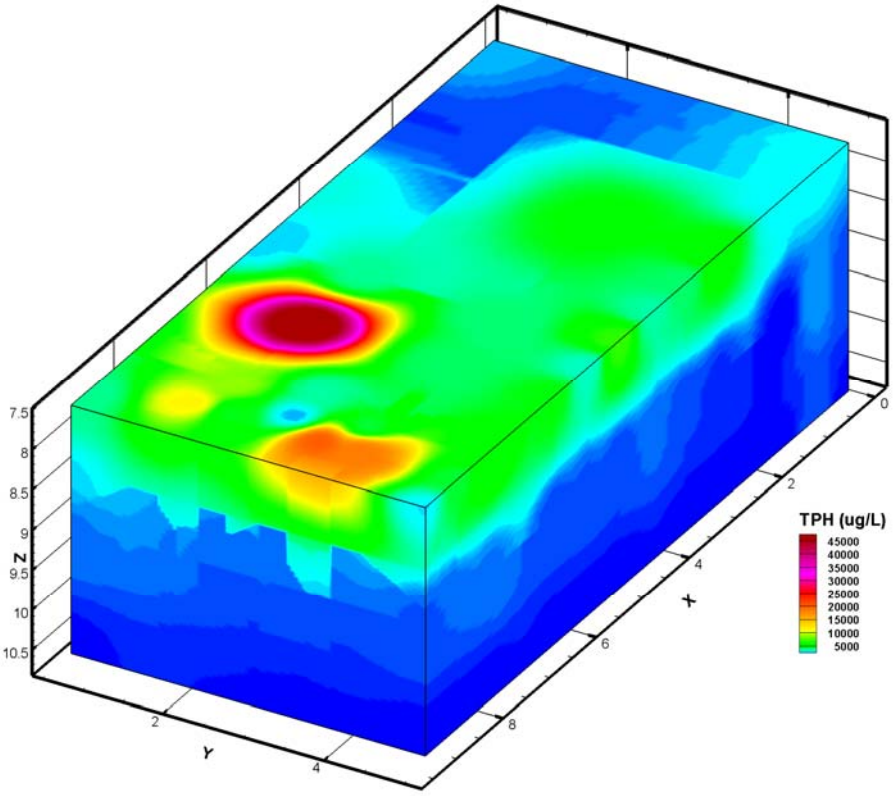

Figure 4-1: Dissolved phase total petroleum hydrocarbon (TPH) within the smear zone at the pilot scale area

4.2 Site Characterization and Field Investigations

Optimal design and implementation of an ISCO remedy rely heavily on knowledge of site history, current conditions, and monitoring of changes in the subsurface as remedial action progresses. A Site-wide observational investigation and soil sampling were implemented to obtain a detailed understanding of Site lithology, nature and extent of contamination, and transport of contamination.

4.2.1 Site Background and History

The Site has a long and complex industrial history (since the early 1900s) with activities that are inferred to have high-risk environmental impact related to storing and handling of petroleum hydrocarbons in either aboveground storage tanks (ASTs) and underground storage tanks (USTs) at various locations at the Site (Figure 4-2). As such, LNAPL releases have occurred from the USTs and ASTs over a long period. A laboratory forensic evaluation of the impacted soil, groundwater, and separate phase floating petroleum hydrocarbons (at some monitoring locations) inferred the presence of weathered diesel fuel,

predominantly F2 and F3. The persistent dissolved PHC concentrations in the groundwater following source removal (e.g., USTs and ASTs) indicated the presence of a residual mass within a smear zone located in the vicinity of the water table at approximate depths of 6 to 9 meters below ground surface (m bgs). The Site was vacant and not in use at the time of pilot-scale studies.

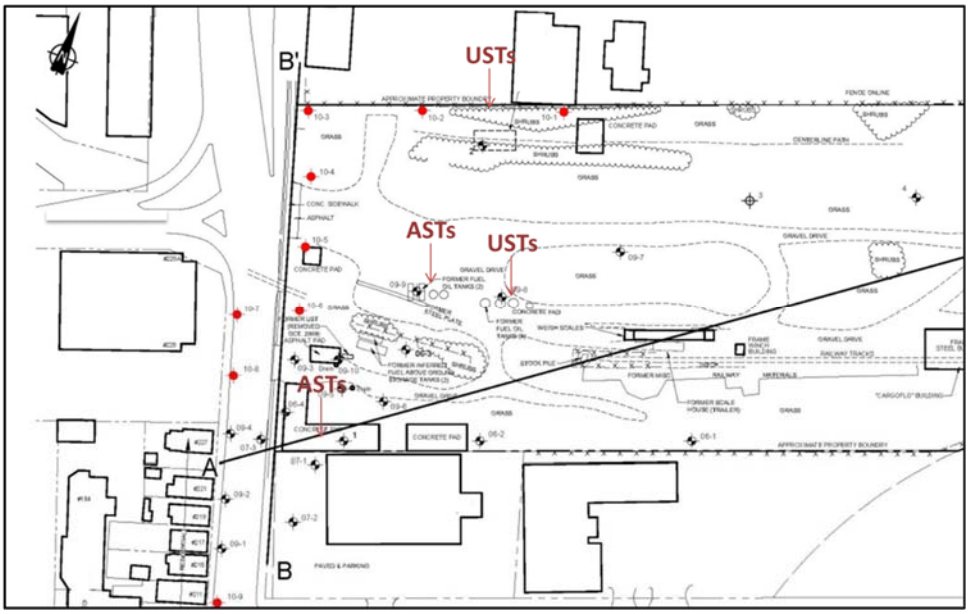

Figure 4-2: Site layout and location of aboveground storage tanks (ASTs) and underground storage tanks (USTs)

4.2.2 Site Geology and Hydrogeology

The surficial geology consists of gravel and sand deposits and deltaic silty sand deposits. Subsurface soil at the Site predominately consists of granular (sandy) fill to depths of about 0.2 to 1.5 m bgs. Fill material was underlain by fine to medium textured native permeable sand interspersed with lenses and layers of silty sands and silts and clay (low permeability) to the maximum investigated depths of 12 m bgs. The groundwater flow direction is in an (overall) southwesterly direction. This flow direction is not entirely consistent with groundwater flow direction at different locations at the Site due to preferential pathways associated with the local aquifer heterogeneities. Hydraulic conductivity had been estimated, utilizing pumping tests, to be in the range of 1.2 to 1.5 x 10^{-5} meters per second ($m.s^{-1}$), and assuming a porosity of 0.35, an average linear groundwater velocity of 2.0 meters per year ($m.yr^{-1}$) was estimated. The depth to the water table was measured at ~6.7 to 8.6 m bgs (Golder, 2009).

4.2.3 LNAPL Delineation Studies

The objective of this investigative effort was to delineate the vertical and horizontal extent of LNAPL impact by soil screening and sampling, to collect and analyze groundwater from the existing monitoring infrastructure at the Site, and to establish a research pilot area. The University of Waterloo's (UW's) geoprobe rig (Geoprobe 7720 DT) was used with the macrocore direct push sampling technology. Drive point (DPT) boreholes were established to the required depths, and soil cores were collected. During these investigative studies, a total of 25 DPT boreholes were established to a maximum depth of ~9.1 m bgs and identified at DPT-1 to DTP-25 throughout the Site, as shown in Figure 4-3. Each borehole was advanced to ~0.6 m above the water table, and then an ~1.5 m long soil core was collected. Each soil core was opened on Site, screened using a photoionization detector (PID), and then inspected for olfactory and visual evidence of source material impacts. Sub-samples were selected from each borehole for potential hydraulic or chemical analyses. Sub-samples for chemical analyses were quickly transferred into wide-mouth sampling jars (500 mL), labeled, and stored in a cooler. At the end of each day, the cooler was transported to the UW laboratory, where the contents were stored at 4 ºC. After each borehole was completed, the boring was backfilled to grade with bentonite chips (Baroid, Holeplug).

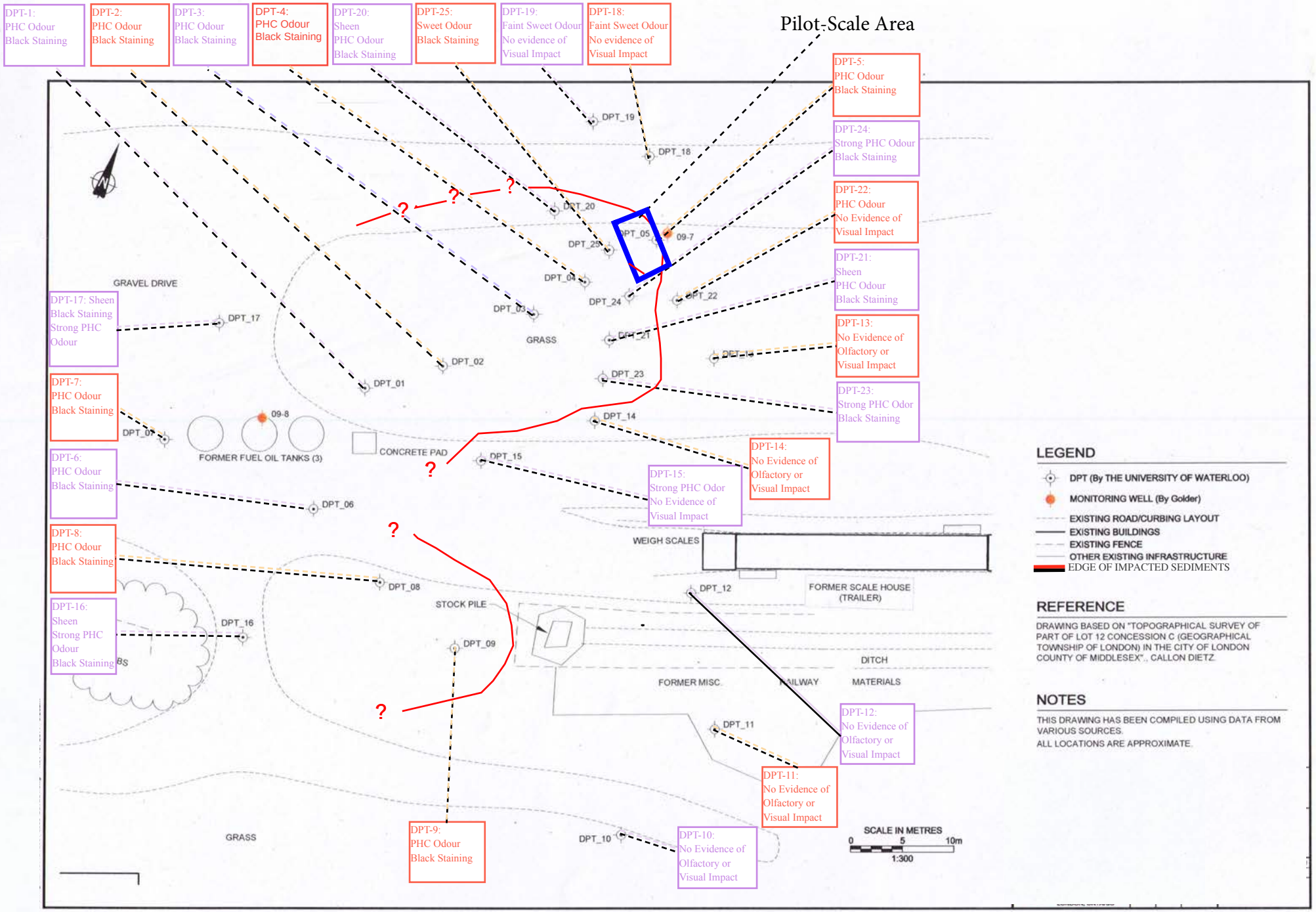

Figure 4-3: Subsurface investigation and observations at DPT locations

Table 4-1: Sediment Description and Visual Observations

Borehole ID	***Borehole Depth (m)***	***Sample Depth Range (m)***	***Description***	***Olfactory Observations***	***Impact Depth (m)***
DPT-1	9.1	0-1.5	Fill material, vegetation, dark brown topsoil and sand, moist	-	-
DPT-1	9.1	1.5-3.0	Dark brown and light brown sand, moist	-	-
DPT-1	9.1	3.0-4.6	Greyish brown sand, trace gravel, moist	-	3.5-5.5
DPT-1	9.1	4.6-6.1	Dark brown sand, trace gravel, moist to wet	PHC like odour	-
DPT-1	9.1	6.1-7.6	Dark brown sand, trace gravel, wet	PHC like odour	7.1-7.6
DPT-1	9.1	7.6-9.1	Black sand, trace gravel, wet	PHC like odour	-
DPT-2	7.6	6.1-7.6	Dark brown sand, trace gravel, wet	PHC like odour	7.2-7.6
DPT-3	7.6	6.1-7.6	Dark brown/black and grey silty sand, trace gravel, wet	PHC like odour	7.1-7.6
DPT-4	7.6	6.1-7.6	Blackish grey sand, trace gravel, moist to wet	PHC like odour	6.2-7.1
DPT-5	7.6	6.1-7.6	Brown and blackish-grey sand, trace gravel and silt, damp	PHC like odour	7.1-7.6
DPT-6	7.6	6.1-7.6	Blackish grey sand, trace gravel, moist to wet	PHC like odour	7.3-7.6
DPT-7	7.6	6.1-7.6	Blackish grey sand, trace gravel, moist to wet	PHC like odour	6.4-6.6 7.5-7.6
DPT-8	7.6	6.1-7.6	Brown sand, trace gravel, moist to wet	PHC like odour	7.3-7.6
DPT-9	7.6	6.1-7.6	Greyish brown sand, trace gravel, moist to wet	PHC like odour	7.6
DPT-10	7.6	6.1-7.6	Greyish brown sand, trace gravel, moist to wet, evidence of oxidation	-	-
DPT-11	9.1	7.6-9.1	Brown sand, trace gravel, moist	-	-
DPT-12	9.1	7.6-9.1	Greyish brown sand, trace gravel, damp to moist	-	-
DPT-13	9.1	7.6-9.1	Brown sand, trace gravel, moist	-	-
DPT-14	9.1	7.6-9.1	Greyish brown sand, trace gravel, moist	-	-
DPT-15	8.2	6.7-8.2	Greyish brown sand, trace gravel, moist	PHC like odour	-
DPT-16	8.2	6.7-8.2	Grey sand, trace gravel, sheen, moist	PHC like odour	7.9-8.2
DPT-17	8.2	6.7-8.2	Grey sand, trace gravel, sheen, moist	PHC like odour	7.7-8.2
DPT-18	8.2	6.7-8.2	Greyish brown sand, trace gravel, moist	Sweet odour	-
DPT-19	8.8	7.3-8.8	Greyish brown sand, trace silt, and gravel, moist	Sweet odour	-
DPT-20	8.8	7.3-8.8	Grey sand, trace gravel, sheen, moist	PHC like odour	8.5-8.8
DPT-21	8.5	7.0-8.5	Brown sand, trace gravel, sheen, moist	PHC like odour	7.6-7.9
DPT-22	8.5	7.0-8.5	Greyish brown sand, trace gravel, moist	PHC like odour	-
DPT-23	8.5	7.0-8.5	Grey sand, trace gravel, moist	PHC like odour	7.3-7.6
DPT-24	8.5	7.0-8.5	Grey sand, trace gravel, moist	PHC like odour	7.6-7.9
DPT-25	8.5	7.0-8.5	Greyish brown sand, trace gravel, moist	Sweet odour	7.6-8.1

Notes:
- *No impact was observed*

4.2.4 Pilot-Scale Area Selection

Based on the field investigations, a pilot-scale area (PSA) of the investigation was selected for further detailed investigation and treatment based on the relative degree of soil impacts observed. The selected area was a 5 x 10 m rectangular area immediately down-gradient of MW 09-7. For the purpose of persulfate based *in situ* chemical oxidation studies, this area was divided into three zones (Figure 4-4):

- Control zone (CZ) (4.5 x 5 x 2 m) was used as the experiment control. During the injection episodes, municipal water (instead of the persulfate solution) was injected into the subsurface throughout this zone;
- Target treatment zone (TTZ) (4.5 x 5 x 2 m) where the persulfate solution was injected for the purpose of PHCs mass destruction; and
- Buffer zone (BZ) (1x 5 x 2 m) was the zone in between the TTZ and CZ. No injections were conducted in this zone. This sub-area was used to mitigate cross-over of persulfate solution to the CZ.

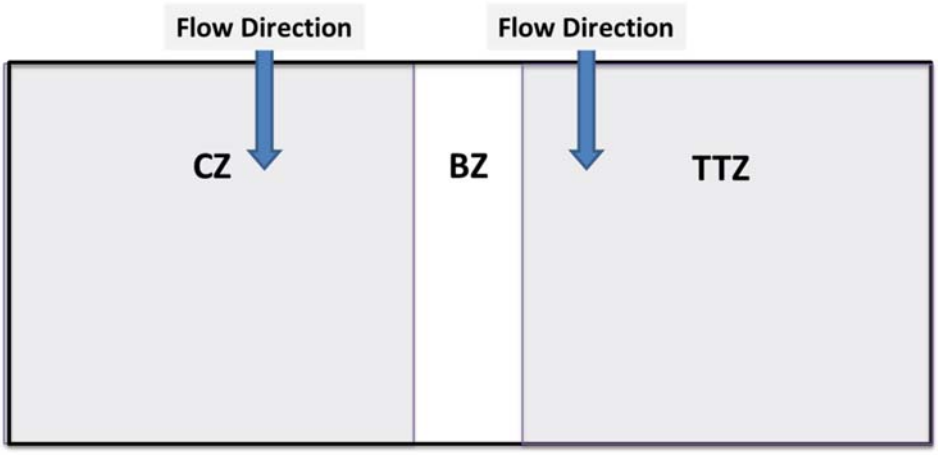

Figure 4-4: Schematic view of the pilot scale area

4.2.5 Laser-Induced Fluorescence Survey

Laser-induced fluorescence (LIF) activities using an ultra-violet optical screening tool (UVOST™) module (Ling & Chen, 2014) were performed to verify the PSA observations from the DPT effort and to delineate the spatial distribution of subsurface impacts further. To adequately delineate the PSA, a combination of adaptive sampling approach (subsequent LIF borehole location was determined based on

the data from preceding boreholes) and grid sampling technique was utilized to select LIF probe borehole locations. The area was gridded into 1 x 1 m segments. LIF-UVOST^{TM} technology uses a pulse laser coupled with an optical probe to determine the presence and quantitate the amount of LNAPL present in the subsurface. The UV light is directed through a sapphire window and absorbed by the LNAPL (present in the subsurface soils), causing them to excite fluorescence. The emitted signal response reaching the same sapphire window is collected and conveyed to a detection system at the surface through optical fibers. The emission data of fluorescence intensity and are normalized to a standard reference emitter. The LIF-UVOST^{TM} results log shows the fluorescence intensity signals (FIS) at the depth they are detected. For more information on LIF UVOST^{TM} technology, please refer to Appendix B. The LIF borehole locations were selected to provide spatial representation across PSA. A total of 18 LIF boreholes were advanced. The LIF boreholes were advanced to depths of ~12 m bgs through the smear zone. In addition, soil cores at the depths corresponding to elevated LIF-UVOST^{TM} responses were collected. The soil core samples were sub-sampled for analysis of F2 and F3 PHCs. LIF borehole locations were plugged and abandoned with granulated bentonite chips (Baroid, Holeplug) by filling the borehole from total depth to grade.

4.3 Monitoring Infrastructure Installations

Monitoring infrastructure was installed at the pilot-scale area to supplement the existing monitoring well network and provide the additional horizontal and vertical definition of the groundwater quality conditions. A total of 22 multilevels wells and one conventional monitoring well (MWUW 01) were installed within the pilot-scale area, as shown in Figure 4-5 and Figure 4-6. Each multilevel monitoring well within the pilot area consisted of 6 monitoring points to collect depth-discrete groundwater samples at 6.1, 6.9, 7.6, 8.4, 9.1, and 10.7 m bgs (Figure 4-7 a). The multilevel wells were constructed of five 0.95 cm outer diameter (O.D.) polyethylene tubes surrounding a 0.64 cm polyvinyl chloride (PVC) Schedule 80 center stock that was advanced to a depth of 10.7 m bgs. Six of the multilevel monitoring wells (ML-13 to ML-18) were used to calculate the radius of influence and injection pressure (Appendix F). In addition, two conventional monitoring wells and a 60-point monitoring fence-line were installed at the downgradient periphery of the pilot area. The fence line included a multilevel well transect consisting of 12 multilevel monitoring wells with 5 sampling points (Figure 4-7 b). The vertical sampling points are spaced 1.5 m from 4.6 to 10.7 m bgs. The material used for the downgradient fence line wells was similar to the multilevel monitoring wells described above. The tubes were grouped together using binding tape.

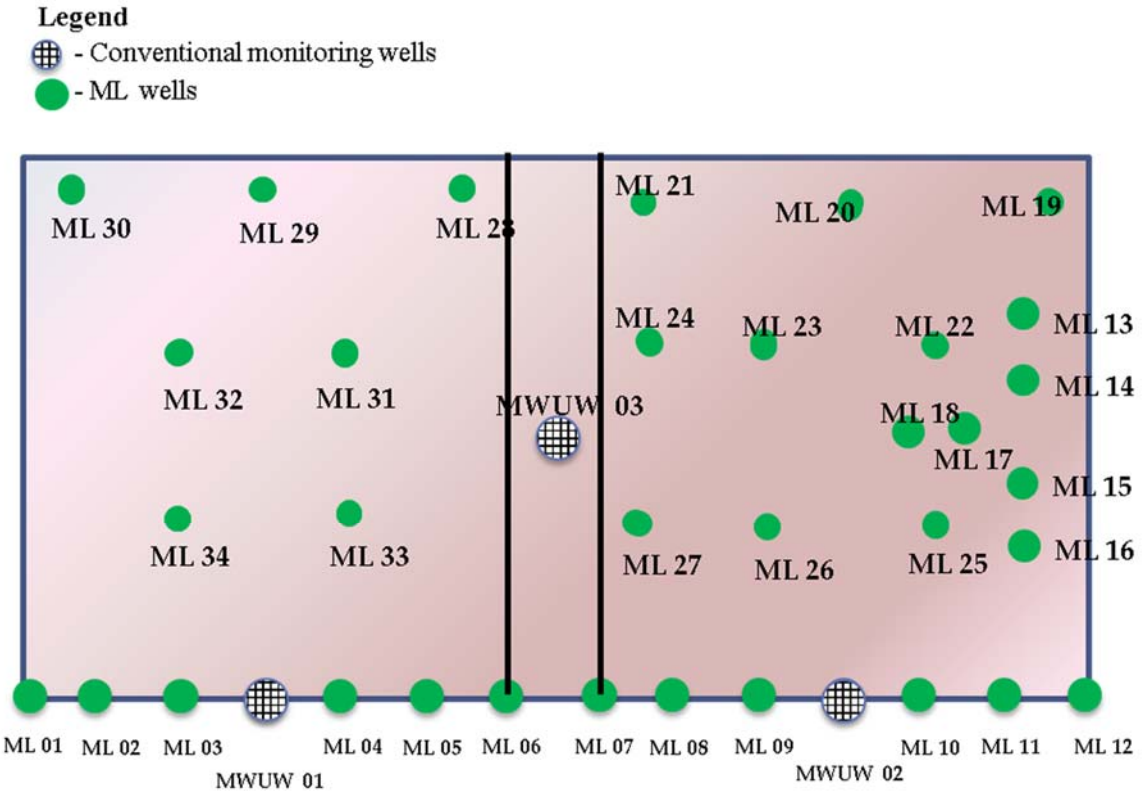

Figure 4-5: Multilevel and conventional monitoring well infrastructure at the Pilot Scale Area

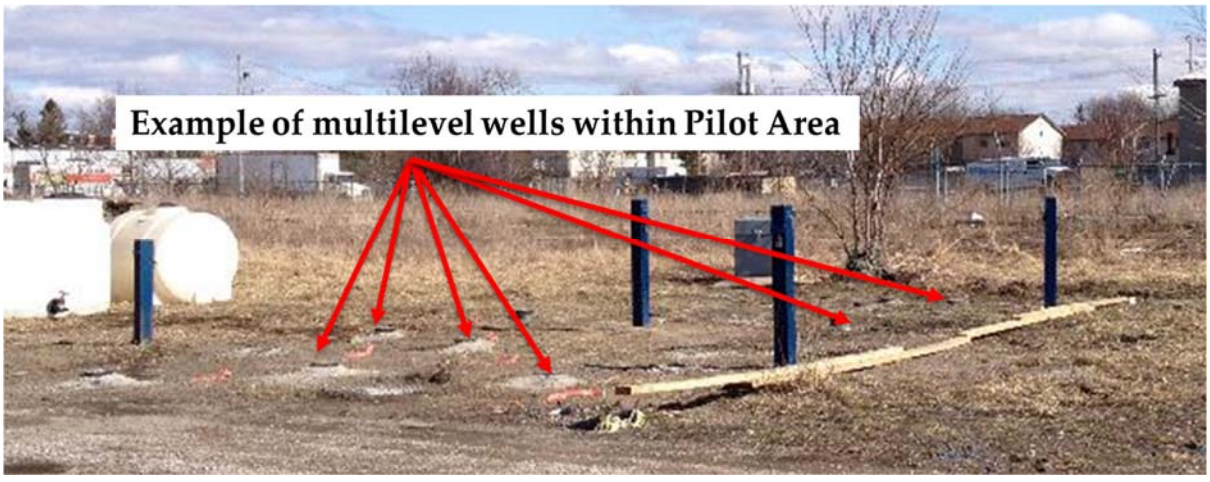

(a)

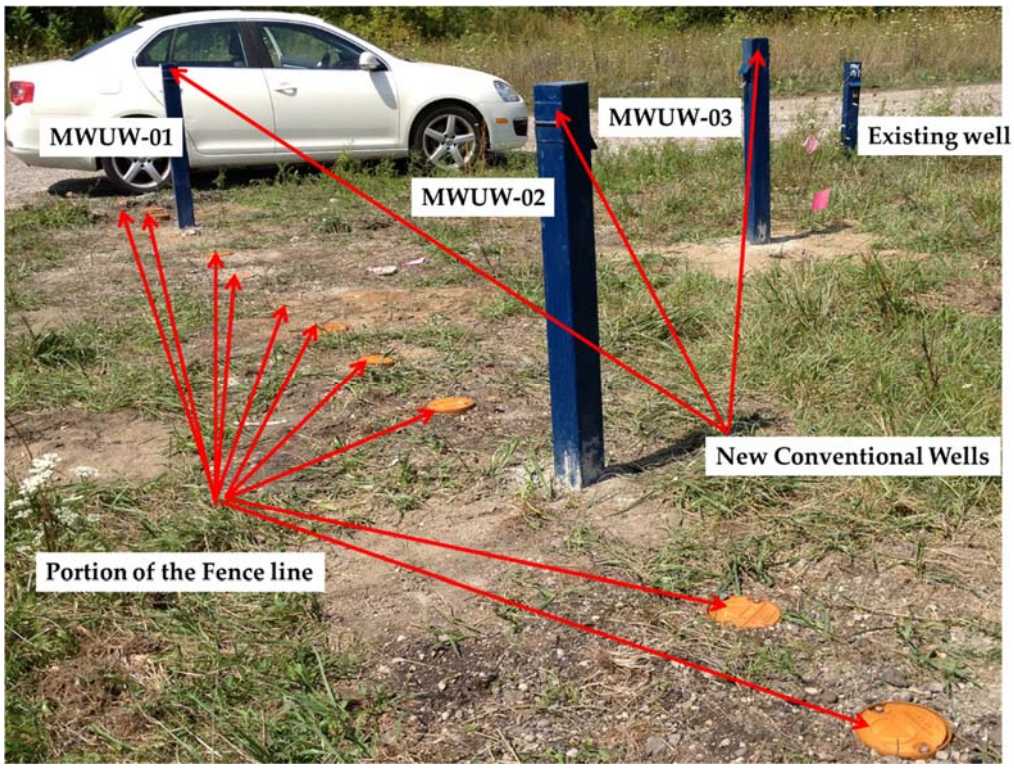

(b)

Figure 4-6: Pictures showing the groundwater monitoring infrastructure (a) multilevel wells within the pilot area and (b) downgradient fence line and newly installed conventional monitoring wells

The bottom 20 cm of each tube was perforated and covered with a 200-micron nylon screen. A dedicated Teflon tube of 0.5 cm O.D. x 0.08 cm wall thickness was inserted in each tube for sampling purposes. Silica sand was placed from the bottom of each multilevel to ~5 cm above the upper sampling port. Bentonite chips (Baroid, Holeplug) were placed above the silica sand and extended to the ground surface. The risers were sealed using duct tape. Protective steel flush-mount casings were installed over the riser tubes and concreted in place. The conventional monitoring wells were constructed using a 3.8 cm diameter Schedule 40 PVC casing with pre-pack 20-slot PVC well screens.

The conventional monitoring wells were advanced to depths of ~8 m bgs and were screened over ~3 m to the depth of completion of 11m bgs. Silica sand was placed around and above each screened interval to establish a filter pack around the well screen. A layer of bentonite chips (Baroid, Holeplug) was placed above the silica sand and was extended to the ground surface. The risers were sealed at the surface with

lockable J-Plug caps. Protective steel stick-up casings were installed over the riser pipes and concreted in place.

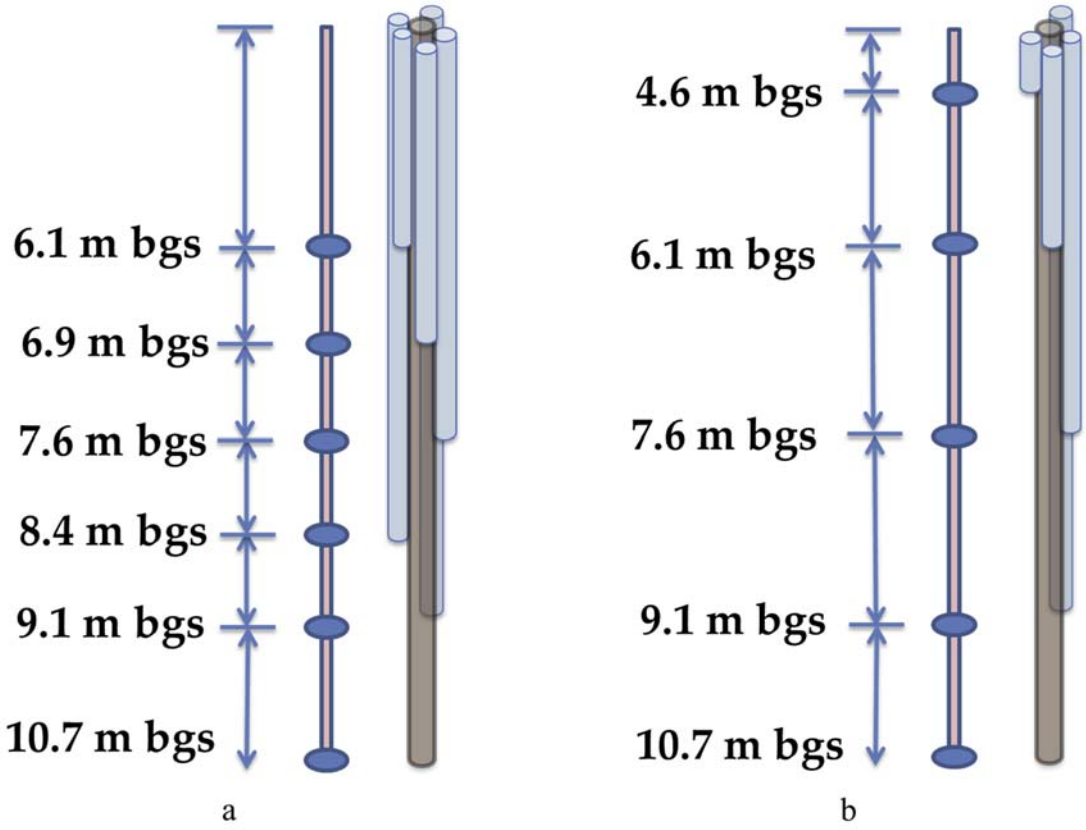

Figure 4-7: Schematic diagram of multilevel wells (a) within the pilot area and (b) in the downgradient periphery of the pilot area

4.4 Monitoring and Remedial Efforts

The monitoring and remedial activities such as well developments, baseline and monitoring well samplings, and *in situ* chemical oxidation using unactivated persulfate were designed and implemented over a 2-year timeframe. The ISCO program was designed based on two injection episodes comparable to the median number of persulfate delivery events for LNAPL contaminated sites (Krembs, 2008). Injection wells are typically used for delivering persulfate into the subsurface. This method allows the use of higher-pressure values for injection compared to drive point boreholes but at the same time limits the location and depth of persulfate introduction. The most common underlying reason for sub-optimal performance and substantial additional cost for ISCO projects appears to be the failure to achieve

adequate distribution and contact between the oxidant and contaminants. Coupling of LIF UVOST™ technology with drive point boreholes for injection can potentially minimize the oxidant solution waste and optimizes the contact of persulfate and contaminants. In this study, a targeted persulfate delivery was utilized using the direct push method to provide the flexibility for injection of persulfate at points of impact to potentially provide adequate time and optimal mixing to facilitate the degradation of contaminants. The median of persulfate concentration injected at the sites is 160 $g.L^{-1}$. Apart from the high cost and considerable impact on the existing geochemical and biological conditions in an aquifer, the persulfate solution at this elevated concentration has a much higher density than the ambient groundwater and sinks down (quicker than a solution of 40 $g.L^{-1}$ persulfate concentration) from the depths that LNAPL presence. The density of the persulfate solution at a concentration of 40 $g.L^{-1}$ is 1027 $kg.m^{-3}$ and is slightly higher than the average ambient groundwater density of 993 $kg.m^{-3}$ at the Site.

4.4.1 Monitoring Well Development

The well development activities were conducted after the installation of the monitoring infrastructure. Development activities at the multilevel sampling wells consisted of purging each well (using three units of the Geopump™ Peristaltic Pump Series II with easy-load II®) until the discharge water was clear and void of soil (~1 L of groundwater was evacuated from each individual sampling point).

4.4.2 Baseline Groundwater Sampling

Prior to each oxidant delivery episode, groundwater samples were collected from the monitoring wells to establish a baseline. Groundwater samples were collected from all monitoring locations were analyzed for F2 and F3, and measurement of field parameters including dissolved oxygen concentration, ORP, EC, temperature, and pH. During these events, groundwater samples (including three field duplicates) were collected from the monitoring locations (34 multilevel monitoring wells and three conventional monitoring wells). No free product was encountered during the groundwater sampling activities. Groundwater samples were collected from each well utilizing a low flow (0.2 $L.min^{-1}$ or less) purge sampling technique via the Geopump™ peristaltic pumps. Samples were collected in 40 mL clear glass septum vial containers containing 10% sodium azide. Conventional monitoring wells were purged three times the standing groundwater volume within the monitoring wells, using Waterra™ tubing and foot valves, or until consistent pH and conductivity readings were achieved. The groundwater samples were placed in coolers, maintained at ~4°C for transport to the UW laboratory under proper chain of custody. Sampling equipment was cleaned before each use by washing with an Alconox-water solution and

double-rinsing with potable water. Development, purge, and equipment rinse water was collected and stored in 55-gallon drums on Site for proper disposal.

4.4.3 Injection Activities

The supporting data from the bench-scale effort was used to select an appropriate persulfate solution and oxidant dosage for the design of the pilot-scale activities. The 40-unactivated persulfate solution was injected at the Site during both injection episodes. Each delivery event (injection episode) was appropriately designed based on the lessons learned from the literature and preceding injection episode. The reader is referred to Appendix F for further details. The persulfate solution injection activities involved the delivery of persulfate solution to the target treatment depths within the target treatment zone (TTZ) and a "clean" water solution using the municipality water to the target treatment depths within the CZ (Figure 4-8). Temporary direct-push boreholes utilizing the UW's Geoprobe were used for solution delivery. A total of 18 temporary boreholes were advanced to ~8 m bgs at the TTZ and CZ within the pilot-scale area. In the event of anomalous behavior (e.g., short-circuiting/daylighting) at the planned injection rate/location/depth, the injection was temporarily suspended and resumed after 15 minutes. If the difficulties with the injection persisted, the injection parameters (i.e., rate, volume, pressure) or injection location were field adjusted, or the injection at the depth was stopped. Sodium persulfate (FMC Klozur) was mixed with municipality water in a 500 L mixing polyethylene tank to yield a persulfate concentration of 40 $g.L^{-1}$. The mixing process was completed as many times as necessary per day to provide the required volume of reagent solution. A direct-push 0.3-meter stainless steel wire wound screened rod (attached to a solid drive tip) was advanced to the target depth, and a prescribed volume of persulfate solution was injected at that interval. The screened rod was then pushed downward to the subsequent injection depth. This process was repeated until injection was completed at each injection borehole. Six of the proposed multilevel wells were used to monitor the spatial distribution of the reagent solution during each injection episode. Based on the data collected from these monitoring locations, the injection design parameters were modified accordingly. The injection pressure was adjusted at some injection locations to maintain a flow rate of ~8 $L.min^{-1}$ for Episode 1; however, some difficulties encountered during this delivery event (e.g., daylighting) resulted in not fully injecting the required volume at some injection depths. Therefore, the flow rate was increased to 15 $L.min^{-1}$ for Episode 2. The target quantity volume for each injection depth was ~200 L. During injection activities, ~5,200 L of persulfate solution were injected at 11 temporary boreholes and 26 depths (based on identified evidence of impact) within the TTZ from ~5 to 8 m bgs. The injection procedure at the CZ was similar to the

procedure described at the TTZ, except that uncontaminated municipal water instead of the persulfate solution along with an appropriate amount of sodium chloride to achieve a solution density similar to persulfate solution were injected. At the CZ, ~5000 L of the solution was injected at 25 depths in 7 temporary boreholes. The injection locations are presented in Figure 4-8. The temporary injection boreholes were backfilled to grade with bentonite chips (Baroid, Holeplug). Waste generated during the activities, including equipment wash, rinse water, and soil cuttings, were contained in approved 55-gallon steel drums and staged on Site until proper off-Site disposal was arranged.

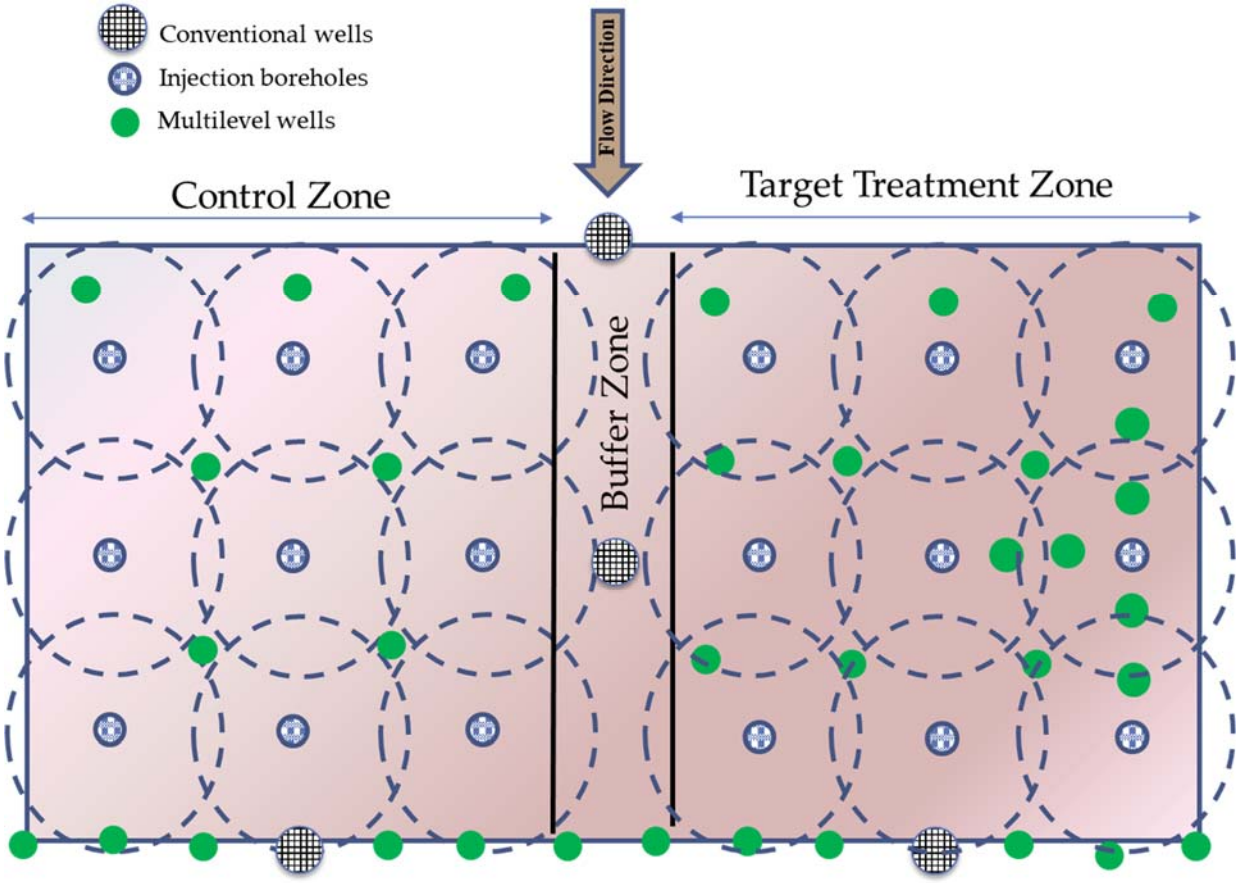

Figure 4-8: A schematic diagram illustrating monitoring well installation and the locations of temporary boreholes used for persulfate injections along with the idealized radius of influence

4.5 Analytical Results and Discussion

4.5.1 Groundwater Sampling

The collected groundwater samples during pre-and post-injection each episode were analyzed for F2 and F3 PHCs. The pre-injection field screenings and laboratory analytical data were used as a baseline against which the post-injection data were compared. Analytical results for groundwater samples are provided in Appendix H, and the interpolated F2 and F3 dissolved plume profiles are shown in Figure 4-9 and Figure 4-10, respectively.

Post-injection monitoring of water quality parameters and field screening analyses were completed to evaluate the distribution and persistence of the persulfate and the resulting changes in aquifer geochemistry. The post-injection results of groundwater EC data and persulfate concentration profile are presented in Figure 4-11 and Figure 4-12, respectively. The results show that persulfate was detected at the selected monitoring locations ~ 3 weeks after the injection activities. The samples collected from the CZ did not show the presence of persulfate, indicating that persulfate did not migrate into the CZ within the 3-week period. The pH values pre-, during, and post-injection activities remained in the neutral range. EC values increased by a factor of ~10, from ~1,000 to 10,000 microsiemens per centimeter ($\mu S.cm^{-1}$) during injection Episode 1, and increased by a factor of ~5, from ~2000 to 10,000 $\mu S.cm^{-1}$, during injection Episode 2. In general, the pilot test data indicate that the aqueous mass of F2 and F3 decreased following each injection episode; however, both the TTZ and CZ showed a similar decrease. Considering the lack of persulfate presence during 3-week monitoring in the post-injection samples collected from the CZ, oxidation of F2 and F3 in the CZ area with persulfate seems unlikely. One potential explanation can be that the injection of water caused a displacement of the dissolved phase and perhaps any mobile non-aqueous phase liquid. Another potential explanation is that by injecting uncontaminated water into this area, oxygen was also supplemented to the subsurface and encouraged microbial activities. Generally, it is believed that oxygen is present within the smear zone, and given the age of this contaminated Site (~70 years), it is expected that aerobic biodegradation had long reached its operational limits. However, the latter explanation is in agreement with the results of groundwater treatment tests in control batch reactors in the absence of persulfate.

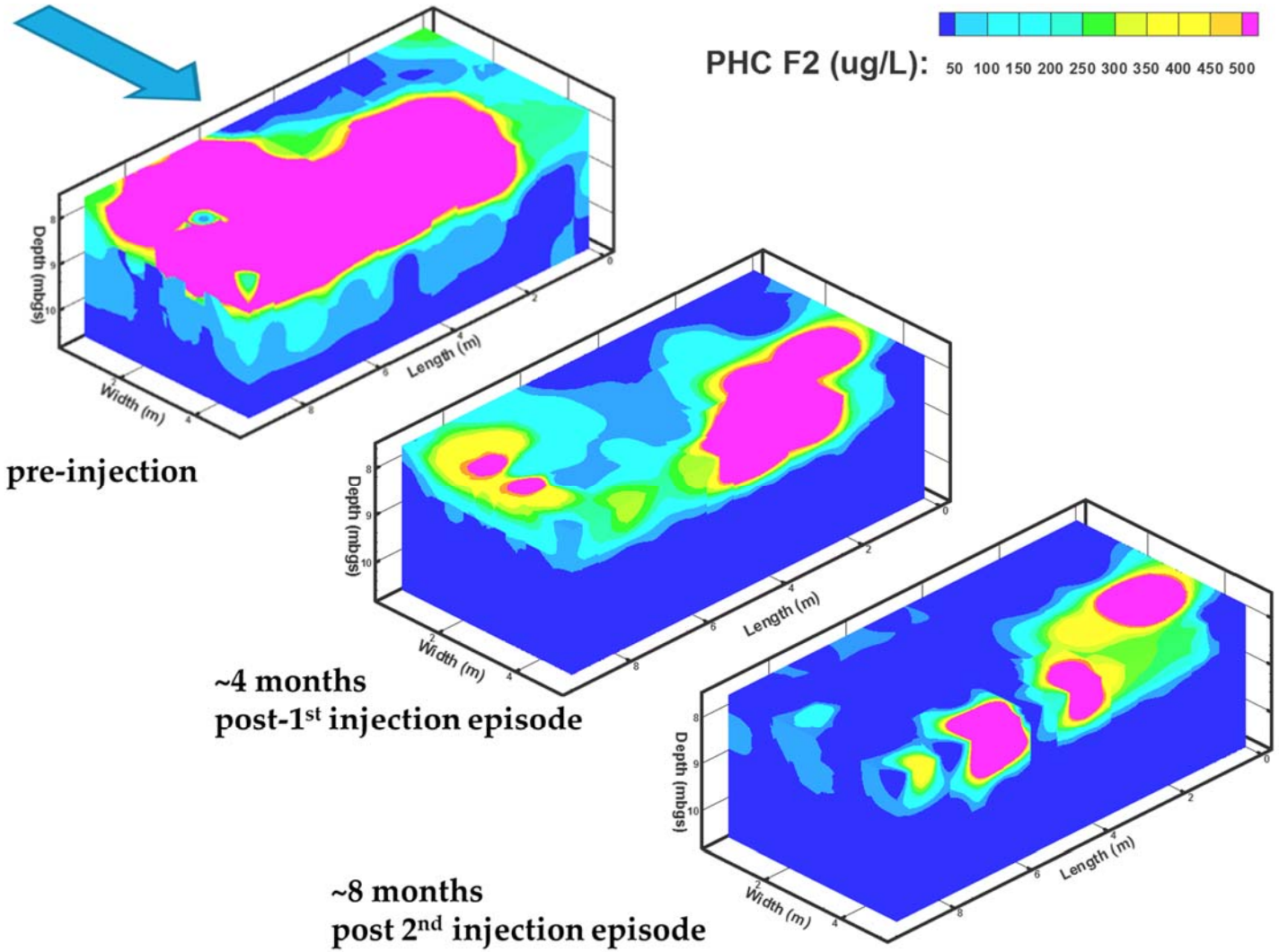

Figure 4-9: Changes in petroleum hydrocarbon F2 dissolved-phase plumes at the pilot-scale area

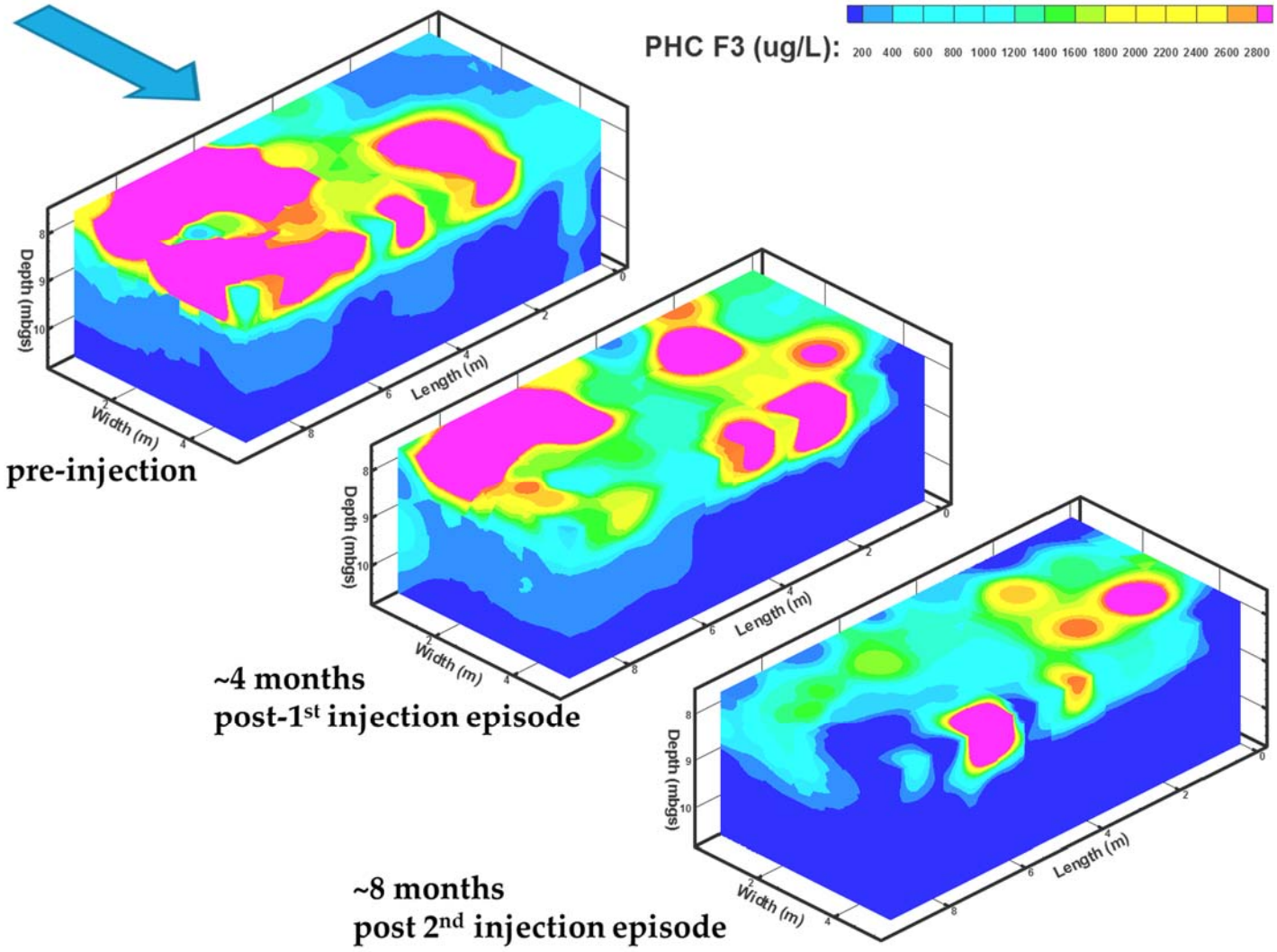

Figure 4-10: Changes in petroleum hydrocarbon F3 dissolved-phase plumes at the pilot-scale area

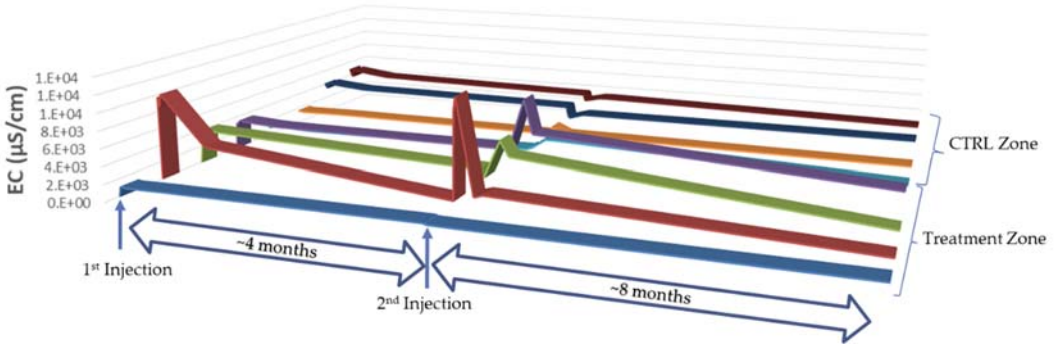

Figure 4-11: Measured electrical conductivity profile at selected monitoring wells

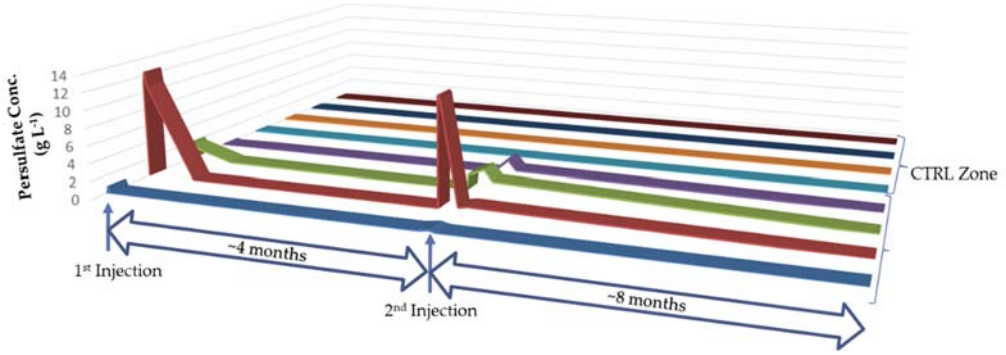

Figure 4-12: Detected Persulfate concentration profile at selected monitoring

4.5.2 Soil Investigation and Sampling

The results of LIF-UVOST™ activities are presented in Figure 4-13. As shown, the intensity of the LIF signals increased with distance towards the downgradient of the MW09-7 monitoring well. The depths[1] at which the intensified signals were detected were generally within the smear zone (Figure 4-14). The LIF-UVOST™ data confirmed the visual observations during the Site characterizations. This data was also used to inform the design of ISCO well depths and locations.

[1] The depth unit depicted in the Figure 4-13 is in feet.

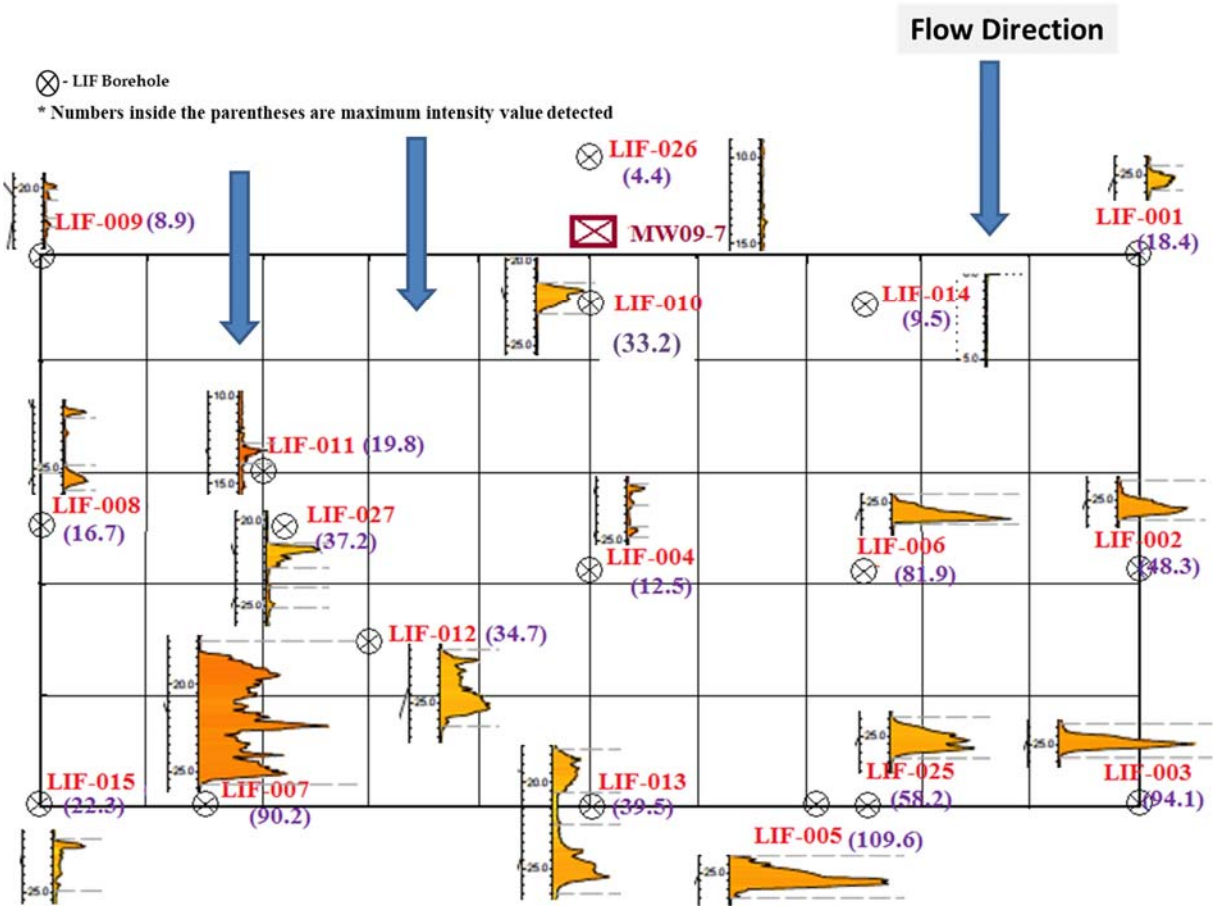

Figure 4-13: Borehole locations at the Pilot-Scale Area and detected LIF response at each location with depth and the maximum value detected

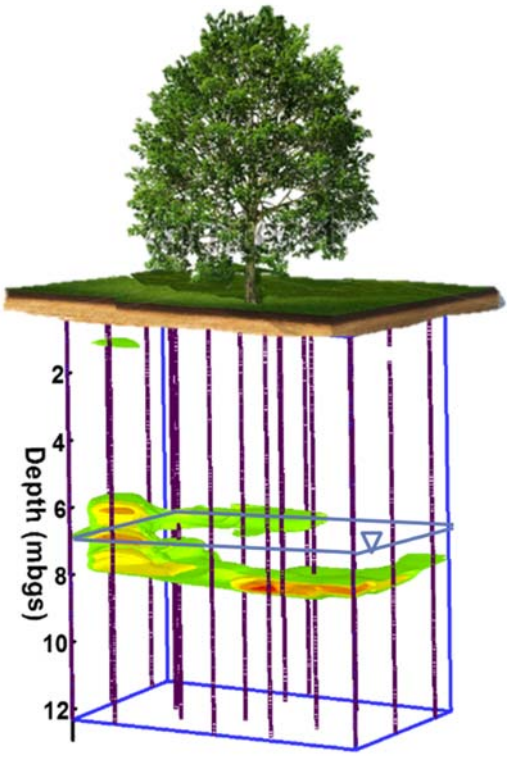

Figure 4-14: 3D LNAPL plume at the pilot-scale area using LIF-UVOST^{TM} data

The soil samples were collected and analyzed pre-injection activities, and after completion of injection Episode 2 corresponding to nearby LIF elevated response data as presented in Table 4-2. Since the places that persulfate can reach during injection are largely unknown, the post-injection soil samples were collected from ~0.5 m above to ~0.5 m below the depths that pre-injection core samples were collected. The values in the post-injection column are the average of concentrations F2 and F3 in the soil samples that were collected within the intervals mentioned above. Overall, collected soil samples within the TTZ showed a decrease of ~50% in F2 and F3. Samples collected from CZ showed overall higher concentrations of F2 and F3 compared to pre-injection samples. Considering the heterogeneity in contaminant distributions, this observation is not uncommon in the field. However, since an overall 50% decrease in contaminant in soil was observed in TTZ, it can potentially be concluded that the two injection episode at the pilot-scale area was successful.

Table 4-2: Soil Sample Analysis Corresponding to the LIF Locations

Area	LIF ID	Depth (m bgs)	Pre-Injection		Post-Injection	
			F2 (ppb)	F3 (ppb)	F2 (ppb)	F3 (ppb)
TTZ	LIF-001	7.6-9.1	924.4	2641.8	610.6	1654.8
	LIF-003	6.7-8.2	2899.5	6288.8	154.4	336.1
	LIF-005	7.6-9.1	700.1	1612.7	1080	2606.8
	LIF-006	6.7-8.2	1884.5	4338.9	1969.6	4354.0
	LIF-002	6.7-8.2	1490.1	3409.0	683.3	2087.5
Buffer	LIF-004	6.4-7.9	3926.8	9085.1	ND	13.7
	LIF-010	6-7.6	ND	75.2	ND	29.2
CZ	LIF-009	5.4-7	71.1	589.7	739.0	3167.3
	LIF-015	6-7.6	1175.8	2542.8	1636.6	3743.3

4.6 Summary

Feasibility and effectiveness of persulfate for remediation of LNAPLs were evaluated at a pilot-scale area impacted with weathered diesel fuel. Two injection episode was conducted at this area. Persulfate solution (at a concentration of 40 $g.L^{-1}$) was delivered into the subsurface at the treatment zone of this area, while clean water was injected at the control zone. Persulfate was persisted in groundwater for three weeks post-injection activities. Even though persulfate was never detected in groundwater collected from the control zone, the decrease in the concentration of F2 and F3 in the aqueous phase was comparable and is consistent with soil column studies. The concentration of pseudocomponents decreased in both control and treatment columns' effluents. One likely explanation for this observation at the field is dilution and displacement of dissolved phase from the area during injection activities. Additional oxygen is also supplemented into the subsurface during injection activities that can result in increased bioactivity and biodegradation of the pseudocomponents. Groundwater has access to oxygen through the unsaturated zone, and it is expected that aerobic biodegradation reaches its limits after several decades. However, the latter

explanation is consistent with the results of groundwater treatment tests in control batch reactors in the absence of persulfate. Overall, collected soil samples within the treatment zone showed a decrease of ~50% in F2 and F3. Soil samples collected from the control zone showed higher concentrations of F2 and F3 compared to pre-injection samples that can be explained by heterogeneity in contaminant distributions in the subsurface.

Chapter 5:
Closure

5.1 Conclusion

The purpose of this research was to develop a combined experimental and numerical simulation approach for the investigation of in situ chemical oxidation of multicomponent weathered LNAPL in the subsurface. The bench-scale experiments were focused on contaminated groundwater and soil in settings that closely resemble a contaminated aquifer. The model developed here to recreate the experimental data simulates groundwater flow, complex chemical oxidation, and advective-dispersive transport of NAPL fractions rather than specific hydrocarbon species. Pseudocomponents were introduced based on carbon number range for the analytical and numerical treatment of the weathered source; these were associated with effective physical and chemical parameters such as diffusion coefficient and reaction rates. The numerical model relied on the aqueous treatability studies to estimate critical kinetic parameters needed to simulate the transport and oxidation of weathered LNAPL. It becomes apparent from aqueous treatability data that the oxidation reactions do not follow a first- or second-order reaction pattern and suggesting that the overall process may follow complex kinetics, most likely involving intermediate products. The coupled aqueous phase oxidation equations were solved numerically, and complex kinetic parameters were obtained for the pseudocomponents. These parameters appear suitable for application in the simulation of soil column studies. The numerical model was able to reproduce the laboratory results of column effluent for each injection event and predict the persulfate efficiency for LNAPL mass removal in soil columns with a reasonable agreement for both unactivated and alkaline-activated persulfate systems. This numerical model is the first to incorporate a phenomenological description of LNAPL oxidation using pseudocomponents as proxies for components, simulates the simultaneous reactive transport, and reproduces such a wide range of experimental data. By using a minimum number of empirical relations and by keeping the equations in the numerical model relatively simple, a powerful and flexible tool has been developed that can be readily adapted to investigate persulfate-based in situ chemical oxidations of LNAPLs for various remedial design and oxidant delivery scenarios. Chapter 4 introduced a detailed pilot-scale persulfate ISCO operation at a contaminated field Site, testing the viability of in situ persulfate ISCO. This experiment yielded insight into the effectiveness of persulfate as an oxidizing agent, with evidence supporting the approximate observation of 50% reduction of source mass eight months after oxidation in the treatment zone. The results from the

treatment zone were consistent with the results obtained from the unactivated persulfate treatment columns. However, analytical data from the control columns show that overall source mass was decreased by ~ 30%, while no change was observed in the control zone at the pilot-scale area. The soil in columns was exposed to oxygen both during packing and with each injection episode. This exposure likely initiated biodegradation activities in column studies and resulted in the LNAPL mass reduction. Although the residual LNAPL blobs are within the smear zone, they are likely trapped within soil pores with no access to oxygen.

5.2 Recommendations

While this investigation achieved its objectives of offering a practical simulation tool that can assist with remedial design and design optimization, this work can be expanded in several directions. This modeling framework may, for instance, be extended to multiple dimensions in order to replicate the results of the *in situ* field test of Chapter 4. In the current simulations, the aqueous phase and LNAPL movements were entirely governed by dissolution and reactive advective-dispersive in one dimension, and they cannot consider scenarios such as movement due to fluid density gradients. A multidimensional model could capture additional key processes involved in "real-world" *in situ* chemical oxidation and provide better predictions.

The model developed in Chapter 3 provided a satisfactory agreement between experimental data and simulated results in treatment columns. It also simulated the column effluent data in control columns with a good accuracy. However, it significantly underestimated the LNAPL removal in soil control columns. The contaminated soil was collected from the smear zone of a several-decades-old impacted site. Generally, it is assumed that oxygen can reach a smear zone. Besides, it was assumed that the natural attenuation, including bioactivity, has reached its limits considering the age of the contaminations. However, it appears the injection of water (in the case of control columns) provided oxygen to the previously inaccessible areas of the subsurface and may have resumed some bioactivity that may have resulted in LNAPL mass reduction. Additional work investigating the increased bioactivity by injection of clean water into the smear zone is required. In addition, the model formulation can be enhanced to accommodate bioactivity in the simulated equations.

Due to LNAPL concentration fluctuations in the pH control column effluent, the experimental results from this system were not used in simulation studies. These columns were injected with the Milli-Q water at an elevated pH of ~12. This system is similar to the alkaline flooding technique utilized in the petroleum industry for enhanced oil recovery. The alkaline chemical reacts with certain oils,

forming surfactants inside the reservoir (Speight, 2009). These reactions can justify the higher LNAPL mass reduction in this system than in the control system, where the Milli-Q at a neutral pH range was injected. However, there is no evidence-based explanation for the observed fluctuations in the effluent concentration data. Therefore, further experimental research is required to provide insights into the behavior of LNAPLs in this system and would be a logical continuation of the current study.

Bibliography

Agaoglu, B., Scheytt, T., & Copty, N. K. (2016). Impact of NAPL architecture on interphase mass transfer: A pore network study. *Advances in Water Resources, 95*, 138-151. 10.1016/j.advwatres.2015.11.012

Anipsitakis, G. P., & Dionysiou, D. D. (2004). Radical generation by the interaction of transition metals with common oxidants. *Environmental Science & Technology, 38*(13), 3705.

Banerjee, S. (1984). Solubility of organic mixtures in water. *Environmental Science & Technology; Environ.Sci.Technol, 18*(8), 587-591. 10.1021/es00126a004

Biswas, N. C. (2011). *In situ Chemical Oxidation using Unactivated Sodium Persulphate at a Former Gasoline Station*. [Master's thesis, University of Waterloo].

Block, P. A., Brown, R. A., & Robinson, D. (2004). Novel activation technologies for sodium persulfate in situ chemical oxidation. . Paper presented at the *Proceedings of the 4th International Conference on the Remediation of Chlorinated and Recalcitrant Compounds, Monterey, CA.*

Bogan, B. W., & Trbovic, V. (2003). Effect of sequestration on PAH degradability with Fenton's reagent: roles of total organic carbon, humin, and soil porosity. *Journal of Hazardous Materials, 100*(1–3), 285-300. 10.1016/S0304-3894(03)00134-1

Brahma, P. P., & Harmon, T. C. (2003). The effect of multicomponent diffusion on NAPL dissolution from spherical ternary mixtures. *Journal of Contaminant Hydrology; J Contam Hydrol, 67*(1), 43-60. 10.1016/S0169-7722(03)00087-1

Brassington, K. J., Hough, R. L., Paton, G. I., Semple, K. T., Risdon, G. C., Crossley, J., Hay, I., Askari, K., & Pollard, S. J. T. (2007). Weathered Hydrocarbon Wastes: A Risk Management Primer. *Critical Reviews in Environmental Science and Technology, 37*(3), 199-232. 10.1080/10643380600819625

Brost, E. J., & DeVaull, G. E. (2000). *Non-aqueous phase liquid (NAPL) mobility limits in soil*. American Petroleum Institute Soil & Groundwater Research Bulletin No. 9.

CCME. (2008). *Canada-Wide Standard for Petroleum Hydrocarbons (PHC) in Soil - Technical Supplement. In: Canada, editor: Canadian Council of Ministers of the Environment.* ().

CCME. (2019). *Canada-Wide Standard for Petroleum Hydrocarbons in Soil, Canadian Council of Ministers of the Environment (CCME), 2018 Progress Report.* ().

Chen, K., Chang, Y., & Chiou, W. (2016). Remediation of diesel-contaminated soil using in situ chemical oxidation (ISCO) and the effects of common oxidants on the indigenous microbial community: a comparison study. *Journal of Chemical Technology and Biotechnology (1986), 91*(6), 1877-1888. 10.1002/jctb.4781

CL:AIRE. (2014). *An Illustrated Handbook of LNAPL Transport and Fate in the Subsurface, Contaminated Land: Applications in Real Environments (CL:AIRE), London, ISBN 978-1-905046-24-9. Download at http://www.claire.co.uk/LNAPL*.

Conrad, S. H., Glass, R. J., & Peplinski, W. J. (2002). Bench-scale visualization of DNAPL remediation processes in analog heterogeneous aquifers: surfactant floods and in situ oxidation using permanganate. *Journal of Contaminant Hydrology; J Contam Hydrol, 58*(1), 13-49. 10.1016/S0169-7722(02)00024-4

Crimi, M. L., & Taylor, J. (2007). Experimental Evaluation of Catalyzed Hydrogen Peroxide and Sodium Persulfate for Destruction of BTEX Contaminants. *Soil and Sediment Contamination: An International Journal, 16*(1), 29-45. 10.1080/15320380601077792

deZabala, E. F., & Radke, C. J. (1986). A Nonequilibrium Description of Alkaline Waterflooding. *SPE Reservoir Engineering, 1*(1), 29-43. 10.2118/11213-PA

Domenico, P. A. (., & Schwartz, F. W. (. (1990). *Physical and chemical hydrogeology*. Wiley.

Drake, S. S., O'Carroll, D.,M., & Gerhard, J. I. (2013). Wettability contrasts between fresh and weathered diesel fuels. *Journal of Contaminant Hydrology; J Contam Hydrol, 144*(1), 46-57. 10.1016/j.jconhyd.2012.09.008

Edwards, D. A., Andriot, M. D., Amoruso, M. A., Tummey, A. C., Bevan, C. J., Tveit, A., Hayes, L. A., Youngren, S. H., & Nakles, D. V. (1997). *Development of Fraction Specific Reference Doses (RfDs) and Reference Concentrations (RfCs) for Total Petroleum Hydrocarbons (TPH).* (No. 4).Total Petroleum Hydrocarbon Criteria Working Group Series.

Fingas, M. (2017). *Oil spill science and technology* (Second ed.). Gulf Professional Publishing. 10.1029/93WR02923

Frind, E. O., Molson, J. W., Schirmer, M., & Guiguer, N. (1999). Dissolution and mass transfer of multiple organics under field conditions: The Borden emplaced source. *Water Resources Research, 35*(3), 683-694. 10.1029/1998WR900064

FSCI. (2019). *Federal Contaminated Sites Inventory (FCSI) Contaminants and Media.* Treasury Board of Canada Secretariat. https://www.tbs-sct.gc.ca/fcsi-rscf/home-accueil-eng.aspx

Golder, A. L. (2009). *2008 GROUNDWATER MONITORING REPORT Report Number 08-1134-139-0-R01.*

Gustafson, J. B., Griffith Tell, J., & Orem, D. (1997). *Selection of Representative TPH Fractions Based on Fate and Transport Considerations.* ().Volume 3, Total Petroleum Hydrocarbon Criteria Working Group Series.

Hauswirth, S. C., Birak, P. S., Rylander, S. C., & Miller, C. T. (2012). Mobilization of Manufactured Gas Plant Tar with Alkaline Flushing Solutions. *Environmental Science & Technology, 46*(1), 426-433.

Heiderscheidt, J. L., Siegrist, R. L., & Illangasekare, T. H. (2008). Intermediate-scale 2D experimental investigation of in situ chemical oxidation using potassium permanganate for remediation of complex DNAPL source zones. *Journal of Contaminant Hydrology, 102*(1-2), 3-16. 10.1016/j.jconhyd.2008.07.002

House, D. A. (1962). Kinetics and Mechanism of Oxidations by Peroxydisulfate. *Chemical Reviews, 62*(3), 185-203. 10.1021/cr60217a001

Huang, K., Zhao, Z., Hoag, G. E., Dahmani, A., & Block, P. A. (2005). Degradation of volatile organic compounds with thermally activated persulfate oxidation. *Chemosphere, 61*(4), 551-560. 10.1016/j.chemosphere.2005.02.032

Huling, S. G., & Pivetz, B. E. (2006). *Engineering Issue: In-Situ Chemical Oxidation*. USEPA Agency Office of Research and Development. https://nepis.epa.gov/Exe/ZyPDF.cgi/2000ZXNC.PDF?Dockey=2000ZXNC.PDF

Imhoff, P. T., Jaffe, P. R., & Pinder, G. F. (1994). An experimental study of complete dissolution of a nonaqueous phase liquid in saturated porous media. *Water Resources Research; Water Resour.Res, 30*(2), 307-320. 10.1029/93WR02675

Johnston, C. D. (2010). *Selecting and assessing strategies for remediating LNAPL in soil and aquifers.* ().CRC CARE Technical Report NO. 18, CRC for Contamination Assessment and Remediation of the Environment, Adelaide, Australia.

Kambhu, A., Comfort, S., Chokejaroenrat, C., & Sakulthaew, C. (2012). *Developing slow-release persulfate candles to treat BTEX contaminated groundwater*. Elsevier. 10.1016/j.chemosphere.2012.06.004

Killian, P. F., Bruell, C. J., Liang, C., & Marley, M. C. (2007). Iron (II) Activated Persulfate Oxidation of MGP Contaminated Soil. *Soil & Sediment Contamination, 16*(6), 523-537. 10.1080/15320380701623206

Kolthoff, I. M., & Miller, I. K. (1951). The Chemistry of Persulfate. I. The Kinetics and Mechanism of the Decomposition of the Persulfate Ion in Aqueous Medium. *Journal of the American Chemical Society, 73*(7), 3055-3059. 10.1021/ja01151a024

Krembs, F. J. (2008). *Critical analysis of the field scale application of in situ chemical oxidation for the remediation of contaminated groundwater*. [Master's thesis, Colorado School of Mines]. 2000-2009 - Mines Theses & Dissertations

Krembs, F. J., Siegrist, R. L., Crimi, M. L., Furrer, R. F., & Petri, B. G. (2010). ISCO for Groundwater Remediation: Analysis of Field Applications and Performance. *Ground Water Monitoring & Remediation, 30*(4), 42-53.

Langbehn, A., & Steinhart, H. (1994). Determination of organic acids and ketones in contaminated soils. *Journal of High Resolution Chromatography, 17*(5), 293-298. 10.1002/jhrc.1240170502

Lee, J., von Gunten, U., & Kim, J. (2020). Persulfate-Based Advanced Oxidation: Critical Assessment of Opportunities and Roadblocks. *Environmental Science & Technology; Environ.Sci.Technol, 54*(6), 3064-3081. 10.1021/acs.est.9b07082

Lemaire, J., Croze, V., Maier, J., & Simonnot, M. (2011). *Is it possible to remediate a BTEX contaminated chalky aquifer by in situ chemical oxidation?*. Elsevier. 10.1016/j.chemosphere.2011.06.052

Liang, C., Bruell, C. J., Marley, M. C., & Sperry, K. L. (2004a). Persulfate oxidation for in situ remediation of TCE. I. Activated by ferrous ion with and without a persulfate–thiosulfate redox couple. *Chemosphere, 55*(9), 1213-1223. 10.1016/j.chemosphere.2004.01.029

Liang, C., Bruell, C. J., Marley, M. C., & Sperry, K. L. (2004b). Persulfate oxidation for in situ remediation of TCE. II. Activated by chelated ferrous ion. *Chemosphere, 55*(9), 1225-1233. 10.1016/j.chemosphere.2004.01.030

Liang, C., Huang, C., Mohanty, N., & Kurakalva, R. M. (2008). A rapid spectrophotometric determination of persulfate anion in ISCO. *Chemosphere (Oxford); Chemosphere, 73*(9), 1540-1543. 10.1016/j.chemosphere.2008.08.043

Liang, C., Wang, Z., & Bruell, C. J. (2007). Influence of pH on persulfate oxidation of TCE at ambient temperatures. *Chemosphere, 66*(1), 106-113. 10.1016/j.chemosphere.2006.05.026

Ling, M., & Chen, J. (2014). Environmental visualization: applications to site characterization, remedial programs, and litigation support. *Environmental Earth Sciences, 72*(10), 3839-3846. 10.1007/s12665-014-3220-y

Lominchar, M. A., Santos, A., de Miguel, E., & Romero, A. (2018). Remediation of aged diesel contaminated soil by alkaline activated persulfate. *The Science of the Total Environment; Sci Total Environ, 622-623*, 41-48. 10.1016/j.scitotenv.2017.11.263

Lu, J. (1994). *Application of a Modified Analytical Derivatization Method to the Determination of Microbial Metabolites in Aquifer Systems,* [Master's Thesis, Western Michigan University]. ScholarWorks at WMU

Matzek, L. W., & Carter, K. E. (2016). Activated persulfate for organic chemical degradation: A review. *Chemosphere, 151*, 178-188. https://doi.org/10.1016/j.chemosphere.2016.02.055

Mendes, G. P., Magalhães, V. M. A., Soares, L. C. R., Aranha, R. M., Nascimento, C. A. O., Vianna, Marilda M. G. R., & Chiavone-Filho, O. (2020). Treatability studies of naphthalene in soil, water and air with persulfate activated by iron(II). *Journal of Environmental Sciences, 90*, 67-77. https://doi-org.proxy.lib.uwaterloo.ca/10.1016/j.jes.2019.11.015

Miller, C. T., & Weber, W. J. J. (1984). Modeling organic contaminant partitioning in ground-water systems. *Ground Water, 22*(5), 584-592. 10.1111/j.1745-6584.1984.tb01429.x

Miller, C. T., Poirier-McNeil, & Mayer, A. S. (1990). Dissolution of Trapped Nonaqueous Phase Liquids: Mass Transfer Characteristics. *Water Resources Research, 26*(11), 2783-2796. 10.1029/WR026i011p02783

Molson, J. W., Frind, E. O., Van Stempvoort, D. R., & Lesage, S. (2002). Humic acid enhanced remediation of an emplaced diesel source in groundwater: 2. Numerical model development and application. *Journal of Contaminant Hydrology; J Contam Hydrol, 54*(3), 277-305. 10.1016/S0169-7722(01)00181-4

Mukherji, S., Peters, C. A., & Weber, W. J. (1997). Mass Transfer of Polynuclear Aromatic Hydrocarbons from Complex DNAPL Mixtures. *Environmental Science & Technology; Environ.Sci.Technol, 31*(2), 416-423. 10.1021/es960227n

NRC. (2013). *Alternatives for Managing the Nation's Complex Contaminated Groundwater Sites.* National Research Council (NRC), Washington, D.C.

NRCAN. (2020). *Frequently Asked Questions Concerning Federally-Regulated Petroleum Pipelines in Canada, Natural Resources Canada (NRCAN) Petroleum Resources Branch* . Natural Resources Canada Petroleum Resources Branch. https://www.nrcan.gc.ca/our-natural-resources/energy-sources-distribution/clean-fossil-fuels/pipelines/faqs-federally-regulated-petroleum-pipelines-canada/5893

Parker, J. C., & Park, E. (2004). Modeling field-scale dense nonaqueous phase liquid dissolution kinetics in heterogeneous aquifers. *Water Resources Research; Water Resour.Res, 40*(5), W05109-n/a. 10.1029/2003WR002807

Perkins, T. K., & Johnston, O. C. (1963). A Review of Diffusion and Dispersion in Porous Media. *Society of Petroleum Engineers Journal, 3*(1), 70-84. 10.2118/480-PA

Petri, B. G., Watts, R. J., Tsitonaki, A., Crimi, M., Thomson, N. R., & Teel, A. L. (2010). *Fundamentals of ISCO Using Persulfate*. Springer New York. 10.1007/978-1-4419-7826-4_4

Potter, T. L., & Simmons, K. E. (1998). *Composition of petroleum mixtures, Volume 2, Total Petroleum Hydrocarbon Criteria Working Group Series*. Amherst Scientific Publishers.

Powers, S. E., Abriola, L. M., & Jr, W. J. W. (1994). An experimental investigation of nonaqueous phase liquid dissolution in saturated subsurface systems: Transient mass transfer rates. *Water Resources Research, 30*(2), 321-332. 10.1029/93WR02923

Powers, S. E., Anckner, W. H., & Seacord, T. F. (1996). Wettability of NAPL-Contaminated Sands. *Journal of Environmental Engineering, 122*(10), 889-896. 10.1061/(ASCE)0733-9372(1996)122:10(889)

Reddi, L. N., Menon, S., & Pant, A. (1998). Pore-scale investigations on vibratory mobilization of LNAPL ganglia. *Journal of Hazardous Materials, 62*(3), 211-230. http://dx.doi.org.proxy.lib.uwaterloo.ca/10.1016/S0304-3894(98)00164-2

Romero, A., Santos, A., Vicente, F., Rodriguez, S., & Lafuente, A. L. (2009). In situ oxidation remediation technologies: Kinetic of hydrogen peroxide decomposition on soil organic matter. *Journal of Hazardous Materials, 170*(2–3), 627-632. 10.1016/j.jhazmat.2009.05.041

Sahloul, N. A., Ioannidis, M. A., & Chatzis, I. (2002). Dissolution of residual non-aqueous phase liquids in porous media: pore-scale mechanisms and mass transfer rates. *Advances in Water Resources, 25*(1), 33-49. 10.1016/S0309-1708(01)00025-2

Sale, T. C., & McWhorter, D. B. (2001). Steady state mass transfer from single-component dense nonaqueous phase liquids in uniform flow fields. *Water Resources Research; Water Resour.Res, 37*(2), 393-404. 10.1029/2000WR900236

Schiesser, W. E. (1991). *The numerical method of lines : integration of partial differential equations*. Academic Press.

Schmidt, J. T., Ahmad, M., Teel, A. L., & Watts, R. J. (2011). Hydrogen peroxide stabilization in one-dimensional flow columns. *Journal of Contaminant Hydrology, 126*(1–2), 1-7. 10.1016/j.jconhyd.2011.05.008

Shafieiyoun, S., & Thomson, N. R. (2019). Intra-NAPL diffusion and dissolution of a MGP NAPL exposed to persulfate in a flow-through system. *Journal of Hazardous Materials; J Hazard Mater, 365*, 366-374. 10.1016/j.jhazmat.2018.10.096

Shafieiyoun, S., Thomson, N. R., Brey, A. P., Gasinski, C. M., Pence, W., & Marley, M. (2018). Realistic expectations for the treatment of FMGP residuals by chemical oxidants. *Journal of Contaminant Hydrology; J Contam Hydrol, 219*, 1-17. 10.1016/j.jconhyd.2018.08.007

Siegal, J., Rees, A. A., Eggers, K. W., & Hobbs, R. L. (2009). In situ chemical oxidation of residual LNAPL and dissolved-phase fuel hydrocarbons and chlorinated alkenes in groundwater using activated persulfate. *Remediation Journal, 19*(2), 19-35. 10.1002/rem.20199

Siegrist, R. L., Crimi, M., & Simpkin, T. J. (2011). *In Situ Chemical Oxidation for Groundwater Remediation*. Springer.

Sra, K. S., Thomson, N. R., & Barker, J. (2013a). Persulfate Treatment of Dissolved Gasoline Compounds. *Journal of Hazardous, Toxic, and Radioactive Waste, 17*(1), 9-15. 10.1061/(ASCE)HZ.2153-5515.0000143

Sra, K. S., Thomson, N. R., & Barker, J. (2013). Persulfate Treatment of Dissolved Gasoline Compounds. Journal of Hazardous, Toxic, and Radioactive Waste, 17(1), 9-15. 10.1061/(ASCE)HZ.2153-5515.0000143

Sra, K. S., Thomson, N. R., & Barker, J. F. (2013b). Persulfate injection into a gasoline source zone. *Journal of Contaminant Hydrology, 150*, 35–44.

Sra, K. S. (2010). *Persulfate persistence and treatability of gasoline compounds*, [Doctoral dissertation, University of Waterloo]

Thomas, K. V., Donkin, P., & Rowland, S. J. (1995). Toxicity enhancement of an aliphatic petrogenic unresolved complex mixture (UCM) by chemical oxidation. *Water Research, 29*(1), 379-382. https://doi.org/10.1016/0043-1354(94)E0111-I

Tratnyek, P., Powell, J., & Waldemer, R. (2009). *Improved Understanding of In Situ Chemical Oxidation. Technical Objective I: Contaminant Oxidation Kinetics Contaminant Oxidation Kinetics.* ().

Tsitonaki, A., Smets, B. F., & Bjerg, P. L. (2008). Effects of heat-activated persulfate oxidation on soil microorganisms. *Water Research, 42*(4-5), 1013-1022. 10.1016/j.watres.2007.09.018

Tsitonaki, A., Petri, B., Crimi, M., Mosbæk, H., Siegrist, R. L., & Bjerg, P. L. (2010). In Situ Chemical Oxidation of Contaminated Soil and Groundwater Using Persulfate: A Review. *Critical Reviews in Environmental Science and Technology, 40*(1), 55-91. 10.1080/10643380802039303

USEPA. (2020). *The National LUST Cleanup Backlog: A Study of Opportunities.* USEPA Underground Storage Tanks (USTs). https://www.epa.gov/ust/national-lust-cleanup-backlog-study-opportunities

USEPA. (2021). *Petroleum Brownfields.* United States Environmental Protection Agency. https://www.epa.gov/ust/petroleum-brownfields

Watts, R., & Teel, A. (2006). Treatment of Contaminated Soils and Groundwater Using ISCO. *Practice Periodical of Hazardous, Toxic, and Radioactive Waste Management, 10*(1), 2-9. 10.1061/(ASCE)1090-025X(2006)10:1(2)

Watts, R. J., & Teel, A. L. (2006). Treatment of Contaminated Soils and Groundwater Using ISCO. *Practice Periodical of Hazardous, Toxic, and Radioactive Waste Management, 10*(1), 2-9. 10.1061/(ASCE)1090-025X(2006)10:1(2)

Weisman, W. (1998). *Analysis of Petroleum Hydrocarbons in Environmental Media, Volume 1, Total Petroleum Hydrocarbon Criteria Working Group.*

Wiedemeier, T., Rifai, H., Newell, C. J., & Wilson, J. T. (1999). *Natural Attenuation of Fuels and Chlorinated Solvents in the Subsurface*. John Wiley and Sons Ltd.

Yang, L. H., Jing, L. X., & Zheng, C. M. (2019). *Evaluation of groundwater remediation strategies at petroleum contaminated sites based on groundwater modelling approach*. IOP Publishing. 10.1088/1755-1315/344/1/012162

Yen, C., Chen, K., Kao, C., Liang, S., & Chen, T. (2011). Application of persulfate to remediate petroleum hydrocarbon-contaminated soil: Feasibility and comparison with common oxidants. *Journal of Hazardous Materials, 186*(2-3), 2097-2102. 10.1016/j.jhazmat.2010.12.129

Yin, Y., & Allen, H. E. (1999). *In Situ Chemical Treatment.* (No. Technol. Eval. Rep. No. TE-99-01). Ground Water Remediation Technology. Analysis Center.

Zhao, D., Liao, X., Yan, X., Huling, S. G., Chai, T., & Tao, H. (2013). Effect and mechanism of persulfate activated by different methods for PAHs removal in soil. *Journal of Hazardous Materials, 254-255*(4), 228-235. 10.1016/j.jhazmat.2013.03.056

Zhao, & Ioannidis, M. A. (2003). Pore network simulation of the dissolution of a single-component wetting nonaqueous phase liquid. *Water Resources Research, 39*(10), 1291-n/a. 10.1029/2002WR001861

Appendices

Appendix A:
Petroleum Hydrocarbon Analysis

Soil and water analytical analysis of fraction 2 (C10 to C16) and 3 (C16 to C34) of PHCs were generally conducted in accordance with applicable sections of the Canadian Council of Ministers of the Environment (CCME) method "Reference Method for the Canada-Wide Standard for Petroleum Hydrocarbons (CWS-PHC) in Soil – Tier 1 Method" (MOE Method DECPH-E3421/CCME). However, the following modifications to the above-referenced method were employed[1]:

Groundwater collection and sample handling:

- In the field: 40 mL glass vials were prepared by adding sodium azide as a preservative (0.4ml of a 10% W/V solution) prior to field activities. Groundwater samples were collected in prepared glass vials with no headspace and immediately capped with Teflon® lined screw caps. Samples were stored at 4°C in coolers before submission to Water and Soil Remediation Laboratory at the University of Waterloo.
- In the laboratory: groundwater samples were equilibrated to room temperature before extraction. A 5 mL of sample was discarded using a glass/stainless syringe to allow for the addition of 2 mL of methylene chloride for solvent extraction purposes. The vial was quickly resealed and agitated on its side at 350 rpm on a platform shaker for 20 min. After shaking, the vial was inverted, and the phases were allowed to separate for 30 min. Approximately 1.0 ml of the dichloromethane phase was removed from the inverted vial with a gas-tight glass syringe through the Teflon® septum. The solvent was placed in a Teflon® crimp sealed autosampler vial for injection into the gas chromatograph.

Soil collection and sample handling:

- In the field: 1.5 m long soil cores were collected at designated locations and depths. Each soil core was opened on Site, screened using a photoionization detector (PID), and then inspected for olfactory and visual evidence of source material impacts. Sub-samples were selected from each

[1] Appendix A is adopted from a document provided by Ms. Shirley Chatten. The version provided in this section may have some editorial differences with the document prepared by Ms. Chattan. The laboratory analytical method has been modified and described by Ms. Shirley Chatten, e-mail: schatten@uwaterloo.ca phone: ext. 36370

core/borehole for chemical analyses. Sub-samples were quickly transferred into wide-mouth sampling glass jars (500 mL), labeled, and stored in a cooler at 4 ºC. At the end of each day, the cooler was transported to the Water and Soil Remediation Laboratory at the University of Waterloo.

- In the laboratory: Approximately 10 g of soil (jars) was collected in the pre-weighed Teflon® screw cap vials (40ml) containing 20ml of methylene chloride (containing internal standard meta-fluorotoluene (MFT) and fluorobiphenyl (FBP)) and were placed on an automatic shaker for 18 hours. Then, samples were allowed to settle, and 1 ml of methylene chloride phase was transferred to a 2ml autosampler vial and crimp sealed with a Teflon® cap.

Sample Analysis:

All prepared samples with solvent were analyzed with an HP 5890 capillary gas chromatograph equipped with an HP7673A autosampler and a flame ionization detector. 3 µL of solvent phase (methylene chloride) was injected in splitless mode (purge on 0.5 min, purge off 10.0 min) onto a 0.25mm x 30M length, DB1 capillary column with a stationary phase film thickness of 0.25µm. Helium column flow rate was 1ml/min with a make-up gas flow rate of 30ml/min. Injection temperature was 275ºC, detector temperature was 325 ºC, and initial column oven temperature was 35 ºC held for 0.5 min, then ramped at 15 ºC /min to a final temperature of 300ºC and held for 2 min. chromatographic run time was 40 minutes. Data integration was completed with an SRI Model 302 Peak Simple chromatography data system. F2 fraction included integration of all area counts beginning just after the end of the decane (nC10) peak to the apex of the nC16 peak, excluding the area of the internal standard fluorobiphenyl (FBP). F3 included the integration of all area counts from the apex of the nC16 peak to the apex of the nC34 peak. The average response factor for nC16 and nC34 was used for the calibration of these two ranges. Calibrations were made in standard internal mode, and standards were run in triplicate at five (or more) different concentrations, covering the expected sample range. Standards were prepared for groundwater by spiking the water with concentrated methanolic and/or toluene stock standards (purchased and certified from Ultra Scientific Analytical Solutions). For soil samples, calibration standards were prepared by spiking quantities of certified methanolic stock into autosampler vials containing 1ml of methylene chloride (with FBP). Similar procedures as described above were followed for extraction and analysis of the standards. A multiple-point linear regression was performed to determine the linearity and slope of the calibration curve. Extraction duplicates (or triplicates) were performed on samples, and results were acceptable when they agreed within 10%. Matrix spikes were performed when necessary by spiking a known amount of midrange standard into

a duplicate field sample and then calculating the amount recovered after extraction. Method Detection Limits (MDL) for the F2 fractions were less than 5 µg/L and less than 100 µg/L for the F3 fraction.

REFERENCES:

1. Canadian Council of Ministers of the Environment (CCME) method "Reference Method for the Canada-wide Standard for Petroleum Hydrocarbons (CWS-PHC) in Soil – Tier 1 Method" (*MOE Method DECPH-E3421/CCME)*

2. EPA Method 8011- 1,2 Dibromoethane and 1,2-Dibromo-3-chloropropane by Microextraction and Gas Chromatography, July 1992.

3. Glaze, William H., Lin, C.-C., Burleson, J. L., Henderson, J. E., Mapel, D., Rawley, R., Scott, D. R., "Optimization of Liquid-Liquid Extraction Methods for Analysis of Organics in Water", Project Report, Contract No's. CR-805472, CR-808561; USEPA/EMSL: Cincinnati, OH, 1983

4. Henderson, J.E., G.R. Peyton and W.H. Glaze (1976). A convenient liquid-liquid extraction method for the determination of halomethanes in water at the parts-per-billion level. IN: Identification and analysis of organic pollutants in water. Keith, L.H. Ed; Ann Arbor Science Publishers Inc., Ann Arbor, MI.

5. Longbottom, James E., Lichtenberg, James J., Ed. (1982). "Methods for Organic Chemical Analysis of Municipal and Industrial Wastewater", EPA-600/4-82-057, USEPA/EMSL: Cincinnati, OH, Appendix A – Definition and Procedure for the Determination of the Method Detection Limit.

6. EPA Method 8015C- Non-Halogenated Organics by Gas Chromatography, February 2007.

Appendix B:
Natural Oxidant Demand Experimental

Uncontaminated materials from the Site were incubated at 80ºC in an incubator (Gallenkamp, 1H-100) and weighted daily until three consecutive weights vary no more than 0.5% calculated as a percentage change from the original weight. The oven-dried soil was sieved to obtain a uniform grade (from 250µm to 2mm) and to remove foreign constituents such as roots and stones. The NOI tests were only conducted for unactivated persulfate in batch reactors over a period of 30 days. Fisherbrand™ clear straight-sided glass 125 mL jars with white polypropylene caps were used for this experiment. Four tests were conducted at 50 grams of soil with varying initial persulfate concentrations of 5, 20, 30, and 40 $g.L^{-1}$ as described in Table B-1. Additional two tests were conducted at an initial persulfate concentration of 30 $g.L^{-1}$ while 40 and 75 grams of soil were used. Four control tests were run in parallel at 5, 20, 30, and 40 $g.L^{-1}$ of initial persulfate in the absence of soil. Chemicals and solutions were used and prepared as described in Chapter 2. Reactors were shaken daily by hand (on sampling days after collection of samples) and stored in the dark at an ambient temperature of ~20 ºC. Aliquots of the supernatant were collected from each reactor on days 0, 1, 4, 7, 15, and 29 and analyzed for persulfate concentration utilizing Huang et al. (2002) spectroscopic method. All tests were conducted in triplicates, and each data point in Figure B-1 is an average of three independent measurements.

Table B- 1: Natural oxidant demand test design

Test ID	*Persulfate ($g.L^{-1}$)*	*Soil (g)*	*solution (mL)*	*Persulfate (g)*	$g_{persulfate}/kg_{soil}$
NOI-1	5	50	50	0.25	5
NOI-2	20	50	50	1.00	20
NOI-3	30	50	50	1.50	30
NOI-4	40	50	50	2.00	40
NOI-5	30	75	50	1.50	20
NOI-6	30	40	67	2.01	50
CTRL-1	5	0	50	0.25	NA
CTRL-2	20	0	50	1.00	NA
CTRL-3	30	0	50	1.50	NA
CTRL-4	40	0	50	2.00	NA

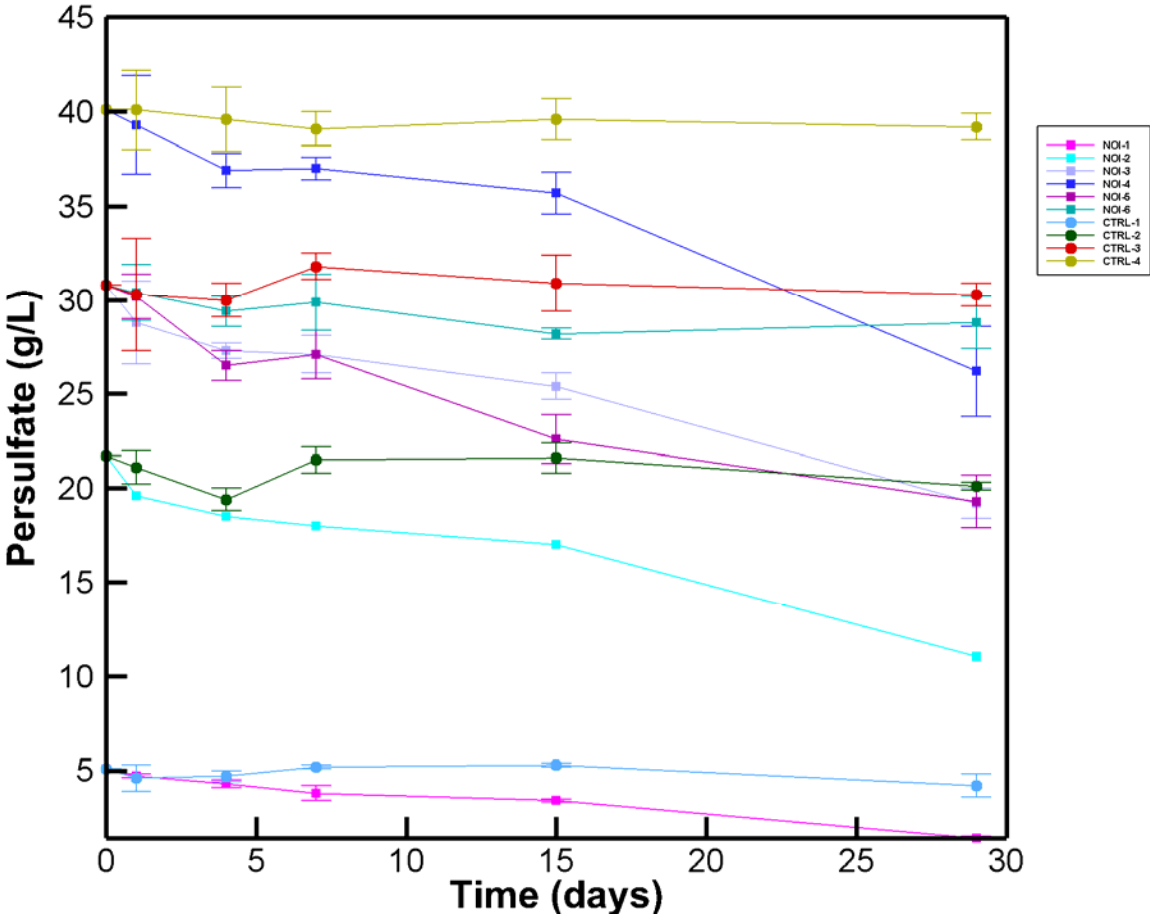

Figure B-1: Persulfate profile during NOD tests

Appendix C:
LNAPL Sorbed Contribution to Dissolved Phase

Investigation focus on dissolved phase in the presence of contaminated porous media should account for the residual and sorbed phases. The LNAPL mass that is partition onto nonpolar aquifer NOM is considered sorbed phase. As the dissolved phase concentration decreases, there is a net flux of LNAPL mass from sorbed phase to the aqueous phase. The mass of LNAPL sorbed is generally estimated by assuming equilibrium between concentrations reside on NOM and dissolved phase. This desorption process can be captured by a first-order approximation described by:

$$K_d = \frac{C_{soil}}{C_{Aqueous}} \quad \text{(C.1)}$$

In the above equation, C_{soil} solute concentration in sorbed phase, $C_{Aqueous}$ solute concentration in the aqueous phase, and K_d is the partitioning coefficient and is estimated fraction of (natural) organic carbon in porous media (f_{oc}) and the LNAPL organic carbon partitioning (K_{oc}) using Equation (C.2):

$$K_d = f_{oc} * K_{oc} \quad \text{(C.2)}$$

Mackay (1991) has provided an equation to calculate LNAPL organic carbon partitioning (K_{oc}) based on more readily available parameters such as octanol-water partitioning coefficient (K_{ow}) that is available for common organic compounds:

$$K_d = f_{oc} * 0.41 * K_{ow} \quad \text{(C.3)}$$

The f_{oc} is a function of soil type and depth and, generally, considered to be ~ 60% of the total soil NOM, and it decreases with depth (Gustafson et al., 1997). Sandy soil has less than 1% NOM (Gustafson et al., 1997). If a soil column in this study is considered, it can be said that the soil in the column is ~$0.131kg$ with a porosity value of 0.32. The analytical results indicated that LNAPL mass in soil for pseudocomponent F2 and F3 is 2.17×10^{-1} and 6.12×10^{-1} grams, respectively. After the soil column was water-saturated and equilibrium was achieved, the mass of F2 and F3 in the aqueous phase was calculated as 3.07×10^{-4} and 3.56×10^{-4} grams, respectively. To estimate the sorption capacity (grams) in the soil for the two pseudocomponents, a 0.5% soil organic matter and estimated $\log K_{ow}$ values of 3.4 and 4.1 for pseudocomponent F2 and F3, respectively, were considered (Gustafson et al., 1997). The maximum sorbed F2 and F3 values of soil in the column can 3.52×10^{-3} and 2.05×10^{-2} grams, respectively. As shown, the analyzed mass of each pseudocomponent in the soil

is one or two orders of magnitude higher than its mass in dissolved and sorbed phases combined. Therefore, in this research, the contribution of sorbed phase to dissolved phase was assumed negligible.

.

Appendix D:
LIF-UVOST™ Tool Description

LIF system is a useful tool that can be used for real-time, high-resolution mapping of NAPLs such as petroleum hydrocarbons. The system consists of a light source (laser), fiber optics strung through the rod string, optical detection, and a computer for processing data. A direct push system is used to push the probe containing the sapphire window into the subsurface ground at a rate of about 2 cm/sec, with a measurement obtained approximately every 0.05 foot (ITRCWEB, 2021; ASTM, 2010). A fiber-optic cable transmits backs the pulsed laser light to the window, where the light exits the probe and illuminates the adjacent soils and sediments and NAPL if present (see Figure D.1 and D-2) (ITRCWEB, 2021). The results are presented on a display in real-time in the form of fluorescence intensity signal (FIS) versus depth log, as presented in Figure D-3.

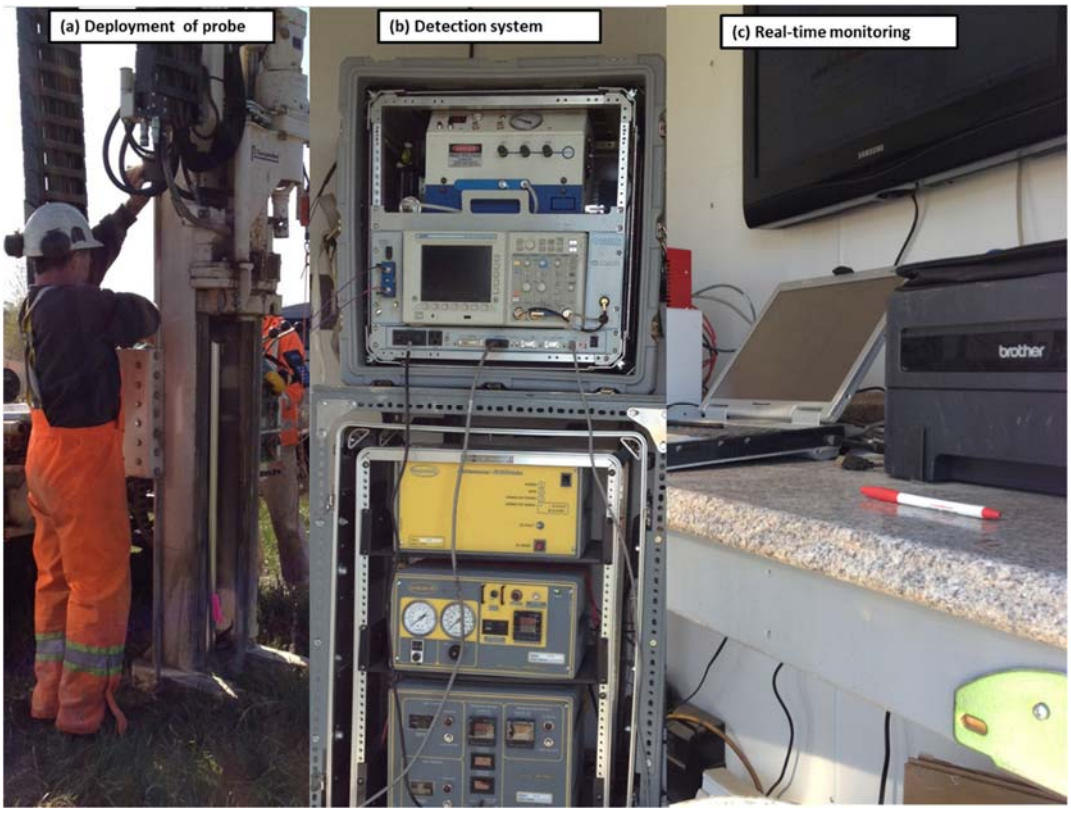

Figure D-1: Equipment for application of LIF-UVOST™ at the Site (a) direct push system, (b) computer receiving data and processing, and (c) the display for real-time observation of result

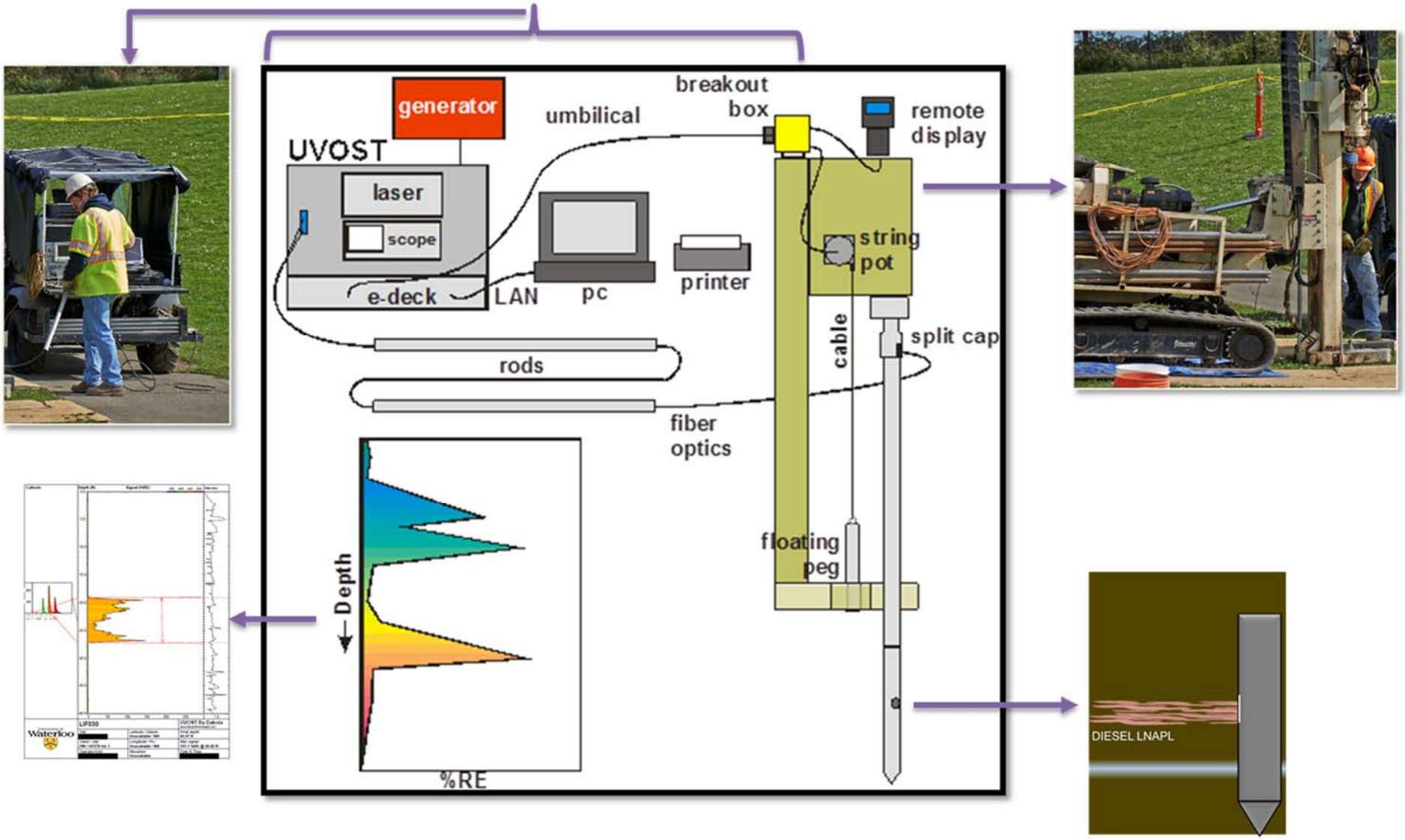

Figure D-2: Illustration of LIF-UVOST^{TM} coupled with direct push system (with modifications and permission from Dakota Technology)

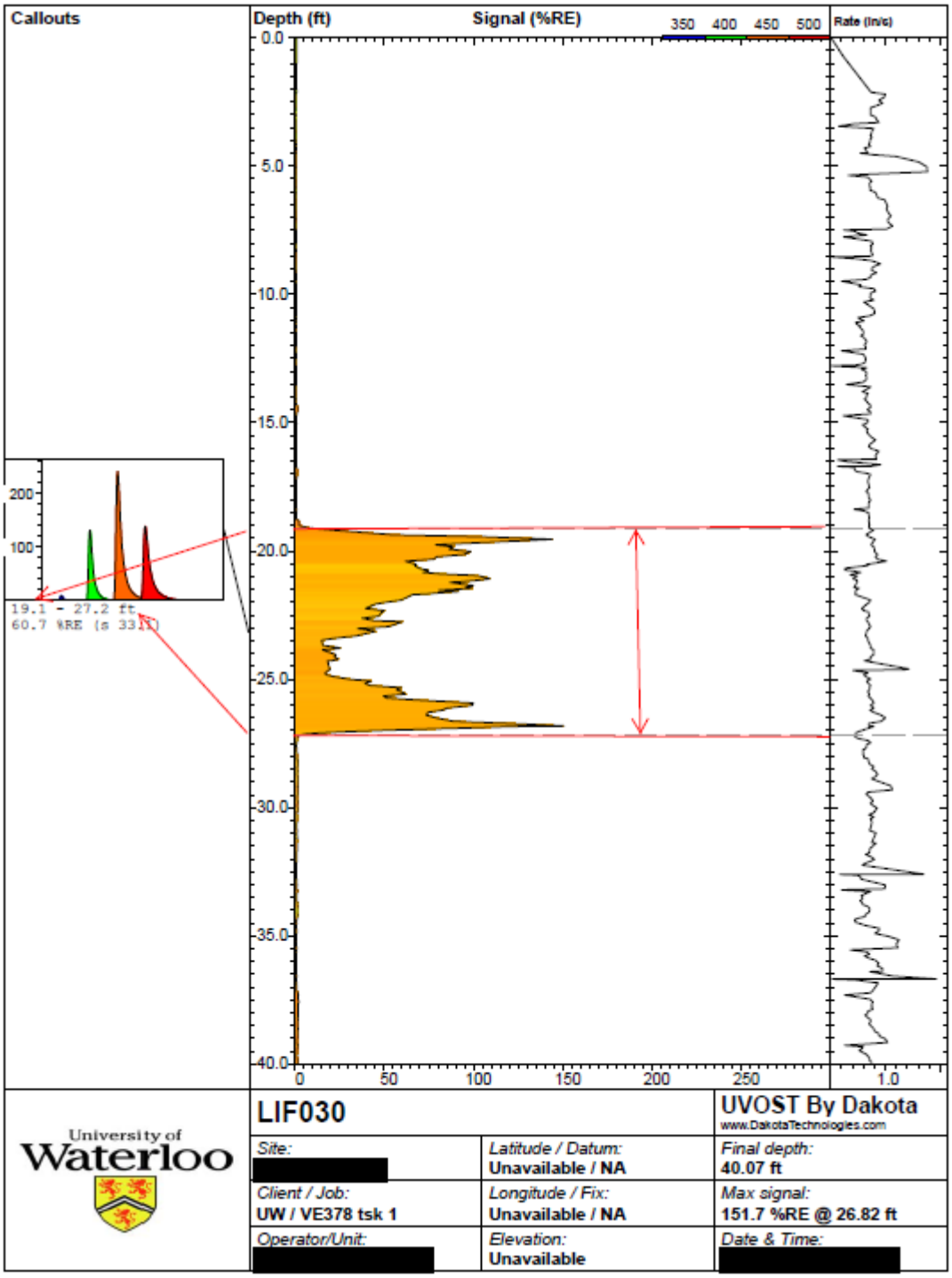

Figure D-3: A sample Fluorescence vs. depth Log presenting the results of UVOST at LIF030

Appendix E:
LIF-UVOSTTM Survey

LIF-UVOST™ profiling was conducted to verify the observations from the DPT effort and to determine the spatial distribution of subsurface impacts. To adequately delineate the pilot-scale area, a combination of adaptive sampling approaches (subsequent LIF borehole location was determined based on the data from preceding boreholes) and a grid sampling technique was utilized to select LIF probe borehole locations. Each PSA was gridded into 1 x 1 m segments. The LIF borehole locations were selected to provide spatial representation across each PSA. A total of 18 LIF boreholes were advanced by Vertex Environmental Inc. (Vertex). The LIF boreholes were advanced to depths of ~12.2 m (40 ft) bgs through the smear zone. Vertex equipped the UW's Geoprobe with a UVOSTTM system. LIF borehole locations were plugged and abandoned with granulated bentonite chips (Baroid, Holeplug) by filling the borehole from total depth to grade. LIF-UVOSTTM technology uses a pulse laser coupled with an optical probe to determine the presence and quantitate the amount of NAPL PHCs present in the subsurface. The UV light is directed through a sapphire window and absorbed by the PHCs (present in the subsurface sediments), causing them to excite fluorescence. The emitted signal response reaching the same sapphire window is collected and conveyed to a detection system at the surface through optical fibers. The emission data are the product of fluorescence intensity normalized to a standard reference emitter (RE). This data was continuously recorded at a 2.54 cm (1 inch)/second vertical resolution as the probe was driven into the subsurface. In grid locations that refusal was encountered, the optical probe was advanced in the neighborhood of the grid locations where favorable subsurface conditions were present. With the exception of LIF-026, which is located ~1.25 m up-gradient of MW 09-7 (used to establish a background LIF response), all LIF borehole locations were advanced down-gradient of MW 09-7 within the pilot-scale area. The LIF results are depicted in Figure E-1 and Figure E-2.

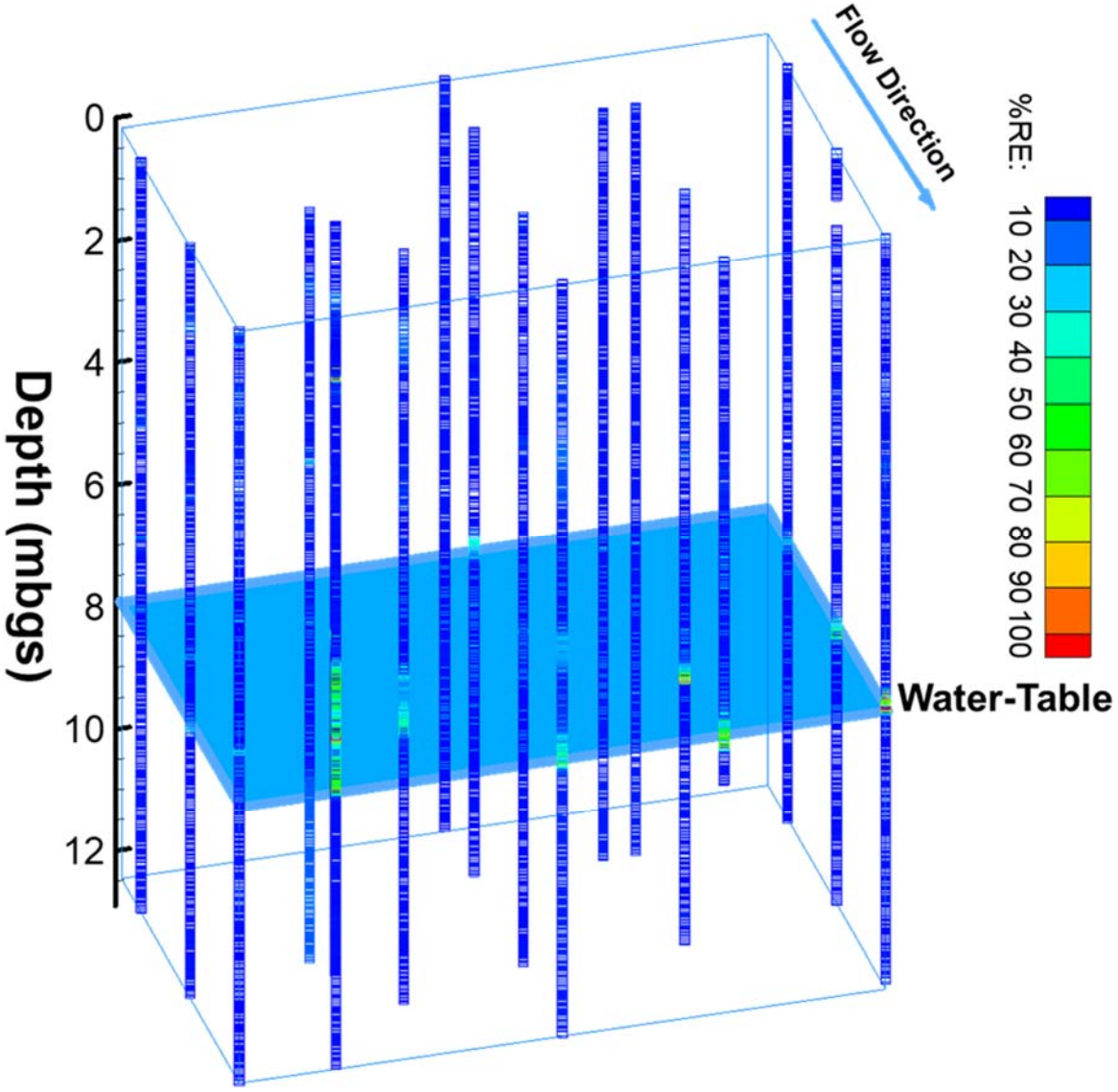

Figure E-1: LIF borehole locations with the presentation of elevated %RE at pilot-scale area

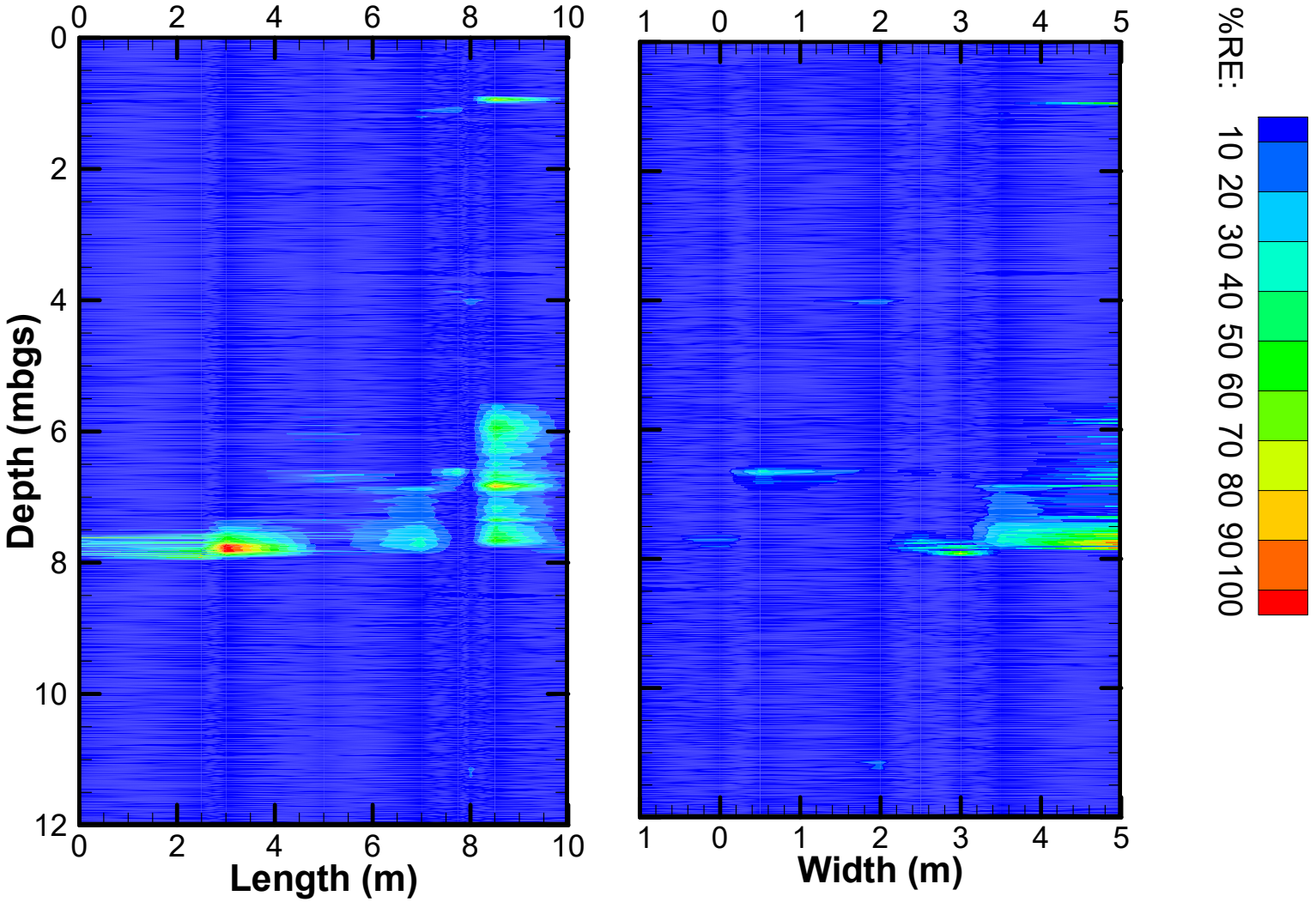

Figure E-2: Cross-sectional LIF-UVOST™ results at pilot-scale area

Appendix F:
ISCO Injection Design Calculations

The injection was designed to achieve a radius of influence (ROI) of 1.1 (m) during the injection. The low-pressure was considered, where possible, to increase the potential for the persulfate solution to mix with contaminated groundwater and to minimize subsurface disturbance, and mitigate daylighting or short-circuiting of remedial fluids. The maximum injection pressure was estimated using the below equation:

$$P_{max} = \rho_{dry} * g * h_{dry} + \rho_{sat} * g * h_{sat} - \rho_{water} * g * h_{sat} \quad \text{(F.1)}$$

where P_{max} is maximum allowable injection pressure, ρ_{dry}, ρ_{sat}, and ρ_{water} are the density of dry soil, density of saturated soil, the density of groundwater, respectively. h_{dry} and h_{sat} are the thickness of the vadose zone and saturated zone, respectively, and g is the gravitational acceleration. It is recommended to apply a 20 to 40 % safety factor to maximum allowable injection pressure to ensure the injection pressure does not cause formation damage. Preliminary ROI testing with tracer was conducted to confirm (Figure F-1) injection spacing and to determine proper injection rate. The design injection pressure was calculated as follows:

φ (porosity)=0.32, ρ_{sand} = 2.65 g/cm^3

Thickness of saturated zone = 300 cm, Thickness of vadose zone = 800 cm

within saturation zone S_r=1➔ $\rho_{sat=}\ \rho_{sand}.(1-\varphi)+\rho_w\ \varphi$ S_r=2.07 g/cm^3

within the vadose zone (dry): S_r=0➔ $\rho_{dry=}\ \rho_{sand}\ .(1-\varphi)+\rho_{water}\ .\ \varphi$ S_r= 1.7 g/cm^3

$P_{max}= \rho_{dry}.g.h_d+ \rho_{sat}.g.h_{sat} - \rho_{water}.g.h_{sat}$ = (1.7*980*10*100+2.07*3*100*980)-1*3*980*100

~2.1x10^{6}dynes/cm^2 =208.5 Kpa➔ P_{design}= 125.1 to 166.8 Kpa

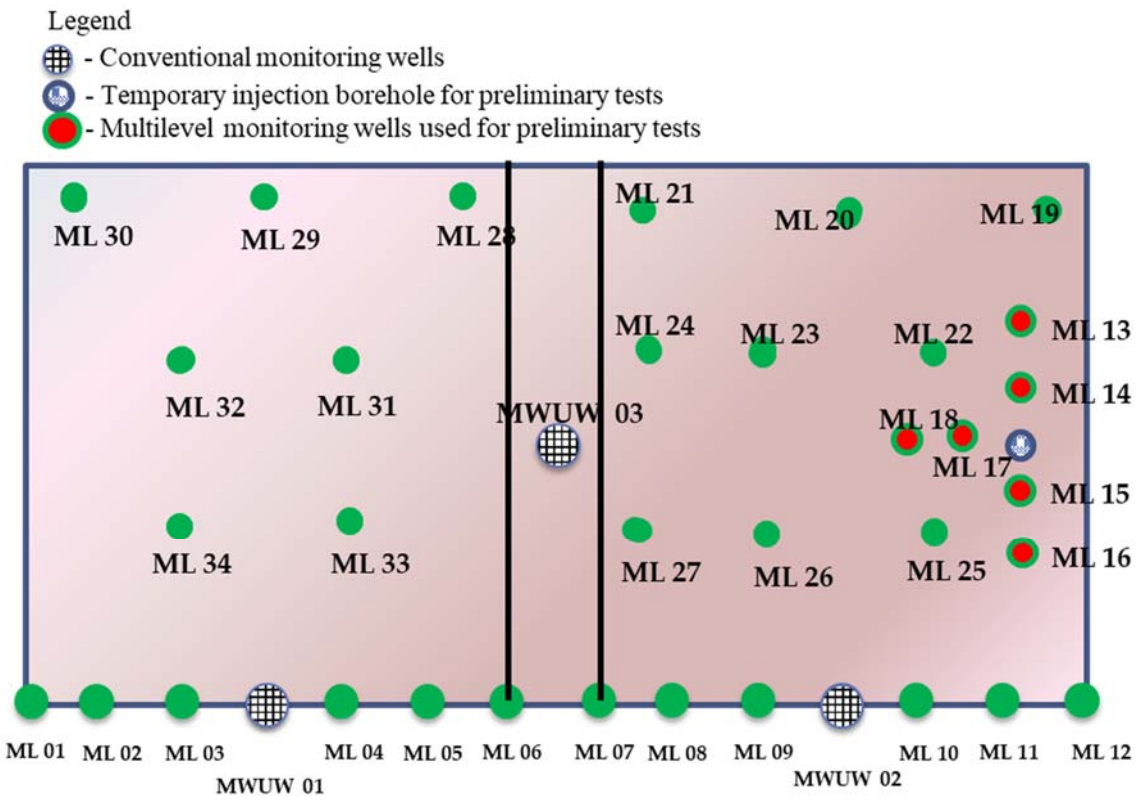

Figure F-1: Schematic diagram illustrating the monitoring wells and temporary borehole used for pre-injection evaluations

Appendix G:
Hydraulic Conductivity Measurements

The primary objective of this laboratory study was to provide some insight on vertical hydraulic conductivity, pilot-scale area and to determine whether the higher hydraulic conductivity layer(s) consisted of higher NAPL mass than the lower hydraulic conductivity layer(s). For this purpose, the hydraulic conductivity of some selected pre-treatment cores collected at the pilot scale area was examined.

The soil core was subsampled at every 10 inches. An adjustment to the length of sampling frequency was made if a change in stratum was observed and could not be captured by the sampling interval. Samples were collected to be used for both hydraulic conductivity evaluation and PHC analysis. The hydraulic conductivity of the core sample was determined using by falling head permeameter apparatus, which was equipped with a manometer. For this purpose, the sample was air or oven-dried before being loaded into the permeameter cell. Carbon dioxide was injected through the sample to displace the oxygen in soil pores. Saturation of the soil was initiated by pumping (de-aired) water through the bottom of the permeameter cell until the water was raised to a selected height in the manometer. The time required for the water level to fall a set distance in the manometer tube was recorded. The hydraulic conductivity estimate was determined using the following equation (Freeze and Cherry, 1979):

$$K = \frac{aL}{At} ln \frac{H_0}{H_1}$$

where a is the cross-sectional area of the manometer, L is the sample thickness, A is the cross-sectional area of the sample tube, t is the average time of three trials, H_0 is the total head at the start of the test, and H_1 is the total head at the end of the test. An example of vertical hydraulic conductivity and total petroleum hydrocarbon concentration profile with depth is provided in Figure G-1.

References

Freeze, R.A., and Cherry, J.A. (1979), *Groundwater*, Englewood Cliffs, NJ, Prentice-Hall

Hazen, A. (1892). *Some Physical Properties of Sands and Gravels, With Special Reference to Their Use in Filtration*. Massachusetts State Board of Health, 24th Annual Report, 539–556.

Rosas, J., O. Lopez, T.M. Missimer, K.M. Coulibaly, A.H.A. Dehwah, K. Sesler, L.R. Lujan, and D. Mantilla. (2014). Determination of hydraulic conductivity from grain-size distribution for different depositional environments. Groundwater 52, no. 3: 399–413. DOI:10.1111/gwat. 12078.

Oldham, T.L. (1998), *Use of falling head permeameters to determine hydraulic conductivity,* Department Of Earth Sciences, University of Waterloo

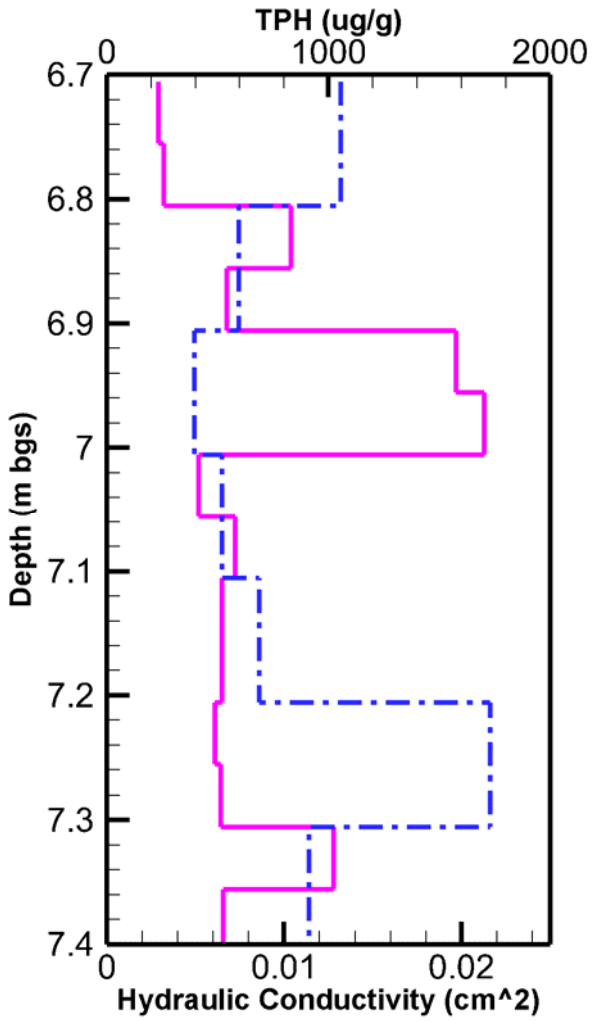

Figure G-1: Example of vertical hydraulic conductivity and total petroleum hydrocarbon concentration profile for a section of the contaminated aquifer

Appendix H:

Groundwater Analytical Results Pre- and Post- Injection Activities

Well ID	Depth (m bgs)	Pre-Injection		~4 months Post Injection 1		~8 months Post Injection 2	
		F2 (ppb) nC10-nC16	F3 (ppb) nC16-nC34	F2 (ppb) nC10-nC16	F3 (ppb) nC16-nC34	F2 (ppb) nC10-nC16	F3 (ppb) nC16-nC34
ML 01	**7.6**	565.9	2023.5	ND	81.5	ND	ND
ML 01	**9.1**	522.7	1923.2	ND	32.4	ND	ND
ML 01	**10.7**	8.3	0.0	ND	ND	ND	ND
ML 02	**7.6**	848.6	2749.7	ND	87.2	ND	ND
ML 02	**9.1**	0.0	0.0	ND	ND	ND	ND
ML 02	**10.7**	0.0	0.0	ND	ND	ND	ND
ML 03	**7.6**	669.9	2671.1	180.9	1264.4	231.0	617.0
ML 03	**9.1**	0.0	0.0	ND	ND	ND	ND
ML 03	**10.7**	-	-	ND	ND	ND	ND
ML 04	**7.6**	528.3	1248.4	851.9	7387.1	280.0	1115.3
ML 04	**9.1**	0.0	0.0	ND	76.3	ND	ND
ML 04	**10.7**	0.0	0.0	ND	ND	ND	ND
ML 05	**7.6**	687.6	1216.6	587.5	1834.8	379.0	795.1
ML 05	**9.1**	0.0	0.0	ND	55.5	ND	ND
ML 05	**10.7**	0.0	0.0	ND	ND	ND	ND
ML 06	**7.6**	702.0	2022.7	1414.9	3739.5	1414.9	3739.5
ML 06	**9.1**	0.0	0.0	ND	39.0	ND	39.0
ML 06	**10.7**	0.0	0.0	ND	47.9	ND	47.9
ML 07	**7.6**	460.3	1076.1	824.8	2614.4	206.5	877.7
ML 07	**9.1**	0.0	0.0	ND	111.0	ND	ND
ML 07	**10.7**	*0.0*	0.0	ND	ND	-	-
ML 08	**7.6**	502.4	1412.3	334.0	699.8	ND	502.9
ML 08	**9.1**	0.0	0.0	37.4	140.2	ND	ND
ML 08	**10.7**	0.0	0.0	ND	ND	ND	ND
ML 09	**7.6**	554.3	1058.4	-	-	2916.3	8579.1
ML 09	**9.1**	0.0	0.0	32.4	256.1	-	-
ML 09	**10.7**	0.0	15.7	ND	ND	ND	ND

Notes:

m bgs- meter below ground surface
DUP field duplicate samples
ML- multi-level monitoring wells
MWUW- conventional monitoring wells
NC- not completed at the time of sampling
ND- not detected = < method detection limit (MDL)
ppb- parts per billion
nC- carbon number

Groundwater Analytical Results Pre- and Post- Injection Activities (Cont.)

Well ID	Depth (m bgs)	Pre-Injection		~4 months Post Injection 1		~8 months Post Injection 2	
		F2 (ppb) nC10-nC16	F3 (ppb) nC16-nC34	F2 (ppb) nC10-nC16	F3 (ppb) nC16-nC34	F2 (ppb) nC10-nC16	F3 (ppb) nC16-nC34
ML 10	**7.6**	541.3	1833.0	312.3	1948.0	ND	ND
ML 10	**9.1**	0.0	0.0	ND	230.8	ND	ND
ML 10	**10.7**	0.0	4.0	ND	ND	ND	ND
ML 11	**7.6**	464.7	1675.6	222.4	1540.1	422.4	674.8
ML 11	**9.1**	0.0	0.0	30.7	332.6	ND	ND
ML 11	**10.7**	0.0	0.0	ND	ND	ND	ND
ML 11-DUP	**10.7**	0.0	0.0	-	-	-	-
ML 12	**7.6**	311.4	1295.7	68.7	553.8	ND	ND
ML 12	**9.1**	0.0	0.0	28.2	246.8	ND	ND
ML 12	**10.7**	0.0	0.0	ND	37.6	ND	ND
ML 13	**7.6**	NC	NC	439.3	6116.6	439.3	6116.6
ML 13	**8.4**	NC	NC	ND	109.3	ND	109.3
ML 13	**9.1**	NC	NC	ND	293.7	ND	293.7
ML 13	**10.7**	NC	NC	ND	50.4	ND	50.4
ML 14	**7.6**	NC	NC	618.7	5952.1	ND	1198.1
ML 14	**8.4**	NC	NC	ND	247.9	ND	553.5
ML 14	**9.1**	NC	NC	ND	290.2	ND	ND
ML 14	**10.7**	NC	NC	ND	ND	ND	ND
ML 15	**7.6**	NC	NC	613.8	2690.4	154.2	1497.7
ML 15	**8.4**	NC	NC	46.5	240.9	76.3	1051.3
ML 15	**9.1**	NC	NC	38.1	302.4	ND	ND
ML 15	**10.7**	NC	NC	ND	44.2	ND	ND
ML 15-DUP	**10.7**	NC	NC	-	-	-	-
ML 16	**7.6**	NC	NC	384.7	2544.0	ND	ND
ML 16-DUP	**7.6**	NC	NC	-	-	-	-
ML 16	**8.4**	NC	NC	ND	255.2	ND	167.4
ML 16	**9.1**	NC	NC	33.5	518.4	ND	ND
ML 16	**10.7**	NC	NC	ND	ND	ND	ND

Notes:
- m bgs- meter below ground surface
- DUP field duplicate samples
- ML- multi-level monitoring wells
- MWUW- conventional monitoring wells
- NC- not completed at the time of sampling
- ND- not detected = < method detection limit (MDL)
- ppb- parts per billion
- nC- carbon number

Groundwater Analytical Results Pre- and Post- Injection Activities (Cont.)

Well ID	Depth (m bgs)	Pre-Injection		~4 months Post Injection 1		~8 months Post Injection 2	
		F2 (ppb) nC10-nC16	F3 (ppb) nC16-nC34	F2 (ppb) nC10-nC16	F3 (ppb) nC16-nC34	F2 (ppb) nC10-nC16	F3 (ppb) nC16-nC34
ML 17	**7.6**	NC	NC	151.0	1746.0	ND	483.1
ML 17	**8.4**	NC	NC	ND	146.5	97.4	1082.4
ML 17	**9.1**	NC	NC	ND	277.3	ND	140.3
ML 17	**10.7**	NC	NC	ND	ND	ND	ND
ML 18	**7.6**	NC	NC	136.8	1788.1	ND	527.8
ML 18	**8.4**	NC	NC	23.9	332.8	ND	444.8
ML 18	**9.1**	NC	NC	40.9	383.8	ND	163.0
ML 18	**10.7**	NC	NC	ND	43.6	ND	ND
ML 19	**7.6**	NC	NC	-	-	ND	211.4
ML 19	**8.4**	NC	NC	35.2	300.2	100.6	699.2
ML 19	**9.1**	NC	NC	23.7	679.6	ND	ND
ML 19	**10.7**	NC	NC	-	-	ND	ND
ML 20	**7.6**	NC	NC	156.0	2878.8	ND	261.9
ML 20	**8.4**	NC	NC	-	-	332.2	970.2
ML 20	**9.1**	NC	NC	ND	158.3	ND	ND
ML 20	**10.7**	NC	NC	ND	ND	ND	ND
ML 21	**7.6**	NC	NC	ND	2376.0	ND	342.9
ML 21	**8.4**	NC	NC	ND	292.5	394.1	5476.2
ML 21	**9.1**	NC	NC	ND	275.0	ND	613.9
ML 21	**10.7**	NC	NC	ND	649.2	ND	ND
ML 22	**7.6**	NC	NC	427.5	4385.7	ND	1447.1
ML 22	**8.4**	NC	NC	ND	246.2	ND	541.2
ML 22	**9.1**	NC	NC	45.1	186.9	ND	284.8
ML 22	**10.7**	NC	NC	ND	ND	ND	ND
ML 23	**7.6**	NC	NC	168.7	9774.2	ND	1752.0
ML 23	**8.4**	NC	NC	96.0	1960.4	ND	954.4
ML 23	**9.1**	NC	NC	164.6	506.2	ND	ND
ML 23-DUP	**9.1**	NC	NC	-	-	-	-
ML 23	**10.7**	NC	NC	ND	ND	ND	ND

Notes:
- m bgs- meter below ground surface
- DUP field duplicate samples
- ML- multi-level monitoring wells
- MWUW- conventional monitoring wells
- NC- not completed at the time of sampling
- ND- not detected = < method detection limit (MDL)
- ppb- parts per billion
- nC- carbon number

Groundwater Analytical Results Pre- and Post- Injection Activities (Cont.)

Well ID	Depth (m bgs)	Pre-Injection		~4 months Post Injection 1		~8 months Post Injection 2	
		F2 (ppb) nC10-nC16	F3 (ppb) nC16-nC34	F2 (ppb) nC10-nC16	F3 (ppb) nC16-nC34	F2 (ppb) nC10-nC16	F3 (ppb) nC16-nC34
ML 24	**7.6**	NC	NC	54.7	1364.5	ND	1191.4
ML 24	**8.4**	NC	NC	ND	445.4	ND	621.0
ML 24	**9.1**	NC	NC	89.4	406.6	ND	ND
ML 24-DUP	**9.1**	NC	NC	53.5	374.0	-	-
ML 24	**10.7**	NC	NC	ND	ND	ND	ND
ML 25	**7.6**	NC	NC	76.3	757.4	ND	ND
ML 25	**8.4**	NC	NC	ND	118.4	ND	281.2
ML 25	**9.1**	NC	NC	120.5	588.2	ND	391.2
ML 25	**10.7**	NC	NC	ND	34.2	ND	ND
ML 26	**7.6**	NC	NC	107.1	1455.5	ND	568.0
ML 26	**8.4**	NC	NC	ND	298.7	ND	773.3
ML 26	**9.1**	NC	NC	ND	312.6	ND	ND
ML 26	**10.7**	NC	NC	ND	99.3	ND	ND
ML 27	**7.6**	NC	NC	81.3	1013.4	ND	672.4
ML 27	**8.4**	NC	NC	58.1	869.2	ND	317.7
ML 27	**9.1**	NC	NC	ND	241.4	ND	ND
ML 27	**10.7**	NC	NC	ND	60.0	ND	ND
ML 28	**7.6**	NC	NC	ND	393.7	ND	450.9
ML 28	**8.4**	NC	NC	ND	312.6	ND	ND
ML 28	**9.1**	NC	NC	ND	132.5	ND	ND
ML 28	**10.7**	NC	NC	ND	2380.8	ND	ND
ML 29	**7.6**	NC	NC	ND	2694.8	ND	ND
ML 29	**8.4**	NC	NC	85.3	719.5	ND	ND
ML 29	**9.1**	NC	NC	ND	31.6	ND	ND
ML 29	**10.7**	NC	NC	ND	ND	ND	ND
ML 30	**7.6**	NC	NC	36.2	1359.2	ND	ND
ML 30	**8.4**	NC	NC	156.2	585.5	ND	ND
ML 30	**10.7**	NC	NC	ND	ND	ND	ND

Notes:
- m bgs- meter below ground surface
- DUP field duplicate samples
- ML- multi-level monitoring wells
- MWUW- conventional monitoring wells
- NC- not completed at the time of sampling
- ND- not detected = < method detection limit (MDL)
- ppb- parts per billion
- nC- carbon number

Groundwater Analytical Results Pre- and Post- Injection Activities (Cont.)

Well ID	*Depth (m bgs)*	*Pre-Injection*		*~4 months Post Injection 1*		*~8 months Post Injection 2*	
		F2 (ppb)	*F3 (ppb)*	*F2 (ppb)*	*F3 (ppb)*	*F2 (ppb)*	*F3 (ppb)*
		nC10-nC16	*nC16-nC34*	*nC10-nC16*	*nC16-nC34*	*nC10-nC16*	*nC16-nC34*
ML 31	**7.6**	NC	NC	148.4	4636.1	26.3	2550.8
ML 31	**8.4**	NC	NC	ND	743.5	ND	ND
ML 31	**9.1**	NC	NC	ND	65.2	ND	ND
ML 31	**10.7**	NC	NC	ND	ND	ND	ND
ML 32	**7.6**	NC	NC	ND	1022.6	ND	1319.4
ML 32	**8.4**	NC	NC	52.6	592.1	ND	ND
ML 32	**9.1**	NC	NC	ND	68.0	ND	5726.8
ML 32	**10.7**	NC	NC	ND	ND	ND	ND
ML 33	**7.6**	NC	NC	657.3	2036.0	447.1	2752.0
ML 33-DUP	**7.6**	NC	NC	-	-	-	-
ML 33	**8.4**	NC	NC	ND	350.6	ND	ND
ML 33-DUP	**8.4**	NC	NC	49.7	340.3	-	-
ML 33	**9.1**	NC	NC	ND	40.4	ND	ND
ML 33-DUP	**9.1**	NC	NC	ND	30.1	-	-
ML 33	**10.7**	NC	NC	ND	42.3	ND	ND
ML 34	**7.6**	NC	NC	860.5	2879.5	1167.3	3695.0
ML 34	**8.4**	NC	NC	85.6	450.6	ND	ND
ML 34	**9.1**	NC	NC	ND	18.2	ND	ND
ML 34	**10.7**	NC	NC	ND	ND	397.6	1940.3
MWUW01	**10.7**	-	-	ND	73.8	-	-
MWUW02	**10.7**	-	-	44.8	144.5	-	-
MWUW03	**10.7**	-	-	31.8	99.2	-	-

Notes:
- m bgs- meter below ground surface
- DUP field duplicate samples
- ML- multi-level monitoring wells
- MWUW- conventional monitoring wells
- NC- not completed at the time of sampling
- ND- not detected = < method detection limit (MDL)
- ppb- parts per billion
- nC- carbon number